1-1-2021

FORECASTING GEOTECHNICAL PARAMETERS FROM ELECTRICAL RESISTIVITY AND SEISMIC WAVE VELOCITIES USING ARTIFICIAL NEURAL NETWORK MODELS

Fatema Tuz Johora
University of Mississippi

FORECASTING GEOTECHNICAL PARAMETERS FROM ELECTRICAL RESISTIVITY AND SEISMIC WAVE VELOCITIES USING ARTIFICIAL NEURAL NETWORK MODELS

A Dissertation
presented in partial fulfillment of requirements
for the degree of Doctor of Philosophy
in the Department of Civil Engineering
The University of Mississippi

By

FATEMA TUZ JOHORA

August 2021

ABSTRACT

Geotechnical measurements of soil parameters used in the design of infrastructure provide information at a specific point of the ground. The use of limited point data may result in greater uncertainty and less reliability in design. Geophysical methods are non-invasive, less time-consuming, and provide continuous spatial information about the soil. However, geophysical information is not in terms of engineering parameters. Correlations between geotechnical parameters and geophysical parameters are needed to facilitate the use of geophysical information in geotechnical designs. The current research is focused on two geophysical methods; electrical resistivity (ER) and seismic wave velocity (S-wave and P-wave). Artificial neural network (ANN) models are developed using published data to predict geotechnical parameters from ER and seismic wave velocity. Results of ANN models from the published data show that ER can predict geotechnical parameters with moderate to good accuracy and also predict cation exchange capacity (CEC) better than saturation. Seismic wave velocity helps to predict water content and dry density. Overall, the performance of ANN is better than regression. Laboratory measurements are performed on proctor-compacted soil samples with varying clay, sand, and silt proportions applicable to earthen dam construction. ER, seismic wave velocity and various geotechnical parameters are measured on the same samples. Results show that ER is most sensitive to Atterberg limits, specific surface area, CEC, cohesion, water content and saturation. ANN models are in agreement with the Waxman-Smits formula. In comparison to ER, S-wave and P-wave velocities are more sensitive to dry density and void ratio. Combining ER and S-wave and P-wave velocities predicts water content, dry density, saturation, and void ratio more accurately than simply using

individual geophysical parameters. The geophysical parameters in conjunction with the soil mix proportions allow for good to high accuracy predictions of multiple geotechnical parameters.

DEDICATION

This work is dedicated to Allah Almighty, my creator,

the unique, omnipotent and only deity and creator of the universe

To my mother Jabunnahar, to my father Taher,

for whom I am here today on the way to achieve my dream

To my dearest husband Sharif and my daughter Sidrat,

the most precious gift from Allah and my best friends

To my sister Khodeja and by brother Omar

thank you for the love, support, and encouragement.

LIST OF ABBREVIATIONS AND SYMBOLS

ρ	Resistivity
r	Resistance
A	Cross-sectional area
L	Length
ρ_b	Bulk resistivity
ρ_w	Resistivity of the pore fluid
F	Formation factor
Φ	Porosity of the sand
m	Cementation component
s_w	Degree of saturation
n	Saturation exponent
C_0	Bulk conductivity of fully saturated soil sample
C_w	Conductivity of the pore fluid
a	Empirical constant
C_e	Conductivity due to the presence of clay content
T	Transverse resistance
h	Thickness
e	Void ratio
BQ_v	Surface conductivity

Θ	Volumetric water content
ε	Standard error
w	Water content
G	Shear modulus
M	Constraint modulus
B	Bulk modulus
d	Mass density of the medium
E	Young's modulus
υ	Poisson's ratio
B_{SK}	Bulk modulus of the skeleton
B_g	Bulk modulus of the grains
B_f	Bulk modulus of the fluid phase
B_{eff}	Effective bulk modulus
G_{eff}	Effective shear modulus
G_{SK}	Shear modulus of skeleton
B_w	Bulk modulus of liquid phase
B_a	Bulk modulus of air phase
C_d	Normalized consistency ratio
G_T	Specific gravity of soil at room temperature (^{0}C)
w_s	Weight of soil (gm)

G_{20}	Specific gravity of soil at 20^0C
G_w	Specific gravity of water
v_w	Volume of water
v_v	Volume of void
v_s	Volume of solid
LL	Liquid limit
PL	Plastic limit
SL	Shrinkage limit
SG	Specific gravity
A_s	Specific surface area
X_i^A	Actual value
X_i^P	Predicted value
$\bar{X}_I$	Mean of X_I^A
N	Total number of data set
$\sigma_{bulk}/\sigma_{pf}$	Normalized conductivity
ER	Electrical resistivity
CEC	Cation exchange capacity
MARE	Mean absolute relative error
ASE	Average squared error
R^2	Coefficient of determination/ regression coefficient

USACE	U.S. army corps of engineers
NID	National inventory of dams
ANN	Artificial neural network
GPR	Ground penetration radar
SP	Self-potential
IP	Induced polarization
SPT	Standard penetration test
DCPT	Dynamic cone penetration test
R	Coefficient of correlation
MES	Mean error squares
MAEP	Mean absolute error percent
V_s	Shear wave velocity
SCPT	Seismic cone penetration tests
q_c	Cone penetration tip resistance
RMSE	Root mean squared error
SMP	Soil mix proportion
Opt	Optimum

ACKNOWLEDGMENTS

I would like to express my sincere gratitude to my research advisor Dr. Craig Hickey, Director at the National Center for Physical Acoustics and Research Associate Professor of Physics and Geological Engineering, for his continuous encouragement and support over the years. The completion of this study would not have been possible without his expertise.

I would also like to express my sincere gratitude to my academic adviser and committee member Dr. Hakan Yasarer, Assistant Professor of Civil Engineering, for his valuable contribution, support, and encouragement. He has devoted his valuable time and energy in helping me navigate my graduate studies. I would also like to thank Dr. Hunain Alkhateb, Associate Professor of Civil Engineering, and Dr. Yacoub Najjar, Chair and Professor of Civil Engineering, for their interest and valuable comments on my work.

I want to thank the U.S. Department of Agriculture under Non-Assistance Cooperative Agreement 58-6060-6-009 for providing financial support. I also thank Dr. Yacoub Najjar, Department Chair and Professor, Civil Engineering Department, University of Mississippi for the ANN software, used for the analysis of this research.

Fatema Tuz Johora

TABLE OF CONTENTS

LIST OF TABLES

LIST OF FIGURES

CHAPTER 1

INTRODUCTION

1.1 General

Geophysics is the study of the earth, and often involves taking measurements at or near the earth's surface by applying the principles of physics. The measurements are influenced by the physical properties of the earth. Historically, geophysical surveys were used to delineate contacts and boundaries in the subsurface and to map the location of these boundaries between boreholes. Geophysical techniques have good spatial resolution in both 2D and 3D. These techniques are non-destructive, thereby allowing for monitoring of changes over time. But geophysical methods have some demerits in engineering applications. The measurements are in terms of geophysical attributes rather than engineering parameters, the spatial resolution depends on the geophysical method and site characteristics, and geophysical anomalies do not necessarily correspond to inferior subsurface locations. Different kinds of geophysical techniques, such as seismic, gravity, magnetic, ER, self-potential and radar (Kearey et al., 1984), are used depending on the purpose.

In the last few decades, geophysical techniques have been used to provide additional information for solving different kinds of civil engineering problems (Sharma, 1997). Some engineering applications include seismic hazard, foundation testing, locating water, and detection of abandoned mine shafts, unlogged pipes, and discarded metallic objects. Determination of the depth and constitution of bedrock, and the physical properties of rock encountered in dam, canal,

tunnel shaft, high-level waste disposal vault, railway, highway, subway, and other construction projects are included in the foundation testing problems. In municipal engineering, the determination of the location of water and its salinity is necessary to solve water supply, sewage disposal, irrigation, and drainage problems. Geophysical methods are also used to collect information on water levels and water-bearing fissures, which are indispensable in the construction of subways and tunnels. To determine the location of older underground excavations, such as shafts and tunnels, and to locate buried ammunition and other metal machinery, geophysical techniques play a very important role (Sharma, 1997). Table 1.1 lists some of the engineering problems and the appropriate geophysical techniques that may be used.

Table 1.1: Engineering and geotechnical applications of geophysical techniques (Sharma, 1997).

Technique	Area of application					
	Depth to and constitution of bedrock	Rip ability/ Rock strength	Fracture/ Flow seepage detection	Location of cavities/voids	Permafrost/ Thaw zones delineation	Pipes/ Metal detection
Gravity	+	-	-	+	-	-
Magnetic	+	-	-	+	-	+
Self-potential	-	-	+	-	-	o
Resistivity +IP[a]	+	-	+	+	+	o
Electromagnetic	o	-	+	o	+	+
Ground radar	+	o	+	+	+	o
Radioactivity	-	-	o	-	-	-
Seismic refraction	+	+	o	o	+	-
Seismic reflection	+	+	o	o	o	-

Note: + applicable; o limited applicability; - not applicable; a Induced polarization

1.2 Research Significance

This research is focused on determining correlations between geophysical and geotechnical parameters for application to earthen dam and levee assessment. However, these correlations could be applied to many investigations involving near-surface soils.

Dams are extremely important life-sustaining resources to the people of the world. Dams can be used for supplying water for domestic, agricultural, industrial, and community use, flood control, erosion control, and for recreational purposes (ASDSO, 2019). Economic and social development in the USA is highly dependent on dams (Ho et al., 2017). According to the U.S. Army Corps of Engineers (USACE), around 20% of dams are used for flood control to reduce the risks of loss of life and property. The current National Inventory of Dams (NID) statistics show that nearly 84,000 dams are already constructed in the USA. The average age of these dams is over 50 years. Figure 1.1 shows the dams according to their age of construction based on data in the NID. In addition to age causing deterioration of the dams, the design criteria and loading estimates considered at the time of construction are insufficient according to modern design code. As a result, most of the dams in the USA are considered as unsafe and vulnerable. Figure 1.2 is a map of the distribution of low, significant, and high hazard potential dams in the USA (FEMA, 2013).

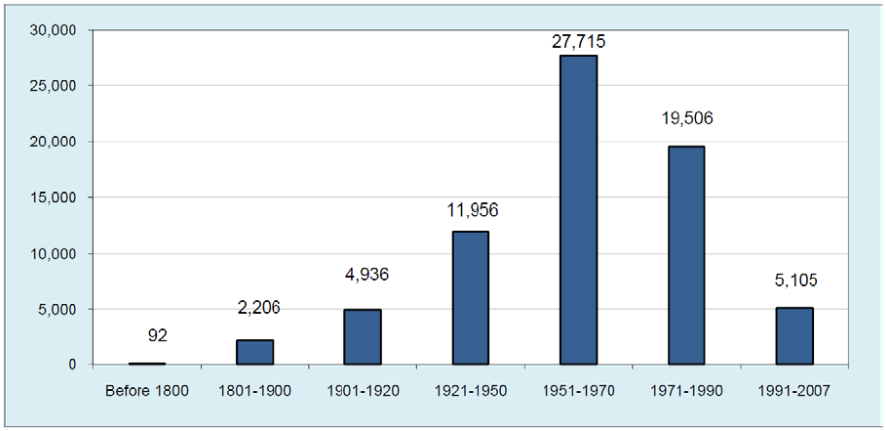

Figure 1.1: Years dams were completed in the United States (NID, 2009)

Preventing failures of these dams requires a rigorous inspection and investigation program. Based upon inspections, engineering solutions have to be proposed and implemented correctly. Geotechnical methods for investigation and inspection are very time consuming and destructive. On the other hand, geophysical methods are noninvasive, have good spatial resolution, and can

cover a large area within a relatively short time in comparison to geotechnical methods. But the geophysical parameters are not engineering parameters, depend on spatial resolution and sometimes difficult to interpret anomalies. Correlations between geophysical and geotechnical parameters can assist in the interpretation problem.

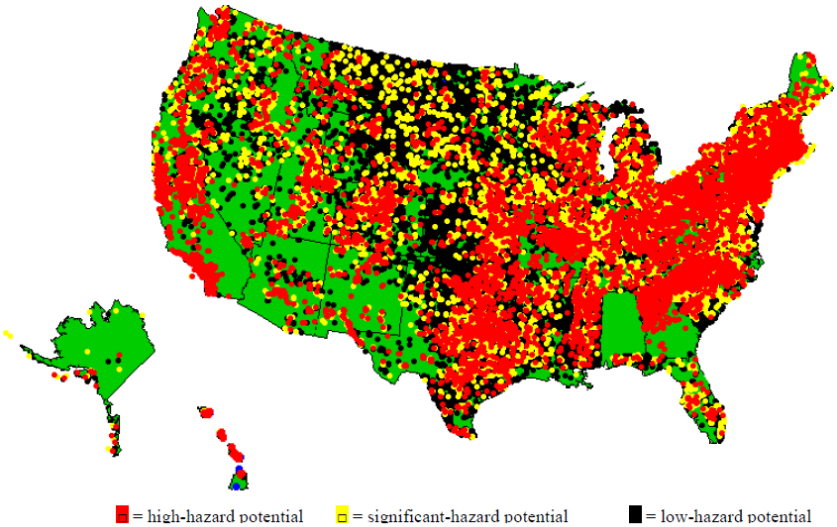

Figure 1.2 : State-regulated dams in the United States according to hazard potential (FEMA, 2010)

For this research, correlations between geophysical and geotechnical parameters and prediction models for geotechnical parameters from geophysical parameters were developed using an artificial neural network (ANN) approach. ANN is very effective in solving complex problems in comparison to traditional methods, such as regression.

1.3 Research Objectives

This research is focused on determining correlations between geophysical and geotechnical parameters. Specific objectives of the research are:

a) Creating a database of measurements for developing ANN models. This requires conducting laboratory experiments to collect: geotechnical parameters, such as Liquid limit (LL), plastic limit (PL), shrinkage limit (SL), water content, dry density, void

ratio, cohesion, specific gravity (SG), degree of saturation, specific surface area; a chemical parameter - CEC; and geophysical parameters, such as ER, S-wave and P-wave velocity. These tests are conducted on common samples prepared using the Proctor compaction method.

b) Predicting geotechnical parameters from ER applying ANN (using existing data from literature).

c) Application of ANN to forecast geotechnical parameters from seismic wave velocity (using existing data from literature).

d) Predicting geophysical parameters from geotechnical parameters (using measured experimental data).

e) Predicting geotechnical parameters from geophysical parameters (using measured experimental data).

f) Predicting geotechnical parameters from combined geophysical parameters (using measured experimental data).

CHAPTER 2

REVIEW OF PREVIOUS WORK

2.1 General

Geophysical information has been used to solve problems in different fields, such as oil exploration and mining exploration (Shirgiri, 2012). More recently, geophysical methods are gaining popularity in archeology, geotechnical engineering, civil engineering, hydrology, and glaciology. Dams and levees are important civil engineering structures and the design and assessment of dams and levees require characterization of the soils. Conventional geotechnical methods for soil characterization are invasive, very expensive, and time-consuming. Sometimes developers are not willing or are unable to conduct site characterization at the appropriate resolution due to the high cost of geotechnical investigation (Adewoyin et al., 2017). On the other hand, geophysical methods can provide subsurface coverage ensuring a cost-effective way of investigation without physical intervention (Mohd et al., 2012). Geophysical methods are non-destructive in nature and less time-consuming. Moreover, geophysical techniques can provide volumetric information and images without disturbing the subsoil physically (Loke, 2015), which is why geophysical methods are becoming a choice for geotechnical engineers for determining the spatial distribution of soil properties. The correlations between geophysical properties and geotechnical engineering properties are necessary to interpret the geophysical data so that geotechnical engineers can utilize the information in the design Five different kinds of geophysical methods commonly used in geotechnical investigations are: (a) seismic-based

methods, which include refraction, reflection, and surface wave method; (b) electromagnetic wave-based methods, including ground electrical conductivity and ground penetration radar (GPR); (c) electrical-based methods that include self-potential (SP), ER, equipotential and induced polarization (IP); (d) gravity methods; and (e) magnetics (Shirgiri, 2012). Among them, ER testing and seismic wave velocity measurements are two well-known geophysical methods.

Soil properties important to dam investigation include: moisture content, unit weight, degree of saturation, N-value, Atterberg limits, cohesion, angle of friction, Specific gravity (SG), void ratio, etc. Strong correlations between these geotechnical properties and geophysical properties will be helpful for using the geophysical information for geotechnical problems.

2.2 Electrical Resistivity

ER method was first designed by Schlumberger in France in 1920 (Loke, 2015). Soil electrical resistivity testing is becoming very popular due to its non-destructive nature and cost-effectiveness. The ER of a volume of soil is determined by measuring the voltage across a pair of electrodes in response to a known imposed current. The electrical resistance depends on the geometric arrangement of electrodes. For measurements on soil samples, it is proportional to the length and inversely proportional to the cross-sectional area of the material being tested. ER of soil is the measure of the resistance of current flow through it (Irfan, 2011). It can be mathematically expressed by the following equation.

$$\rho = r * A/L \qquad 2.1$$

where, ρ is the resistivity (ohm*m), r is the resistance (ohms), A is the cross-sectional area (m^2), L is the length of soil (m).

ER is sensitive to many soil properties, such as LL, plasticity index, particle size, porosity, degree of saturation, moisture content, etc. (Kibria, 2014). It is commonly considered as a soil

property that is affected by soil particle size distribution (clay content), porosity, and moisture content.

Archie's (1942) first law is a relationship between the bulk resistivity of soil and the porosity for a fully saturated clean sand or coarse-grained material. This model assumes that the primary pathway for electric current is through the pore fluid. Archie's first law is expressed as

$$F = \rho_b/\rho_w = a\Phi^{-m} \quad 2.2$$

where ρ_b is bulk resistivity, ρ_w is the resistivity of the pore fluid, F is formation factor, Φ is the porosity of the sand, a is an empirical constant close to 1 and m is the cementation exponent.

For partially saturated sand Archie's (1952) second law is

$$\rho_b/\rho_w = a\Phi^{-m} * s_w^{-n} \quad 2.3$$

where s_w is degree of saturation, and n is the saturation exponent.

The assumption of clean sand is usually not valid for most soils because they contain clay minerals. The presence of clay minerals allows for electric current to flow along the surface of the clay minerals. Waxman-Smit (1968) developed a relationship for the effective electrical conductivity of soils that includes surface conduction. The electrical conductivity is the inverse of ER. The formula provided by Waxman-Smit is

$$C_0 = \frac{1}{F}(C_w + C_e) \quad 2.4$$

where C_0= bulk conductivity of fully saturated soil sample with clay, C_w = conductivity of the pore fluid, and F is the formation factor of Shaley sand. C_e =Conductivity due to the presence of clay content.

2.3 Developed Correlation with ER

A significant amount of research has been published on correlations between ER and various geotechnical parameters. Sudha et al. (2009) developed correlations between transverse

resistance of soil with the number of blow counts (N values). N values are obtained from the Standard Penetration Test (SPT) and Dynamic Cone Penetration Test (DCPT). Two locations were chosen (Aligarh and Jhansi) in Uttar Pradesh, India. ER data were calibrated with borehole data, and finally, the transverse resistance was calculated, which was co-related with the N-values. The resistivity of the sites varies from 1 to 1000 Ωm, which indicates the variation in soil matrix, grain size distribution, and water saturation. The percentage of sand is dominant at Aligarh. Fine sand is dominant at Jhansi with a percentage of >70%. At both the sites the percentage of gravel is very small (<10%). Jhansi contains a higher percentage of clay than the Aligarh site. Figure 2.1 illustrates the fact that they found no specific correlation between resistivity and N-value.

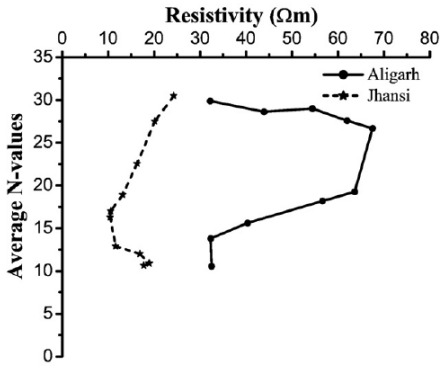

Figure 2.1: Variation of resistivity values derived from the interpreted section (Sudha et al, 2009).

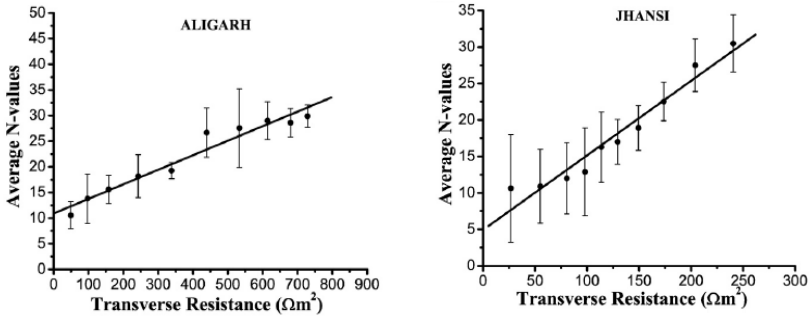

(a) (b)

Figure 2.2: Linear relationship between number of blow counts (N-values) and transverse resistance obtained at (a) Aligarh; (b) Jhansi (Giao, 2003).

Then they used the transverse resistance to determine a correlation with N-values. The transverse resistance (T) for an m-layer section was calculated as

$$T = \sum_{i=1}^{m} \rho_i h_i \qquad 2.5$$

where ρ_i and h_i are the resistivity and thickness of the i^{th} layer, respectively. Figure 2.2 represents the linear relation between average N-values and the transverse resistance.

Equations 1 and 2 represent the linear relationships at the Aligarh and Jhansi sites as,

$$y = 0.028x + 10.909 \qquad 2.6$$

$$y = 0.102x + 4.922 \qquad 2.7$$

where x is the transverse resistance (Ωm^2) and y is the number of blow counts (N values). The coefficients of correlation (R) for Aligarh and Jhansi sites are 0.974 and 0.975, respectively. Equations represent the positive correlations between the transverse resistance and average N values. The coefficients of the linear relationship are influenced by the clay content and lithology at the investigated sites. The changes in slope in the equation and are due to the change in clay content. At the Aligarh site, the percentage of clay content is less than the Jhansi sites.

P. H. Giao et. al. (2003) measured ER of Pusan clays of 50 core samples taken from five sites in the Nakdong river plain (Kimhae, Shinho, Eulsookdo, Yangsan, and Jangyu) in the laboratory to correlate it with geotechnical parameters such as salinity, organic content, water content, plasticity, unit weight and sampling depth. The soft clay samples were prepared with a diameter of 75 mm and a length of 110 mm and the four-electrode configuration. Figure 2.3 illustrates the ER versus geotechnical parameters. They found that ER of Pusan clays varied within the range of 1 to 3 Ω m. The resistivity of clays located in Kimhae, Yangsan, and Jangyu was higher (~ 2 to 3 Ω m) than Eulsookdo and Shinho (~ 1 Ω m). No definite relationship was found

between ER and geotechnical parameters (water content, plasticity, unit weight, and depth). Only salinity showed a closer correlation with ER.

Bryson and Bathe (2009) determined correlations between the void ratio (e) and normalized conductivity ($\sigma_{bulk}/\sigma_{pf}$), void ratio and surface conductivity (BQv), and volumetric water content (Θ) and surface conductivity. Void ratio is the ratio of volume of voids to the volume of soil in a soil specimen. Normalized conductivity is the ratio of bulk conductivity and the conductivity of pore fluids.

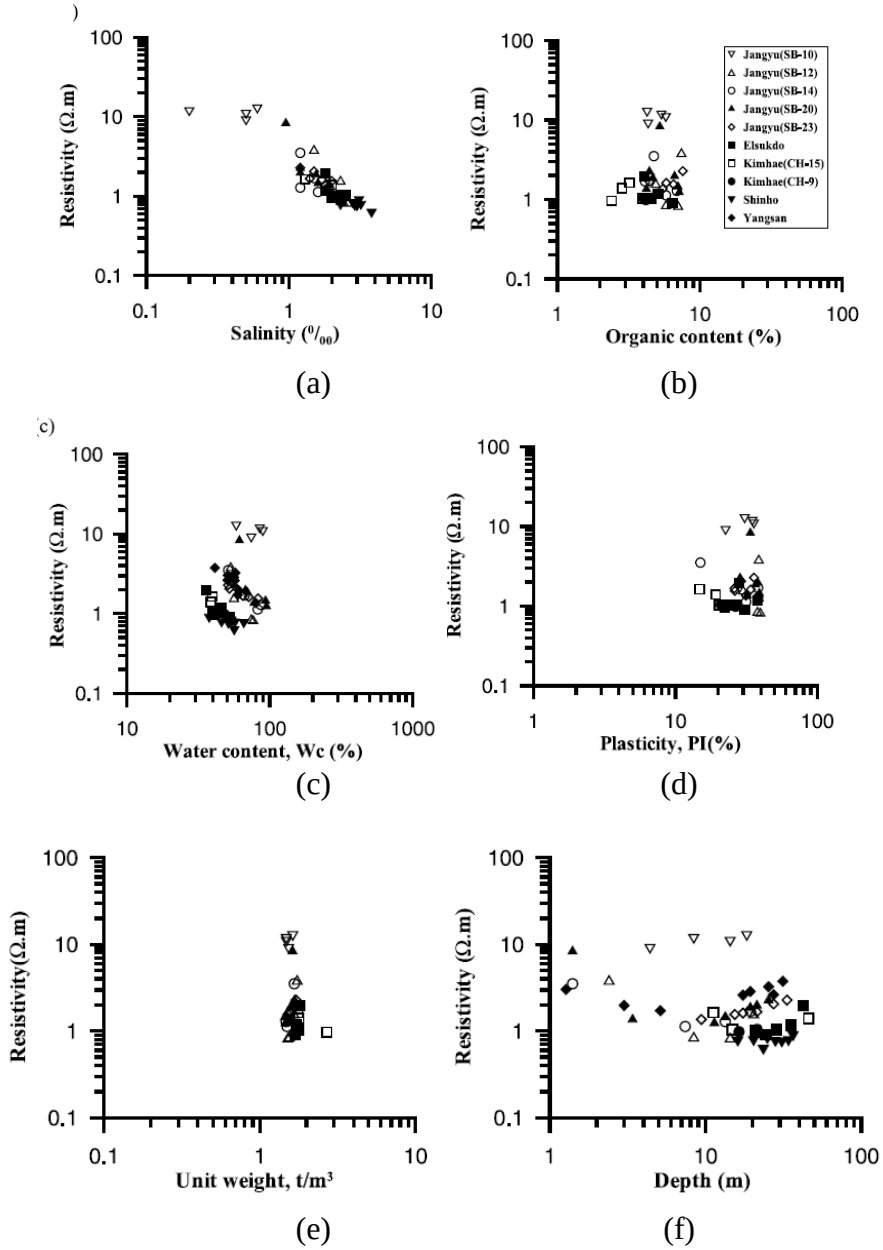

Figure 2.3 : Relationship between the ER and other parameters for Pusan clays, i.e., (a) salinity; (b) organic content; (c) water content, (d) plasticity, (e) water content (d) depth (Giao, 2003).

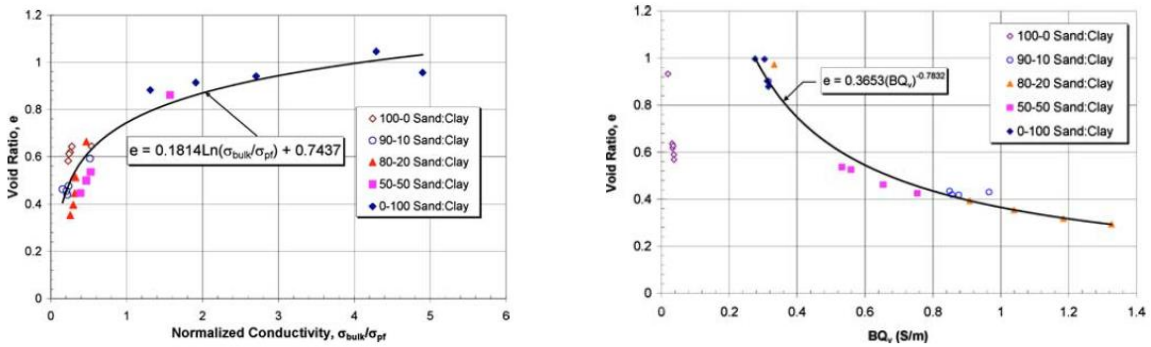

(a) (b)

Figure 2.4: Relationship between (a) void ratio and normalized conductivity (b) void ratio and surface conductivity (Bryson and Bathe, 2009).

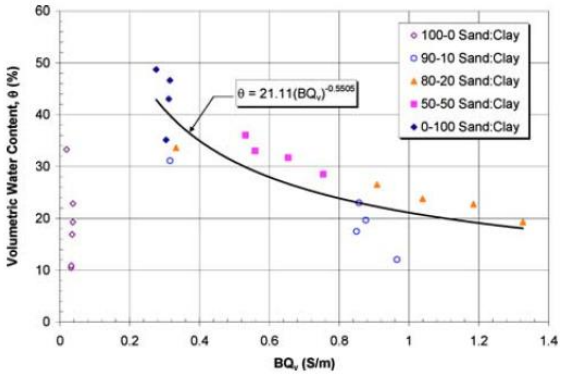

(c)

Figure 2.5: Relationship between volumetric water content and surface conductivity (Bryson and Bathe, 2009).

Figure 2.4a depicts that the normalized conductivity increases with an increase of clay content although the relative magnitude of the void ratios remains the same. The graph shows a logarithmic trend represented by

$$e = 0.18 \ln \left(\sigma_{bulk}/\sigma_{pf}\right) + 0.74 \qquad 2.8$$

Figure 2.4b illustrates the correlation between void ratio and surface conductivity. The graph shows that there exists a strong correlation between void ratio and surface conductivity. They represented the correlation using the following power function

$$e = 0.37 \left(BQv^{-0.78}\right) \qquad 2.9$$

The surface conductivity increases with a decrease in clay content. They attributed this phenomenon to greater dispersion of clay particles into the sand matrix than into the clay matrix. The orientation of clay particles is more aligned in the sand matrix and, for that reason, the particles can hold more water - which results in increased surface conductivity. Figure 2.5 shows the strong correlation between volumetric water content with surface conductivity, which can be expressed by the following equation:

$$\Theta = 21.11\ (BQ_v)^{0.55} \qquad 2.10$$

In Figure 2.5, the points below the curve represent the soil mixtures with degree of saturation less than 70%. The volumetric water content is strongly correlated with the surface conductivity for the degree of saturation greater than 70%.

Kibria and Hossain (2012) determined the relationships between soil resistivity and geotechnical properties of soil (i.e. moisture content, unit weight, degree of saturation, and specific surface area). They conducted soil resistivity tests in the laboratory at varying unit weights and moisture contents. They collected disturbed soil samples from Midlothian, Ellis County, Texas, and considered soil samples of similar geologic information.

The moisture contents were varied from 10 to 50%. Compaction was done at the optimum(opt) dry unit weight. Four samples, denoted A-B2-D15, A-B3-D10, A-B3-D15, and A-B3-D20, were considered to determine the correlations, where A represents the site location highway US 287, the second letter and number are for the borehole and third letter and number indicate the depth of samples. Figure 2.6 represents the variation of soil resistivity with gravimetric moisture content. The relationships and coefficients are also shown in Figure 2.6. ER decreases with an increase in water content up to around 20%. For moisture content above 40%, the soil resistivity does not change.

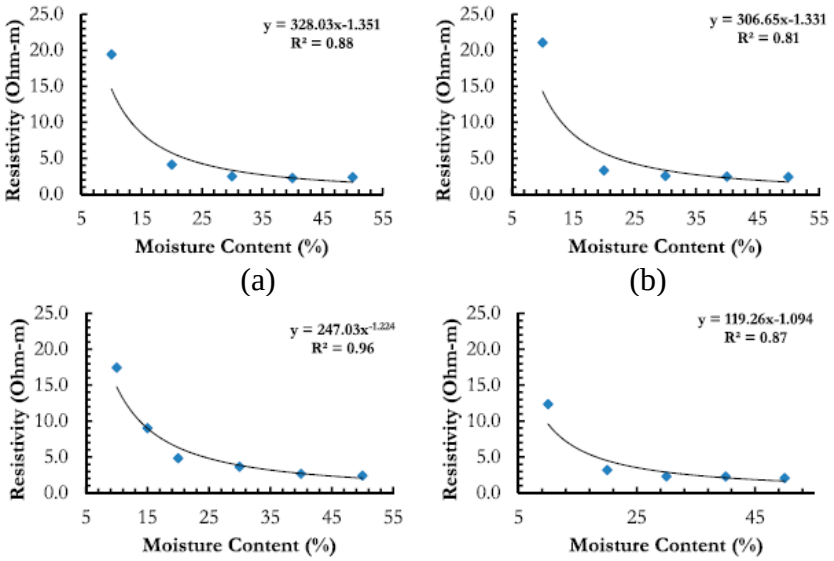

Figure 2.6: Variation of soil resistivity with gravimetric moisture content: (a) A-B2-D15; (b) A-B3-D10; (c) A-B3-D15; (d) A-B3-D20 (Kibria, 2014).

Figure 2.7 shows the relationship of soil resistivity with moist unit weight at a constant 18% moisture content. For determining the correlation, they varied the unit weight from 11.8 KN/m3 to opt. The soil resistivity decreases with an increase in unit weight. Comparing the influence of moisture content and unit weight, they found that the soil resistivity changes more with the variation of moisture content than unit weight. They studied the relationship between resistivity and dry unit weight for three different moisture contents - 18%, 24%, and 30%. Figure 2.8 shows that with increasing dry unit weight, resistivity decreases. They found the co-relation between volumetric moisture content and soil resistivity. They found the regression coefficient of the proposed relationship as 64%. Figure 2.9 represents the inversely proportional relationship between resistivity and volumetric water content.

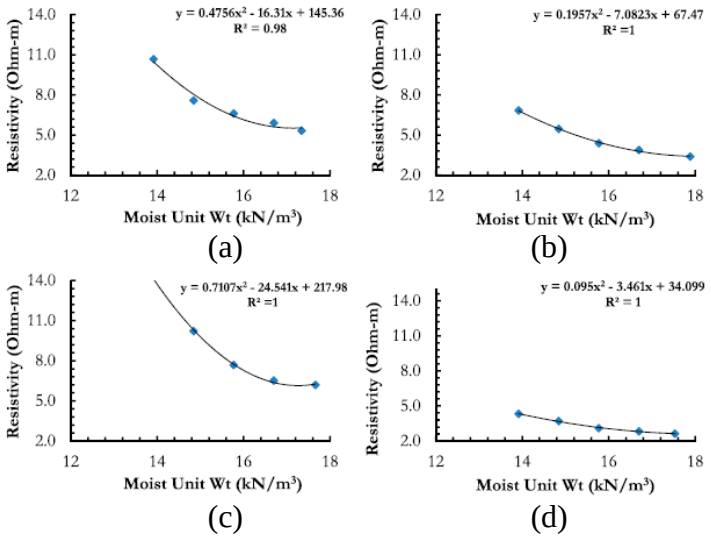

Figure 2.7: Variation of resistivity with moist unit weight at 18% moisture content: (a) A-B2-D15; (b) A-B3-D10; (c) A-B3-D15; (d) A-B3-D20 (Kibria, 2014).

The correlations between the degree of saturation and ER for four different types of samples shown in Figure 2.10 were also developed. The variations of soil resistivity with the degree of saturation for 18%, 24%, and 30% moisture content were studied. Four pre-defined soil samples were considered for that purpose. With an increase in the degree of saturation, soil resistivity decreases. Soil resistivity increases more for 18% water content. ER decreases with an increase in the degree of saturation. Figure 2.11 shows the variation of specific surface area with the soil resistivity at dry unit weights of 11.8 KN/m3, 12.6 KN/m3, 13.4 KN/m3, and 14.2 KN/m3. With an increase of specific surface area, soil resistivity also increases. Soil resistivity increases more for the 18% moisture content.

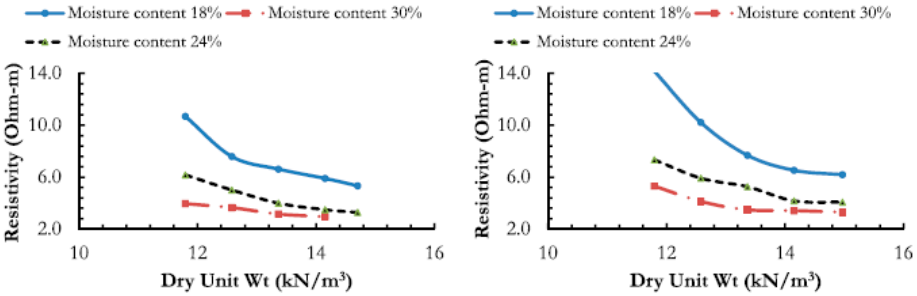

Figure 2.8: Comparison of the effect of moisture content and unit weight with soil resistivity: (a) A-B2-D15; (b) A-B3-D15 (Kibria, 2014).

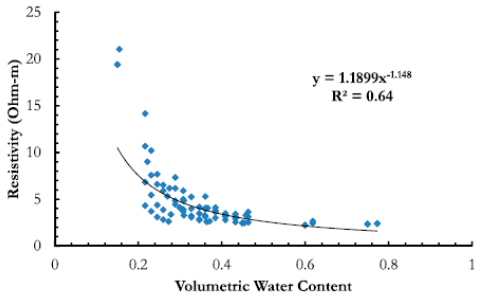

Figure 2.9: Variation of soil resistivity with volumetric water content (Kibria, 2014).

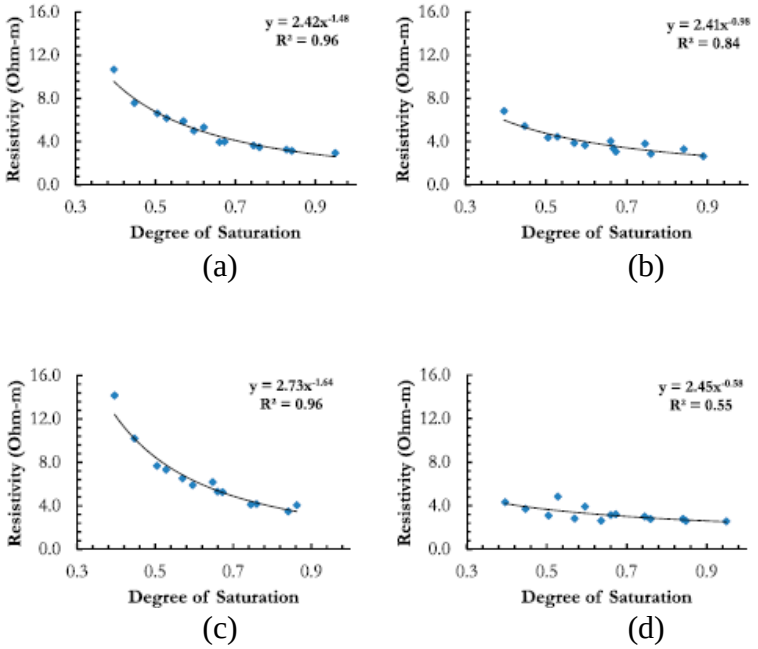

Figure 2.10: Variation of soil resistivity with the degree of saturation: (a) A-B2-D15; (b) A-B3-D10; (c) A-B3-D15; (d) A-B3-D20 (Kibria, 2014).

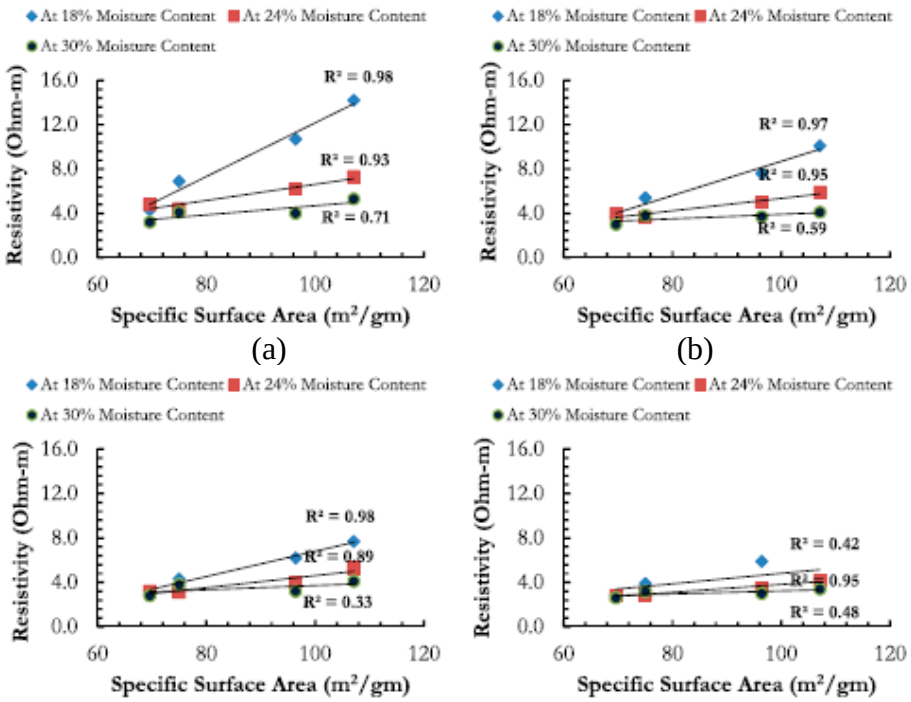

Figure 2.11: Variation of soil resistivity with specific surface area at dry unit weight: (a) 11.8 KN/m3, (b) 12.6 KN/m3, (c) 13.4 KN/m3, (d) 14.2 KN/m3 (Kibria, 2014).

Bhatt and Jain (2014) used a statistical approach to determine the correlation between ER and water content of sand. They prepared the samples in the laboratory at constant dry density and water contents were varied from dry to saturated condition. Through non-linear regression analysis, they found the following correlation equation:

$$\rho = 388.97e^{0.08w} + \varepsilon \qquad 2.11$$

where ρ is ER (Ωm), w is water content, and Ɛ is standard error.

Figure 2.12 shows the fitted exponential curve which represents the correlation between ER and water content. The R^2 value was 0.908, which indicates a good correlation between ER and water content.

They performed another statistical analysis to determine the correlation between water content and ER. In that case, they kept ER as a variable. They established the following correlation between water content and ER:

$$w = 29.536\, e^{0.006\rho} + \varepsilon \qquad 2.12$$

with an R^2 is 0.839, which indicates good correlation. Figure 2.12 represents the correlation between water content and ER. In both cases with an increase of water content, ER decreases.

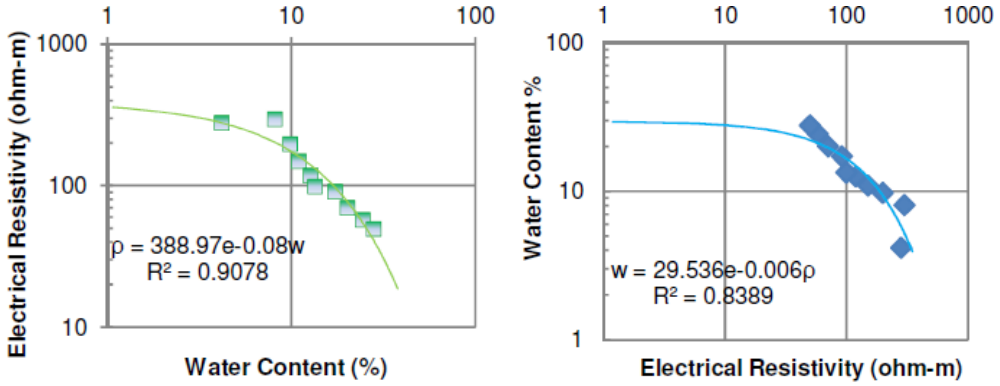

(a) (b)

Figure 2.12: (a) plot of water content variable for ER (b) plot of ER variable for water content (Bhatt and Jain, 2014).

Ozcep et. al. (2009) used artificial intelligence techniques to develop correlations between ER and soil-water content. They also compared conventional regression analysis to artificial intelligence techniques. The ranges of ER considered were 1-50 ohm-m and water content 20-60%. Geotechnical measurements were taken at depths up to 15m. Soil samples for this study were sandy soils. Three types of artificial intelligence techniques were used: artificial neural networks (ANN), Fuzzy-Mamdani method, and the Fuzzy-Sugeno method. Again, these methods were compared with conventional regression analysis methods. Figure 2.13 represents the results of regression analysis for the correlation between ER and soil-water content for sites near Istanbul and Golcuk, and Figure 2.14 illustrates all data.

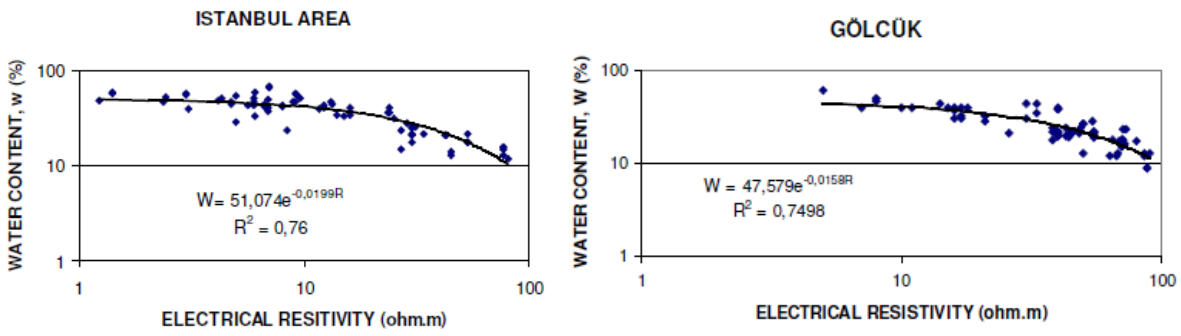

(a) (b)

Figure 2.13 : Relationship between soil ER and water content for (a) Istanbul area (b) Golcuk area (Ozcep et al., 2009).

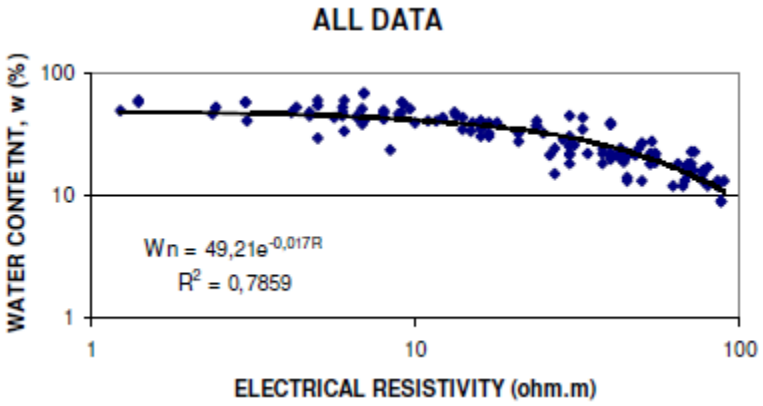

Figure 2.14: Relationship between soil ER and water content for all data (Ozcep et al., 2009).

The regression coefficient (R^2), Mean error squares (MES) and mean absolute error percent (MAEP) for the four methods are shown in Table 2.1. It was found that even though the regression analysis method easily estimates a value of water content from ER, the prediction accuracy and the evaluation of performance of estimation of AI systems are good enough. The ANN method showed better performance than the other methods.

Table 2.1 : Statistics for three artificial intelligence and regression methods.

	ANN	MAMDANI	SUGENO	REGRESSION
MAEP	17.76	19.99	17.63*	20.85
MES	33.62	43.12	32.598*	50.39
R^2	0.8844*	0.82688	0.8825	0.7859

Note: Best results are indicated by the sign '*'

Tiwari and Shah (2015) studied the relationship between index properties and ER of periodically hydrocarbon contaminated clays. They used 3%, 6%, and 9% hydrocarbon for periods of 15, 30, 45, and 60 days, and compared the results with non-contaminated marine clay. Soil resistivity was measured in the laboratory by fabricating a soil resistivity box. Figure 2.15 (a) represents the correlation between ER and percentage of hydrocarbon contamination. ER increases by 28%, 40%, and 33%, respectively, for 3%, 6% and 9% of hydrocarbon contamination. But ER decreases with the increase of period of contamination. Figure 2.15 (b) shows the ER decreases with an increase in LL. LL of hydrocarbon contaminated clay is lower than the non-contaminated clay. ER shows a proportional relationship with PL, but PL shows an inversely proportional relationship with period of contamination as shown in Figure 2.16 (a). PL of contaminated clay is higher than non-contaminated clay. With an increase in period of contamination, shrinkage limit (SL) increases; with an increase in SL, the ER increases as shown in Figure 2.16 (b). Figure 2.17 shows the correlation between ER and SG. ER shows an inversely proportional relationship with SG, and SG shows a proportional relationship with period of contamination.

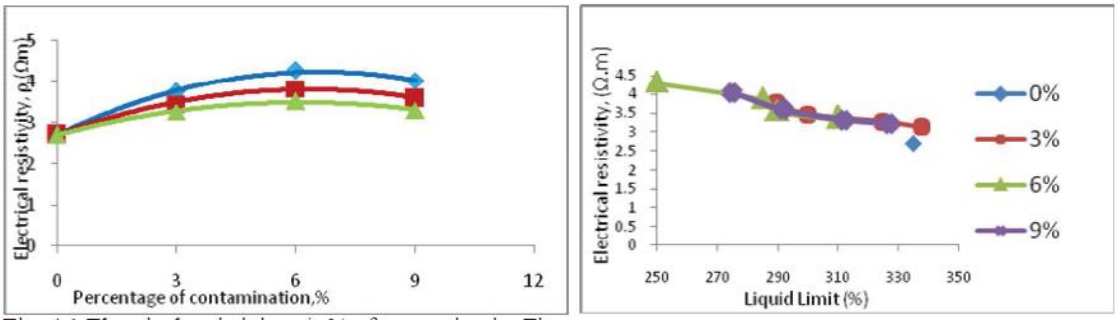

(a) (b)

Figure 2.15: (a) ER versus % of contamination. (b) ER versus LL (Tiwari and Shah, 2015).

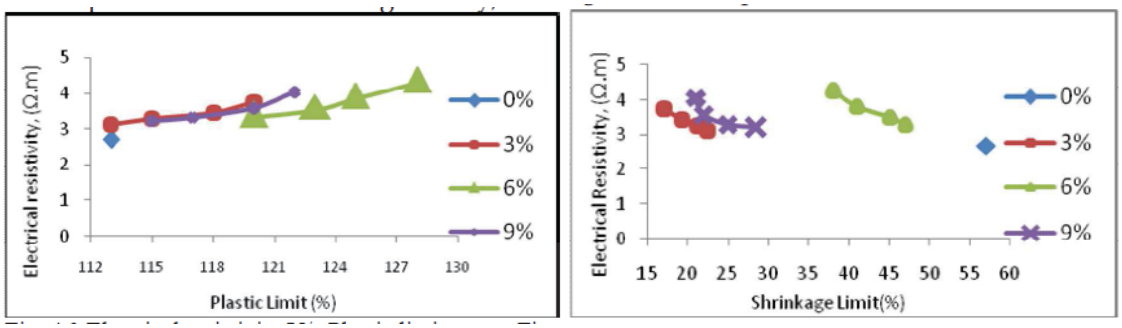

(a) (b)

Figure 2.16: (a) ER versus PL (b) ER versus SL (Tiwari and Shah, 2015).

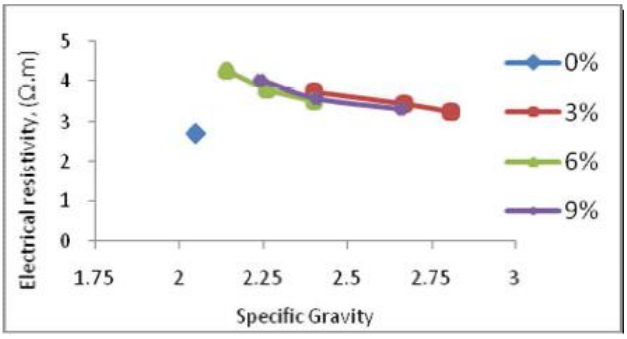

Figure 2.17: ER versus SG (Tiwari and Shah, 2015).

Osman et. al. (2014) established correlations intended to help determine soil strength parameters, such as cohesion and angle of friction, using ER. They conducted ER tests in the laboratory for different types of soils by varying compaction energy and moisture content. They used three types of soil samples - namely clay, silt and sand. Figure 2.18 shows the relationship between moisture content and ER for three types of soil. Strong correlation was observed for clay samples (R^2 of 0.818) whereas silt showed the lowest correlation (R^2 of 0.694). They explained that the lower correlation for the silt sample was a consequence of using a lower moisture content (10% to 25%) for the silt sample. Figure 2.18 (d) represents the combined correlation for silt and clay. In this case, they found a better correlation and suggested that fine-grain soil shows better correlation between moisture content and ER.

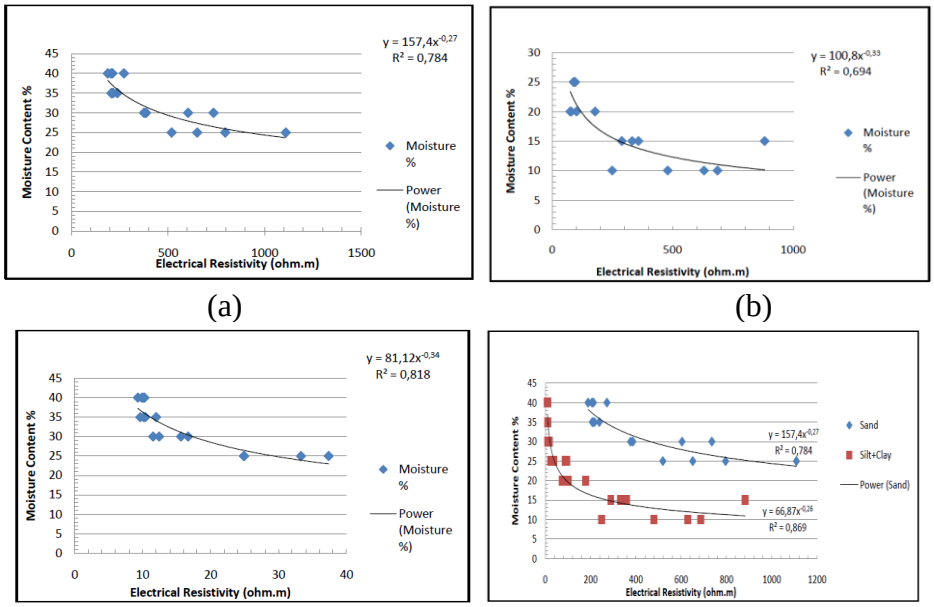

Figure 2.18: Moisture content versus ER for (a) sand (b) silt (c) clay (d) sand and silt + clay (Osman et. al.,2014).

The correlations between angle of friction and ER are shown in Figure 2.19. This graph demonstrates that with an increase of internal friction, ER also increases. Again, the strongest correlation was for clay ($R^2 = 0.824$) and weakest correlation for silt ($R^2 = 0.012$).

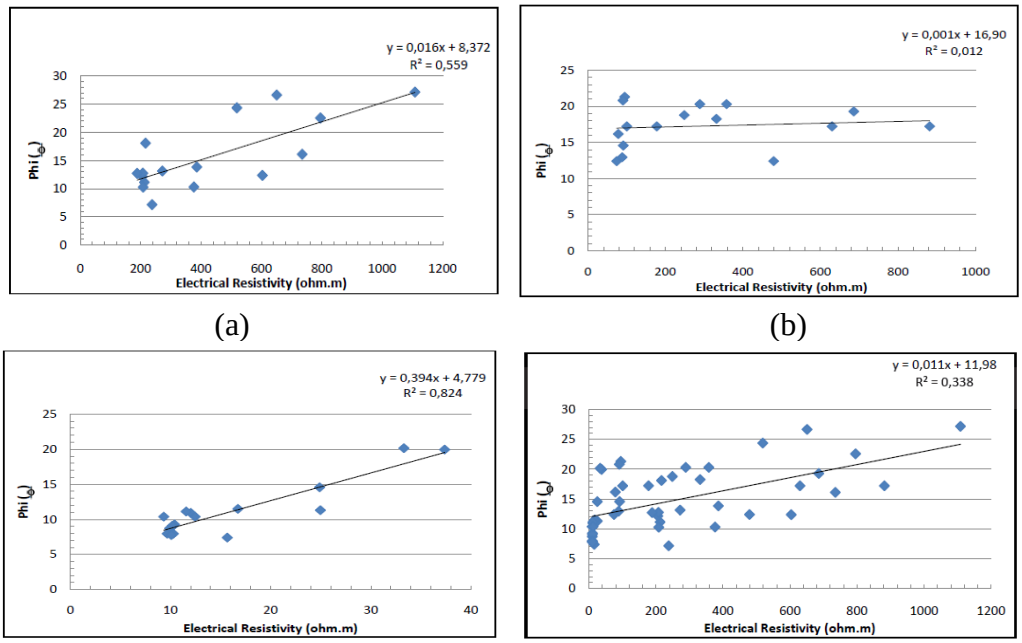

Figure 2.19 : Angle of friction (phi) versus ER for (a) sand (b) silt (c) clay (d) sand and silt plus clay (Osman et. al.,2014).

Siddiqui and Osman (2012) also developed correlations between ER and strength properties of soil. They conducted field measurements of electrical resistivity survey and soil boring. In laboratory, they performed ER tests and direct shear tests, and they also measured moisture content and unit weight. Their resistivity values measured in laboratory were higher than the field resistivity values. They explained that this was due to the change in saturation condition, temperature difference, and overburden pressure. They combined the field and laboratory resistivity data for simplicity and generalization. Figure 2.20 describes the relationship between ER and moisture content, unit weight, angle of internal friction, and cohesion of soil. They indicated the bad data points by red-circles in the graphs. Figure 2.20 (c) shows that ER increases with an increase of friction angle. A good correlation exists between angle of internal friction and ER. The correlation between cohesion and resistivity shown in Figure 2.20 (d) is weak. Moisture content in Figure 2.20 (a) shows good correlation with resistivity; on the other hand, unit weight shows a weak correlation with resistivity in Figure 2.20 (b).

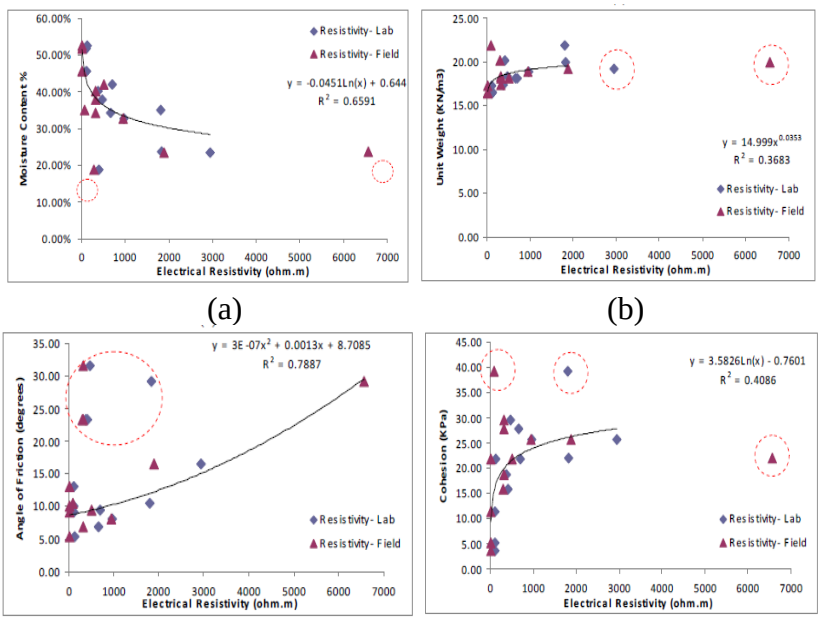

Figure 2.20: Correlation of ER with (a) moisture content (b) unit weight (c) angle of internal friction and (d) cohesion of soil (Siddiqui and Osman, 2012).

Abidin et. al. (2013) performed 24 resistivity tests to determine the correlations between ER and moisture content and soil density. The disturbed soil samples were collected to conduct the geophysical and geotechnical experiments in the laboratory. For resistivity testing, Nilsson model 400 soil resistance meters were used. Soil samples were prepared by mixing an original mass of 1500g of oven-dried soil with 1-5% of distilled water. Moisture content was determined by taking the average of the two samples from each soil box test. Figure 2.21 shows curvilinear resistivity between water content to ER and bulk density to ER. ER decreased with increasing water content and bulk density.

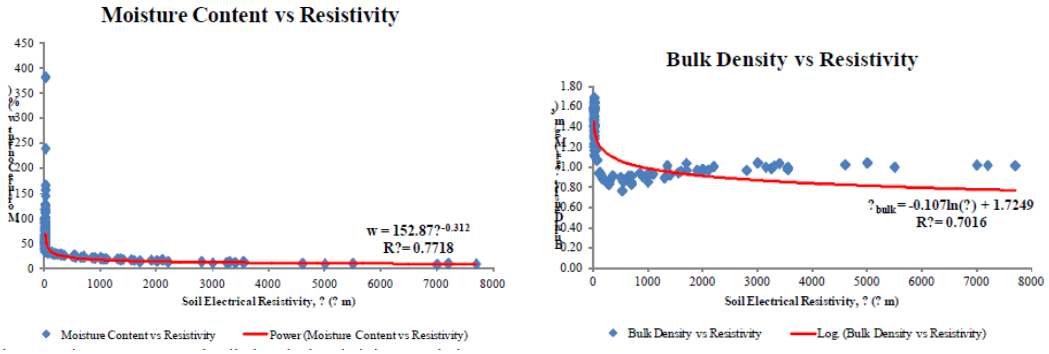

(a) (b)

Figure 2.21: Correlation of ER with (a) moisture content, (b) bulk density (Abidin et. al., 2013)

Abidin et. al. (2013) developed correlations between field ER values and basic geotechnical properties. Basic geotechnical properties include soil moisture content, grain size of geomaterial, density, porosity, void ratio, and Atterberg limit. They collected three disturbed soil samples from three different sites along the same resistivity line. Based on particle size distribution, they classified the soil as clayey silt. The three soil samples were different from each other in terms of percentages of coarse and fine soil. Soil A contains the highest amount of coarse soil (C- 24.19%) and lowest amount of fine soil (F- 75.81%) followed by soil C (C-22.86% and F-77.14%) and B (C-20.51% and F-79.49%), respectively. They presented the general relationship using a bar chart as shown in Figure 2.22.

Figure 2.22 illustrates that moisture content is inversely proportional to the field ER. Sample A holds the least moisture content and highest field ER whereas sample B holds the highest moisture content and lowest field ER. They also showed that ER is proportional to the grain size. ER increases with an increase of grain size. Sample A has the highest ER and greatest amount of coarse soil; on the other hand, sample B has lowest ER with the smallest amount of coarse soil.

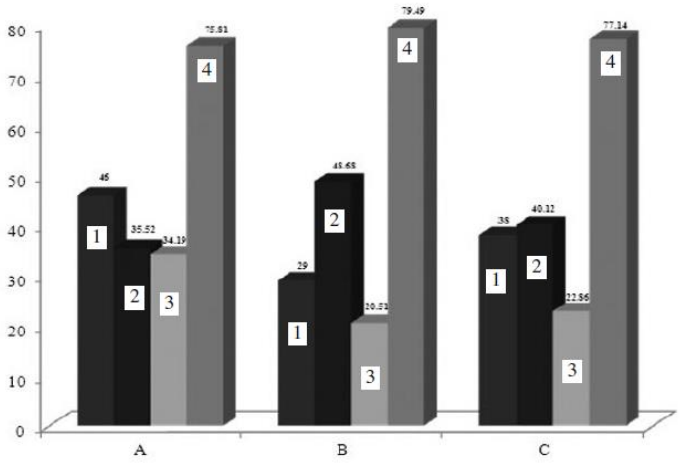

Figure 2.22: Relationship of field ER to the moisture content and particle size of soil: (a) 1- field ER ρ, Ωm; (b) 2- moisture content w, %; (c) 3- particle size (coarse soil) d, mm; (d) 4- particle size (fine soil) d, mm-μm (Abidin et. al., 2013).

Figure 2.23 indicates that ER is proportional to the high soil density. Sample A was denser than C and B, and C was denser than B. They found the highest ER for sample A, then C, and lowest for sample B.

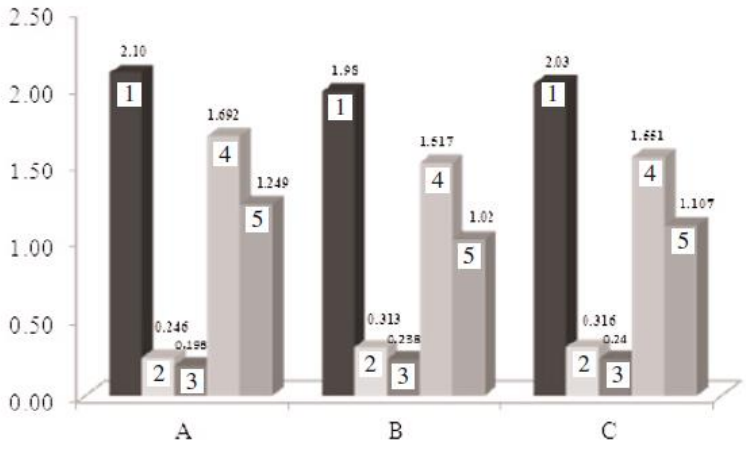

Figure 2.23: Variations of (basic geotechnical properties) with particular reference to SG, void ratio, porosity, and density: (a) 1- specific gravity Gs; (b) 2-void ratio e; (c) 3- porosity φ; (d) 4- bulk density ρbulk, Mg/m3; (e) 5- dry density ρdry, Mg / m3 (Abidin et. al., 2013).

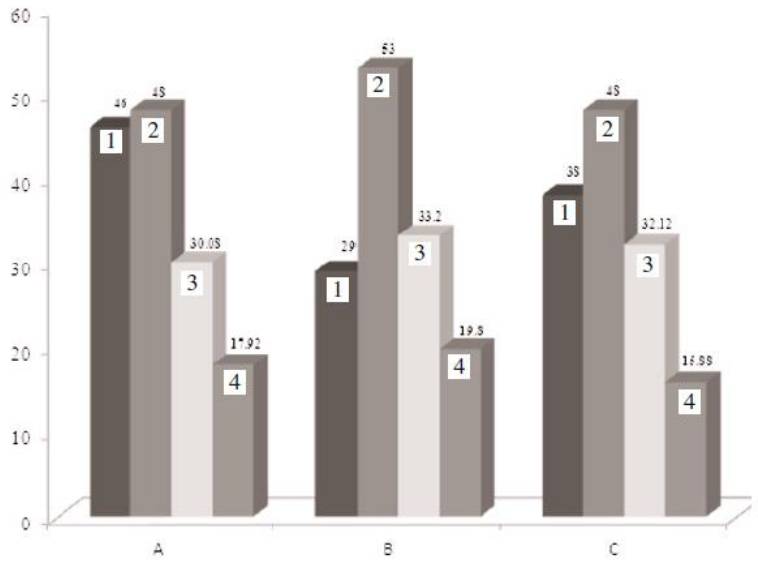

Figure 2.24: Relationship of field ERV to the Atterberg limit (a) 1- field ER ρ, Ωm (b) 2- LL, %; (c) 3- PL, %; (d) 4- PI, % (Abidin et. al., 2013).

Figure 2.24 showed that field ER is inversely proportional to Atterberg limit. Such as sample B has lowest ERV and highest Atterberg limit.

2.4 Seismic Wave Velocity

Seismic wave methods are sensitive to the mechanical properties of the soil. Soil allows for the propagation of different types of seismic waves. Waves that deform the material through shear are referred to as shear waves and those that produce volumetric deformations are referred to as compressional waves. These are often referred to as S-waves and P-waves, respectively. There are numerous methods for measuring seismic wave velocity in the field and the laboratory. In the laboratory, the "time of flight" approach is common. A seismic wave is generated using a source in contact with one end of the sample, the disturbance passes through the soil and is detected by a receiver at the opposite end of the sample. Velocity is calculated by dividing the distance (sample length) by the measured travel time. Typical P-wave and S-wave velocities are shown in Table 2.2.

Table 2.2: Seismic wave velocities for different materials.

Material	P-wave velocity, m/s	S-wave velocity, m/s
Air	330	0
Water	1450	0
Sands and clays	300-1900	100-500
Glacial till	1500-2700	600-1300
Chalk	1700-3000	600-1500
Strong limestone	3000-6500	1500-3500
Weathered granite	100-3000	500-1500
Fresh granite	3000-6000	1500-3000
Slate	5000-7000	2500-3800
Rock salt	4000-5500	2000-3200

Longitudinal P-wave and the transverse S-wave in an infinite elastic continuum are related to the elastic properties of the soil:

$$V_p = \sqrt{\frac{M}{d}} = \sqrt{\frac{B + \frac{4}{3}G}{d}} \quad \text{P-waves} \tag{2.13}$$

$$V_s = \sqrt{\frac{G}{d}} \quad \text{S-waves} \tag{2.14}$$

where M is the constraint modulus, B is the bulk modulus, G is the shear modulus, and d is the mass density of the medium. Hence, the propagation velocity increases with the stiffness of the material and decreases with its mass density (inertia). Velocity of S-waves is smaller than the velocity of P-waves (Santamarina et al., 2001) The soil shear modulus is sometimes used to derive some geotechnical properties, such as maximum shear modulus (Gmax), bulk modulus (B), Young's modulus (E) and Poisson's ratio (υ).

The coexistence of solid and fluid phases adds significant complexity to the behavior of particulate or granular materials like soil. Phenomena include the formation of double layers, seepage, time-dependent pressure diffusion, and the partition of applied stresses into pore fluid

pressure and effective skeletal stress. Under dynamic loading, differences in inertia, shear stiffness, and bulk compressibility add further complexity to the analysis.

For fluid-filled porous media, the effective bulk modulus provided by Gassmann (Dikmen, 2009) is

$$B_{eff} = B_{SK} + \frac{(1-\frac{B_{SK}}{B_g})^2}{\frac{\varphi}{B_f}+\frac{1-\varphi}{B_g}-\frac{B_{SK}}{B_g^2}} \quad 2.15$$

where B_{SK} is the bulk modulus of the skeleton, B_g is the bulk modulus of the grains, B_f is the bulk modulus of the fluid phase, and φ is the porosity. In the Gassmann model, the shear modulus of the soil, G_{eff}, remains unaffected by the presence of the fluid at low excitation frequencies,

$$G_{eff} = G_{SK} \quad 2.16$$

For partially saturated soils, the mass density of the mixture d_{mix}, changes due to the different densities of the saturating fluids. Ignoring granular effects, fluid substitution can be used to modify the expression for the effective bulk modulus of the soil. For a soil with a water saturation of S_w the fluid bulk modulus in equation 2.17 given by

$$\frac{1}{B_f} = \frac{S_w}{B_w} + \frac{1-S_w}{B_a} \quad 2.17$$

where B_w is the bulk modulus of the liquid phase and B_a is the bulk modulus of the air phase. Small volumes of fluid produce a large decrease in the modulus of fluid.

Seismic wave propagation in granular materials like soil is more complicated due to the complex behavior of solid skeleton and the influence of capillary forces. The skeletons B_{SK} and G_{SK} depend on the "strength" of the grain contacts and are therefore dependent upon the applied effective stress. The concept of effective stress for soils at low saturation is still an area of active research because internal forces associated with capillary forces and electrical forces and grain

surface play an important role. That's why empirical relationships are necessary to predict the seismic wave propagation in partially saturated particulate mediums.

The velocity of propagation of P-waves reflects the bulk B and shear G stiffness of the medium, while the velocity of S-waves only depends on the shear stiffness G. Since fluids do not support shear, P-waves velocity is more sensitive to changes in water content. In general, S-waves velocity has low sensitivity to water saturation and as such is correlated with soil matrix behavior. Combining P-waves and S-waves results in a powerful tool for distinguishing the water table from other geological features.

2.5 Developed Correlation with Seismic Wave Velocity

Various studies have presented correlation between seismic wave velocity and geotechnical parameters. Dikmen (2009) examined the statistical correlation of uncorrected standard penetration test (SPT)-N values and shear wave velocity (V_s) for different kinds of soil categories (i.e. all soil, sand, silt and clay-type soil). He used 193 uncorrected SPT-N and V_s data pairs considering 82 sand, 76 silt, and 35 clay samples. For statistical analysis, he separated all data according to high or low plasticity for cohesive soils and uniform or poor gradation for sand soils. Figure 2.25 represents the correlations between SPT-N values and the shear wave velocity. The following empirical formulas were derived and it was concluded that the type of soil has no significant effect on the estimation of V_s. Equation (2.18-2.21) shows that SPT-N values have a strong correlation with the shear wave velocity.

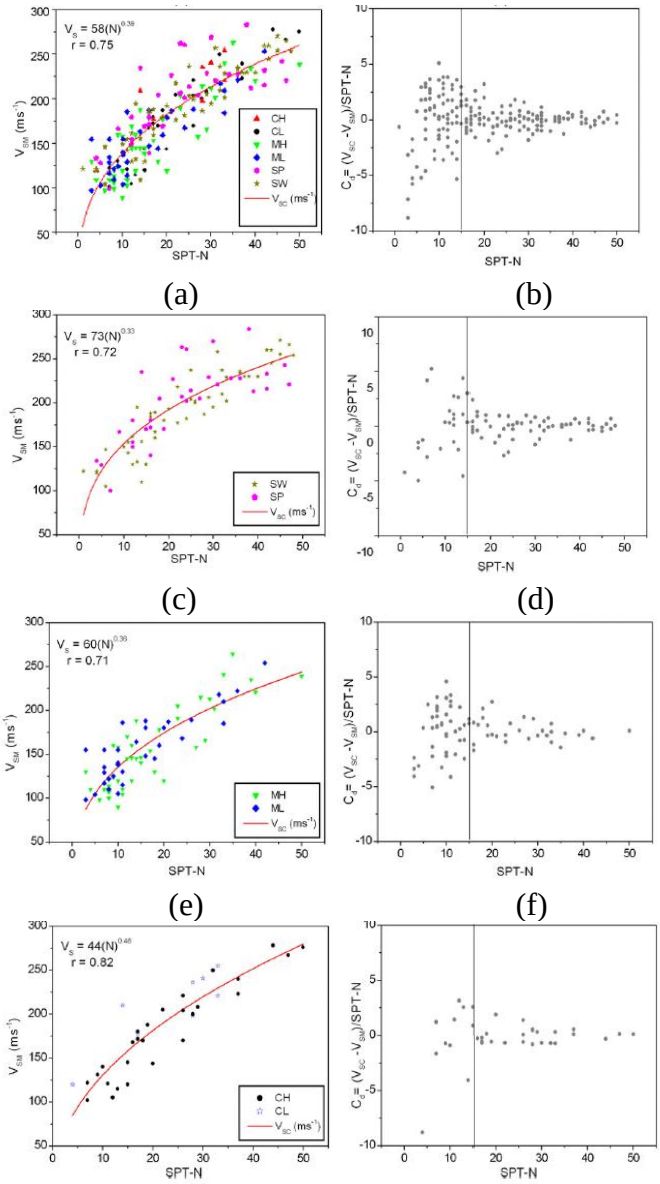

Figure 2.25: Correlations between SPT-N and shear wave velocity (Vs) values: (a) for all soils, (b) normalized consistency ratio for all soils, (c) for sand soils, (d) normalized consistency ratio for sand soils, (e) for all silt soils, (f) normalized consistency ratio for silt soils (g) for clay soils and (h) normalized consistency ratio for clay soils (Dikmen, 2009).

$$V_s = 58N^{0.39} \quad (R = 0.75 \text{ for all soils}) \qquad 2.18$$

$$V_s = 73N^{0.33} \quad (R = 0.72 \text{ for sand soil}) \qquad 2.19$$

$$V_s = 60N^{0.36} \quad (R = 0.71 \text{ for silt soil}) \qquad 2.20$$

$$V_s = 44N^{0.48} \quad (R = 0.82 \text{ for clay soil}) \qquad 2.21$$

$$C_d = (V_{SM} - V_{SC}) / \text{SPT-N} \qquad 2.22$$

Dikmen (2009) calculated a normalized consistency ratio C_d using equation 2.22, where V_{SM} is the measured V_s from seismic cone penetration tests (SCPT) and seismic experiments, V_{SC} is the calculated V_s from the equation and SPT-N is the uncorrected SPT-N blow counts corresponding to V_{SM}. Figure 2.25 (h) shows a comparison between V_{SM} and V_{SC}. The values of C_d are close to zero, which ensures the good performance of the proposed empirical formula.

Mayne and Rix (1995) estimated the empirical correlations between shear wave velocity (V_s) and cone penetration tip resistance (q_c) using the field data collected from 31 different natural clays. Figure 2.26 shows the correlation between V_s and q_c for both intact and fissured clay deposits. The increasing trend of shear wave velocities and cone penetration resistance is observed with consistency from soft to stiff to hard clay materials. Through log regression analysis the following empirical equation was found with n = 481 and $R^2 = 0.736$:

$$V_s = 1.75\ (q_c)^{0.6278} \qquad 2.23$$

where V_s is in units of meters/sec and q_c in kpa

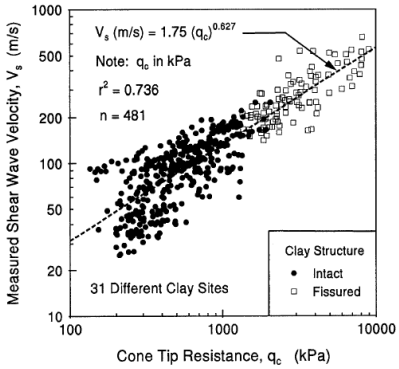

Figure 2.26: Direct correlation between shear wave velocity and cone tip resistance in intact and fissured clays (Mayne and Rix,1995).

Gautam (2017) developed correlations between shear wave velocity and uncorrected standard penetration resistance for all soils, sand, and clays using 500 secondary data pairs. The depth, overburden pressure, geological age, fine content, and soil types were not considered, which

may also influence the relationship. He conducted a simple power regression analysis to develop correlations between uncorrected SPT-N values and VS. Data were collected up to 30m in depth. The correlations were developed for all soils, silt, and sand separately. Figure 2.27 shows the correlations for all soils, silt, and sand, respectively. The coefficient of determination for silt is relatively low. Gautam (2017) explained that the coefficient of determination is lower due to a limited database and to scattered data records. For sand, the coefficient of determination is also low because of the limited number of data points available for formulation of the governing equation. He also showed that the developed correlations are in good agreement with existing correlations.

Hoover and Handy (1970) investigated relationships between seismic wave velocity, water content, and dry density. Both laboratory and field experiments were conducted on three types of soils. Microseismic refraction tests were conducted to collect seismic velocities in the field. In the lab, velocities were measured on compacted samples. Lab velocities were correlated with conventional dry density and moisture content, and field velocities were correlated to in place moisture-density.

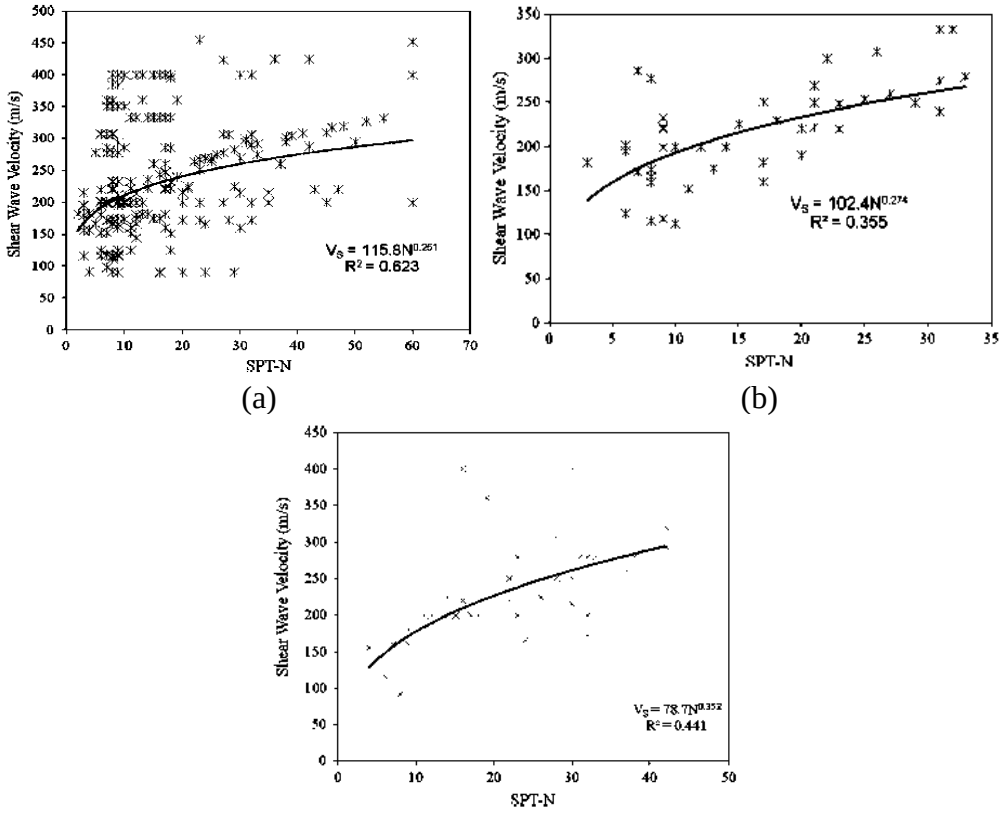

Figure 2.27 : Vs-N correlations for (a) all, (b) silt, and (c) sand of Kathmandu valley (Gautam, 2017).

2.6 Artificial Neural Network

During the past few years, artificial neural network (ANN) based modeling has been gaining popularity in the field of engineering. ANN can predict by learning the complex nonlinear relationships between parameters from a large number of data sets (Yasarer and Najjar,2014). The working method of ANN is based on the human brain activity of processing data. Like the human brain, ANN has large numbers of interconnecting cells called neurons (Najjar and Huang, 2007). ANN consists of three different layers - input layer, hidden layers, and output layer. Information is passed from the input layer, through hidden layers to the output layer. There are connecting links between the neurons to transfer signals from one neuron to others. The hidden layers process the received signals from the input layer and then transmit the information to the output layer. The

output layer receives the processed information from the hidden layer and executes the outputs. ANN is capable of learning highly complex relationships that are difficult to solve by traditional computational techniques. The accuracy of the performance of an ANN model depends on the accuracy of the data and the size of the data set. Erroneous and too small data sets affect the accuracy of the performance of the model. Depending on the number of layers, activation function, and training algorithm, ANNs can be of different types, such as feed-forward neural networks, recurrent networks, and stochastic neural networks (Najjar and Huang, 2007). Another important part of ANN is the activation function. The activation function introduces nonlinearity to the network to solve complex problems. It can be of different types (i.e. linear activation function, binary step activation function, sigmoidal activation function, or hyperbolic tangent sigmoid activation function).

2.7 Application of ANN in Geotechnical Engineering

ANN has been playing an important role in the field of engineering for research. To solve critical geotechnical engineering problems, the use of ANN is of great interest to researchers. The behavior of soil is a complex physical process and formation mechanism (Jaksa, 1995). Complex behavior and spatial variability introduce difficulties in geotechnical design. One way to mitigate these difficulties is to simplify the design model by making justified assumptions. Another alternative technique is the application of ANN (Shahin et al., 2001). ANN was applied in various fields of geotechnical engineering, such as prediction of load-bearing capacity of deep foundation, settlement of the shallow foundation, liquefaction potential, evaluation of slope stability, development of correlations between different parameters, etc. Shahin et. al. (2001) published a review paper on the application of ANN in the field of geotechnical engineering. Table 2.3 has been produced to represent the summary of ANN applications discussed in the review paper.

Table 2.3: Application of ANN in geotechnical engineering.

Branch	Topic	Author and published year
Deep foundation	Load-bearing capacity of the driven pile in clay and cohesionless soil	Goh (1995 a, 1996 b)
	Driven pile capacity	Chanet al. (1995)
	Ultimate load caring capacity of pile	Lee and Lee (1996)
	Static pile capacity	The at al. (1997)
Settlement prediction	Settlement of shallow foundation on granular soil	Sivakugan et al (1998)
	Settlement of shallow foundation on cohesionless soil	Shahin et al (2000)
	Settlement of tunnel	Shi et al. (1998)
Liquefaction	Liquefaction potential investigation	Goh (1994 b)
	Liquefaction potential from cone penetration test	Goh (1996 a), Najjar and Ali (1998)
	Liquefaction potential from standard penetration test	Agrawal et al. 1997
Soil properties and behavior	Correlation between relative density and cone resistance	Goh (1995a, 1995 c)
	Correlation between ER and soil-water content	Ozcep et al. (2009)
	Grain size distribution and stress history model for sands	Ellis et al (1995)
	Modeling the behavior of sand and clay soil	Penumadu and Jean-Lou (1997)
Slope stability	Evaluation of slope stability	Ni et al (1996)
Site characterization	Prediction of soil permeability variation	Basheer et al. (1996)
	Site characterization method	Rizzo et al. (1996)

2.8 Developed Correlations using ANN

ANN has been applied successfully to different branches of geotechnical engineering. The current research proposes to use ANN to predict geotechnical parameters from geophysical parameters. Two studies where ANN was used to develop correlations between soil parameters are discussed below.

For normally consolidated and overconsolidated sands, Goh (1995 a, 1995 c) developed a correlation between cone penetration resistance and relative density. Calibration chamber tests were performed in the laboratory to collect the data used for training the ANN network. The

nonlinear relationship between parameters was successfully developed using the ANN technique. The ANN model showed high coefficients of correlation of 0.97 and 0.91 for training and testing data.

2.9 Findings from Literature Review

An extensive literature review was completed to determine previous work in the field of developing correlations between geophysical parameters and geotechnical parameters. To develop trustworthy correlations between geophysical parameters and geotechnical parameters, the following are recommended:

- Correlations should be developed for all types of soils, such as clay, sand, silt, as well as for synthetic samples (mixing different types of soil with varying percentages) in the laboratory with varying dry density and water content. Percentages of soil type (clay, sand, silt) fractions can be included as input parameters in prediction models for better predictability.
- Cohesion and angle of friction are two important strength parameters of soil. There is little research on correlation between angle of friction, cohesion, and geophysical parameters (Osman et al, 2014, Siddiqui et al., 2012). These strength parameters can also be considered with drained and undrained conditions for developing correlations with geophysical parameters. Correlations should also be developed for permeability and seepage. Especially for sand type soils, permeability of compacted clay soils is very low. Those are two important parameters for earthen dams.
- Large numbers of research articles support that ER is affected by water content (Giao et al., 2003, Mohd et al., 2012, Kibria, 2014, Bhatt and Jain, 2014, Ozcep et al., 2009, Osman et al., 2014). Researchers attempted to develop correlations with others parameters (degree

of saturation, void ratio, dry density, and so on) but those correlations are still not well established.

- Literature shows that liquid limit (LL), plastic limit (PL), shrinkage limit (SL), and specific gravity (SG) are not well correlated with electrical resistivity (ER) (Tiwari and Shah, 2015).
- A large number of correlations have been done with shear wave velocity and N value (Dikmen, 2009, Mayne and Rix 1995, Gautam, 2017). Other parameters, such as void ratio, dry density, degree of saturation, and CEC, can be considered in developing correlations with shear wave velocity.
- P-wave velocity is not commonly used to predict geotechnical parameters. P-wave can also be considered for developing correlations with the geotechnical parameters.
- No attempt has been made to use ER and seismic wave velocities together to predict geotechnical parameters. These geophysical parameters can be used together to predict geotechnical parameters for better predictability.
- Artificial neural networks are capable of solving complex problems (Giao et al., 2003). ANN has been applied in different fields of geotechnical engineering (Table 2.3) including for development of correlations between parameters (Goh, 1995a,1995b). Very limited amounts of research have been done using ANN to predict geotechnical parameters from geophysical parameters (Ozcept, 2009), but early results indicate that ANN can be effectively used to get more reliable results and better correlations than has been achieved with just regression analysis.

CHAPTER 3

METHODOLOGY

3.1 General

Selection of soil types for laboratory experiments are associated with earth dam and levee construction materials. Geotechnical and geophysical parameters are determined in the laboratory for compacted soil samples. Soil parameters that are important for earth dams are considered for prediction models.

3.2 Soil Type and Parameter Selection

Earth dams consist of three main components: core, upstream, and downstream. Figure 3.1 shows the main components of an earth dam. Usually, the core is constructed with clay-type soil to make it impermeable, the upstream, which is relatively impermeable, is made with sandy clay soil, and the downstream is made with sandy soil to allow drainage (Stephens,2010).

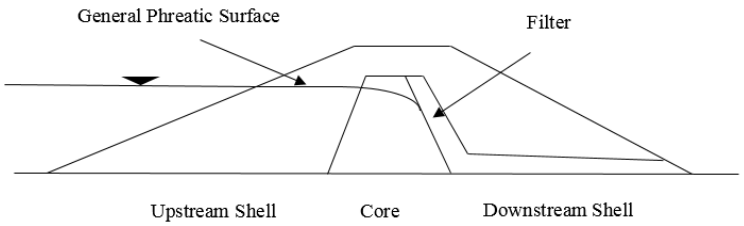

Figure 3.1: Earth dam section

This research is focused on soil types optimal for the core and the upstream construction. The soil types are presented on the soil triangle shown in Figure 3.2 and the soil samples investigated are listed in Table 3.1

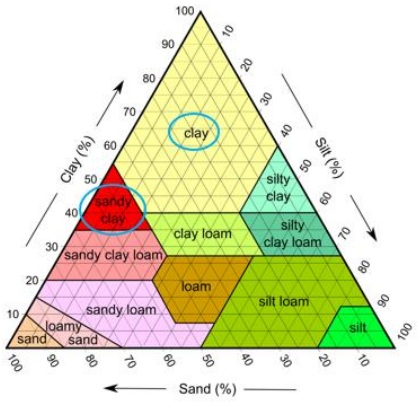

Figure 3.2: Selected soil type for laboratory measurement

Geophysical information would be most beneficial for studying excessive seepage and piping, foundation defects, and slope stability issues. Subsurface indicators that correlate with erodibility, water velocity, geometry of earth embankment, soil gradation, hydraulic conductivity, pore pressures, and degree of compaction would be very useful. Erodibility depends on water content, plasticity index, undrained shear strength, and clay mineral content (Shidlovskaya et al., 2016).

Table 3.1 : Selected soil mixing proportion for laboratory measurements.

No	Sand	silt	clay
1	45	0	55
2	45	5	50
3	45	10	45
4	45	15	40
5	50	0	50
6	50	5	45
7	50	10	40
8	50	15	35
9	60	0	40
10	60	5	35
11	65	0	35
12	20	0	80
13	20	10	70
14	20	20	60
15	25	0	75
16	25	10	65
17	25	20	55
18	30	0	70
19	30	10	60
20	30	20	50
21	35	0	65
22	35	10	55
23	35	20	45
24	40	0	60
25	40	10	50
26	40	20	40

As discussed earlier, ER is sensitive to water content, saturation, and clay content. Seismic wave velocity is affected by mechanical parameters which are in turn related to porosity, saturation, degree of compaction, and effective stress. So considering all of these criteria, this research attempts to establish correlations between the geotechnical and geophysical parameters listed in Table 3.2. Geotechnical and geophysical parameters and ranges obtained from experiments are shown in Table 3.3.

Table 3.2: Geophysical and geotechnical parameters chosed for developing correlation.

Geophysical parameters	Geotechnical parameters
Electrical resistivity P-wave velocity S-wave velocity	Moisture content Degree of saturation Void ratio Dry unit weight Specific surface area Cation exchange capacity Liquid limit Plastic limit Shrinkage limit Specific gravity Cohesion

Table 3.3: Geotechnical and geophysical parameters and ranges.

Parameters	Max	Min
Clay (%)	80	35
Silt (%)	20	0
Sand (%)	65	20
LL (%)	73.5	34
PL (%)	22.7	13.02
SL (%)	15.94	4.40
Specific gravity	2.65	2.54
Specific Surface Area (m2/kg)	97321.43	26785.71
Cation exchange capacity (cmol/kg)	21.21	9.20
Cohesion (kPa)	50.33	1.07
Dry density Kg/m^3	1734.90	1335.80
wet density Kg/m3	2061.42	1513.17
Water Content %	28.35	11.39
Void Ratio	0.915	0.483
Degree of Saturation (%)	98.41	33.50
True resistivity (Ohm-m)	50.64	3.43
P-wave velocity (m/sec)	670.5	256.9
S-wave velocity (m/sec)	496.8	158.3

3.3 Laboratory Measurements

3.3.1 Sample preparation

Soil behavior depends on compacted conditions. For this study, compacted soil samples are used to determine the ER, seismic wave velocity, and other geotechnical parameters. To produce a suite of consistent samples, the soil is compacted following a standard proctor test

method (ASTM D698). This approach is used in sample preparation because it simulates the field compaction. The aim is to find the opt water content at maximum dry density. ASTM D698 procedure is followed to perform the test. The procedure involves mixing water with the soil and, after assembling the compaction mold, adding soil to the mold in three layers. Each layer is compacted with a hammer by applying 25 blows per layer. After that, the weight of the soil in the mold is determined by deducting the weight of the empty mold from the weight of soil with mold to calculate the dry density. Some soil is taken from the top and bottom of the soil samples to determine the water content. Dry density increases with the increase of water content up to opt, which is defined as dry side. Beyond opt moisture content, dry density decreases with the increase of water content, which is defined as wet side. Compaction changes hydraulic conductivity, compressibility, and strength of compacted clay by changing soil structure. At dry side of opt, an undeveloped diffuse double layer of ions around the clay particles results in reduced repulsion between the particles. This reduction in repulsion makes the particles more flocculated or randomly oriented. With an increase of moisture content, the double layer expands, and repulsion increases, which results in less flocculent orientation and an increase in dry unit weight. Dry unit weight reaches its maximum at opt water content. Beyond opt water content, dry density decreases even though the double layer expands more, repulsion increases and particles become parallel to each other. The reason is that after opt, the added water dilutes the concentration of soil solids per unit volume, which results in decreased dry unit weight. Permeability decreases with the increase of moisture content until it reaches a minimum value at opt moisture content due to the reduction of pore spaces. Beyond the opt, permeability increases slightly. The random orientation of the particles is the reason for the high value of permeability at dry side. Under low pressure, soil compacted on the dry side is less compressible than the soil compacted on the wet side. At low

pressure, the orientation of the particles is more random in dry side than in wet side. At high pressure, it is possible to have the same type of parallel orientation of the particles at both wet and dry sides (Stephens, 2010). High earth dams are compacted at 2% dry to 3% wet of opt water content (Sharma, 1997). To conduct ER measurements, the soil samples must be compacted in an ER sleeve reducing the traditional volume and cross-sectional area of soil within the Proctor cell. The ER sleeve is designed in such a way that it can be inserted into a standard compaction mold. A plastic collar is also placed at the top of the ER sleeve to protect the wires from being broken during compaction (Figure 3.3).

Figure 3.3: Compaction test

The cross-sectional area of the ER sleeve is approximately 15% less than the standard compaction mold. Modification of the compaction effort is required due to the reduction of the cross-sectional area and was determined by testing on clay soils. The number of blows per layer (bpl) is adjusted for the clay samples using the ER sleeve until the results match a standard compacting curve. Figure 3.4 represents the matched compaction with and without the ER sleeve.

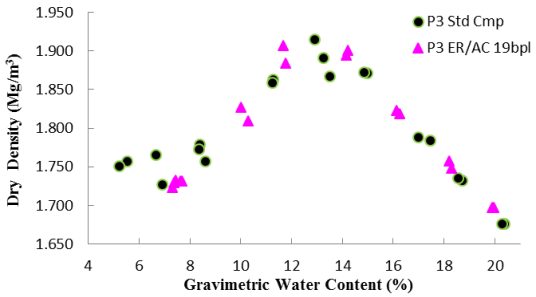

Figure 3.4: Adjusted compaction effort compared to standard compaction effort (Hickey, 2012).

3.3.2 Geophysical tests

3.3.2.1 Electrical resistivity test

ER is measured by passing current through the soil and measuring the resulting potential difference. Different apparatus have been designed based on the electrode array system, two electrodes, four electrodes, eight electrodes, and AC- versus DC input current. In the laboratory, researchers have used different kinds of sample holders or resistivity cells and boxes to measure the ER. For this research, an acrylic cylindrical mold shown in Figure 3.5 is used to measure the ER of compacted samples.

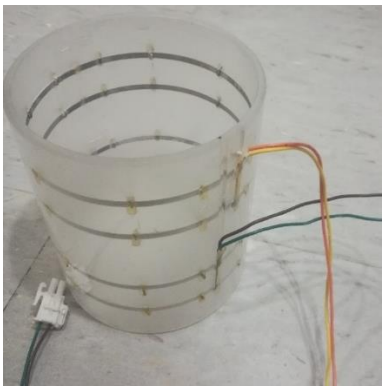

Figure 3.5: Acrylic mold with four electrodes.

This acrylic cell is a modified setup used by Kalinski and Kelly (1993). They used a circular non-conductive resistivity cell with eight equally spaced electrodes around the cell. Our cell consists of four steel rings; the outer two are current electrodes, and inner two measure the potential

difference. The resistance of the compacted soil sample is measured using an Agilent E4980A LCR meter connected with the resistivity cell. Figure 3.6 shows the entire setup for the ER measurements of compacted samples. The resistance must be converted to resistivity using a calibration curve shown in Figure 3.7 (Hickey, 2012). For resistance measurements < 560ohm:

$$\rho = 0.1788r^{1.0032} \quad 3.1$$

where, ρ = true resistivity (ohm-m), r = electro resistivity sleeve measured resistance (ohm).

For resistance measurements > 560ohm:

$$\rho = 0.0459r^{1.2044} \quad 3.2$$

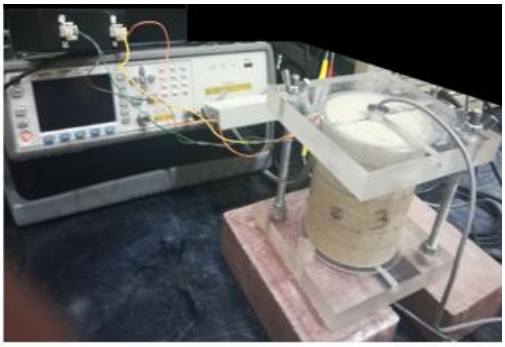

Figure 3.6: ER measurement.

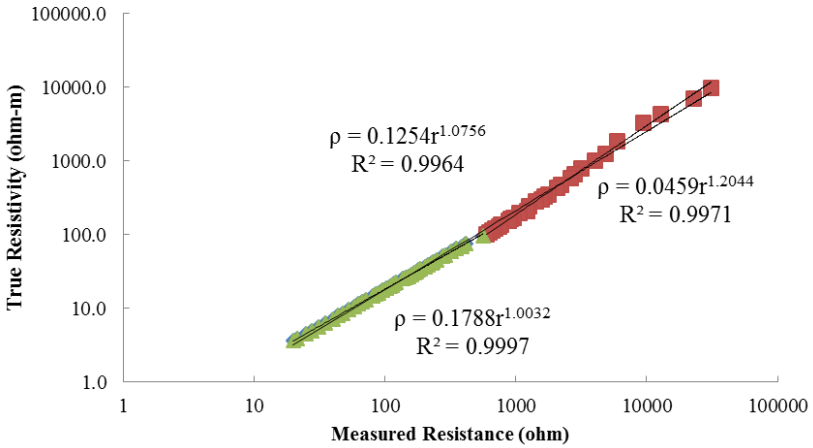

Figure 3.7: Calibration curve for measured resistance compared to true resistivity.

3.3.2.2 Seismic wave velocity test

To measure the S-wave and P-wave velocity, the compacted soil sample is placed between two end plates holding GDS bender elements. The system uses a pair of bender elements for source and receiver as shown in Figure 3.8. Each transducer is a combined P and S-wave transducer consisting of two elements. The elements are wired differently to produce and receive S-waves and P-waves. The element with the stripy markings works as a S-wave source/ P-wave receiver and the other element works as P-wave source/ S-wave receiver. The two elements are inserted at the top and bottom of the soil sample as shown in Figure 3.9. GDS bender element software is used to run the test. Appropriate amplitude, gain, length of sample, sample frequency, and sampling time must be selected for the test. Figure 3.10 shows the reference signal that is used to excite the source (same for both sources), and the vibration signal recorded after it had traveled to the sample as a P-wave and as an S-wave. The time it takes for the wave to propagate through the sample is determined from the peak of source to the first peak of the received P-wave or S-wave signal. The velocities are calculated by dividing the length of the sample by the measured time.

Figure 3.8: Bender element. P source / S receiver (left side), S source / P receiver (right side).

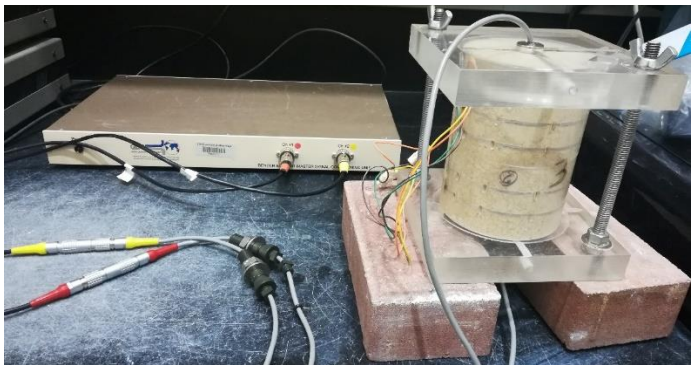

Figure 3.9: Seismic wave velocity measurements using GDS bender element.

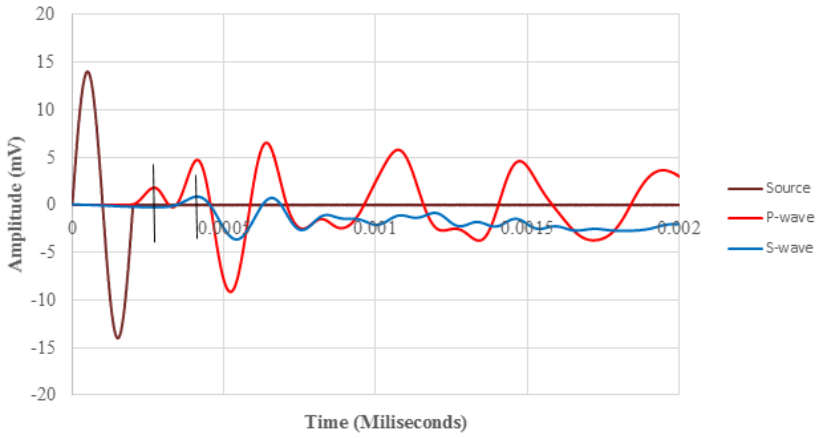

Figure 3.10: Seismic wave velocity (source, P-wave, S-wave).

3.3.3 Geotechnical tests

3.3.3.1 Atterberg limits

In the presence of moisture, cohesive soil can be remolded without crumbling. Fine-grained soil in the presence of clay mineral changes its consistency with varying moisture content. A Swedish scientist named Atterberg in the early 1900s developed a method to describe the phenomenon. At very high moisture content, soil behaves like a liquid; at very low moisture content, soil behaves like a solid. Depending on moisture content, the consistency of soil can be divided into four basic states; solid, semi-solid, plastic, and liquid. The transitions from one stage to another are defined by parameters called LL, PL, and SL. These parameters are known as Atterberg limits (Das and Sobhan, 1985). Figure 3.11 shows the different stages of soil with the

increase of moisture content. LL and PL are used to classify fine-grained soil. These parameters are related to several other engineering parameters, such as permeability, compressibility, conductivity, compaction, and characteristics of clay-shale minerals subjected to repeated wetting and drying cycles. Shrinkage potential, swell potential and crack development potential of cohesive soils depend on SL.

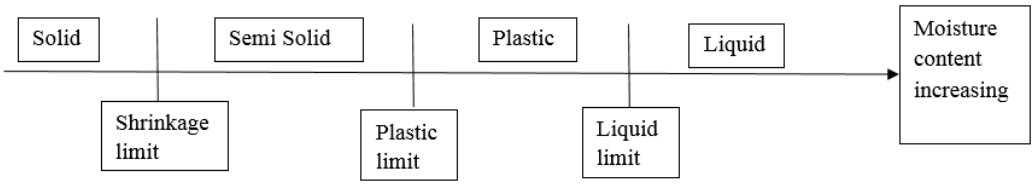

Figure 3.11: Atterberg limit.

3.3.3.1.1 Liquid limit test

Liquid limit is defined as moisture content at the point of transition from a plastic to a liquid state. Casagrande (1932 b, 1958) developed a LL test which is shown in Figure 3.12. According to this method, a remolded soil sample is spread into the cup to a depth of about 10 mm. After that, a standard-groove is cut in the soil using a grooving tool. Then blows are applied to close the groove over a distance of 13 mm (1/2 in). The LL is defined as the water content at which the groove closure occurs at exactly 25 blows. In practice, it is difficult to close the groove at exactly 25 blows. A plot of water content versus the number of blows count, which gives a straight line, helps to determine the water content at 25 blows. This requires a couple of samples with different water content to be mixed to have groove closure approximately from 18 to 35 blows. For this reason, ASTM D4318-00 standard test procedure for multipoint LL Method A is used to determine the LL.

Figure 3.12 : LL test.

3.3.3.1.2 Plastic limit test

Plastic limit (PL) is the water content at which the transition from plastic to semisolid state occurs. A soil is considered non-plastic if a thread cannot be rolled out down to 3.2 mm at any moisture possible. For the current research, the ASTM D 4318 standard test method of PL of soils is used. A soil sample is mixed with water less than the LL. The sample is then rolled between the palm and a ground-glass plate by applying sufficient pressure to roll it into a thread of uniform diameter throughout its length. The sample is rolled until a 1/8 in diameter thread shows signs of crumbling. The rolled samples are shown in Figure 3.13. The crumbling soil was collected to determine the water content. The whole procedure is repeated three times to get three determinations of water content which is averaged to determine the PL of the sample.

Figure 3.13: Plastic limit test.

3.3.3.1.3 Shrinkage limit test

Shrinkage limit (SL) is the water content at which further loss of moisture will not result in any more volume reduction. In other words, it is the amount of water required to fill the voids of a given cohesive soil. For this current research, ASTM D4943-08 standard test method by

shrinkage factors of soil by wax method is used. A soil sample is mixed with water content close to its LL to form a uniform paste and placed in a small dish. The initial moisture content of the soil paste is measured and then the soil pat is oven-dried and the volume change is determined using the water submersion technique. To prevent the dry soil pat from absorbing moisture during volume determination, it is coated with wax. The final moisture content of the soil pat is determined. Then the change in moisture content from the initial condition is determined to calculate the SL. Figure 3.14 describes the SL test.

(a) (b) (c)

Figure 3.14: Shrinkage limit test (a) shrinkage of soil pat after drying (b) wax coating of soil pat (c) water submersion technique.

3.3.3.2 Specific gravity test

Specific gravity (SG) of material represents the ratio of the mass of a given volume of that material to the mass of an equal volume of distilled water at 20°C. SG of soil is an important parameter in geotechnical engineering. It is used to calculate the phase relationship of soils, such as void ratio and degree of saturation, and also the density of soil solids. For this current research, SG of soil solids is determined using a water pycnometer following ASTM D854-02 standard test. Figure 3.15 shows the SG test of soil passing through the 4.75mm (No.4) sieve. 100 gm of oven-dry soil sample is placed in a 500 ml dry pycnometer with the help of a funnel. To prepare the soil, slurry water is added between $^1/_3$ and ½ of the depth of the main body of the pycnometer. The

mixture is agitated to form a soil slurry. Entrapped air in the soil slurry is removed by the heat-only method by boiling it for 2 hours. After that, the pycnometer is filled with water up to the mark and allowed to cool to approximately room temperature. The weight of the pycnometer and the room temperature is recorded. After cleaning the pycnometer it is filled with water and weight is determined. The SG of the soil is determined by using the following equations:

$$G_T = \frac{w_s}{w_s - w_1 + w_2} \quad 3.3$$

$$G_{20} = G_T * \frac{(G_w) \text{ at } T^0c}{(G_w) \text{ at } 20^0c} \quad 3.4$$

where GT = SG of soil at room temperature (0C), w_s = weight of soil (gm), w_1 = weight of pycnometer + water + soil (gm), w_2 = weight of pycnometer + water (gm), G20 = SG of soil at 20° C, (G_w) at T^0C = SG of water at room temperature, and (G_w) at 20^0C = SG of water at 20°C

.

(a) (b) (c)

Figure 3.15: Specific gravity test. (a) dry soil (b) soil with water (c) boiling soil-water mixture.

3.3.3.3 Unconfined compression test

Unconfined compression test is used to determine the unconsolidated undrained shear strength of clay soil. The unconfined compression strength is the stress at which a cylindrical soil specimen will fail after applying axial load under an unconfined condition. For this research, the

unconfined compression strength of clay and sandy clay are determined according to ASTM D 2166 method. A total of 26 samples are tested following this method. Samples are prepared in a standard proctor compaction cell at opt water content. The samples are extruded from the compaction mold and cut into a cylindrical shape with a length to width ratio of between 2 to 2.5. After taking an initial measurement of diameter and length of the sample, it is placed in a unconfined compression test machine. Load is applied to produce an axial strain rate of 0.5% to 2% per minute. Load and deformation dial readings are recorded at 30 sec intervals until the sample fails. Figure 3.16 (a) shows the unconfined compression test of sample 1. Figure 3.16 (b) shows the stress versus strain graph for sample 1 used to determine the maximum stress (unconfined compression strength) at failure. Cohesion is half of the unconfined compression strength.

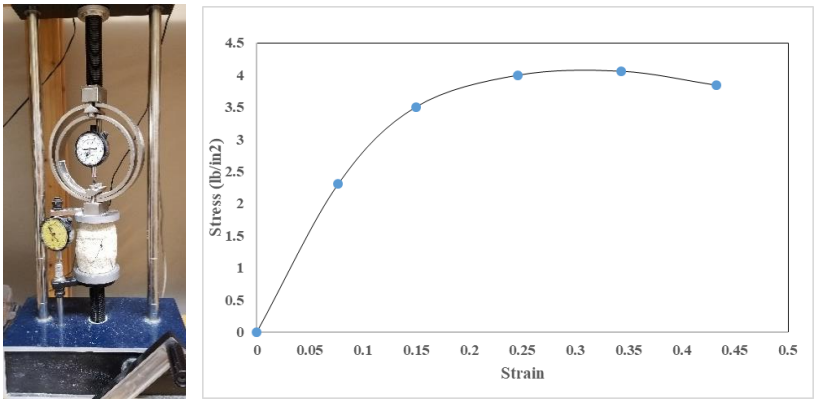

(a) (b)

Figure 3.16: (a) unconfined compression test, (b) stress versus strain graph of sample 1.

3.3.3.4 Parameters obtained using weight volume relationship

Void ratio, degree of saturation and specific surface area are determined from the measured geotechnical parameters using the weight volume relationship.

The degree of saturation is the ratio of the volume of water to the volume of voids.

$$S_w = \frac{v_w}{v_v} \qquad 3.5$$

Void ratio is the ratio of volume of void (air and water) to the volume of solids.

$$e = \frac{v_v}{v_s} \quad 3.6$$

Specific surface area is a property of solids defined as the total surface area of a material per unit of mass. Specific surface area is determined from the LL using the following correlation given by Farrar and Coleman (1967),

$$LL = 19 + 0.56*A_s \quad 3.7$$

where A_s is in m^2/gm.

3.3.4 Chemical test (CEC)

CEC of a soil is the total amount of negative charge on soil surfaces that can hold positive cations such as calcium, magnesium, and potassium. From a practical standpoint, CEC indicates the holding capacity for nutrients and water. CEC depends on soil type and the CEC will increase with clay fraction. Geotechnical properties and geophysical properties depend on soil type and water content. So it is expected that geotechnical and geophysical properties could have correlations with CEC. For this current research, CEC of soil is determined according to ASTM D7503-10. The ammonium acetate pH 7 measuring method is followed. At first, a 25 g oven-dry soil sample is placed in a 500 mL Erlenmeyer flask. After that, 125 ml of the 1 M NH4OAc is added to the soil and shaken thoroughly. The mixture is then kept in the laboratory for 24 hours. The soil sample is transferred to a 5.5 cm Buchner funnel with moistened filter paper. Then the soil is gently washed four times with 25 mL of additional NH4OAc. Suction is applied when necessary to ensure slow filtering. Next, the soil is washed with eight separate additions of 95% ethanol to remove any excess saturating solution. The adsorbed NH4 is extracted by washing the soil with eight separate 25 mL additions of 1 M KCl. The leachate is collected in a 250 mL volumetric flask and diluted to volume with additional KCl. The amount of ammonia is determined using a spectrophotometer following the salicylate method in the high range. Blank (sample that

contains everything except for the analyte of interest) and the sample are prepared by adding ammonia salicylate and ammonia cyanurate reagents. After that, the concentration of ammonia is determined using a spectrophotometer. Figure 3.17 (a) and (b) shows diluted leachate in the chemical and determination of ammonia of sample 15.

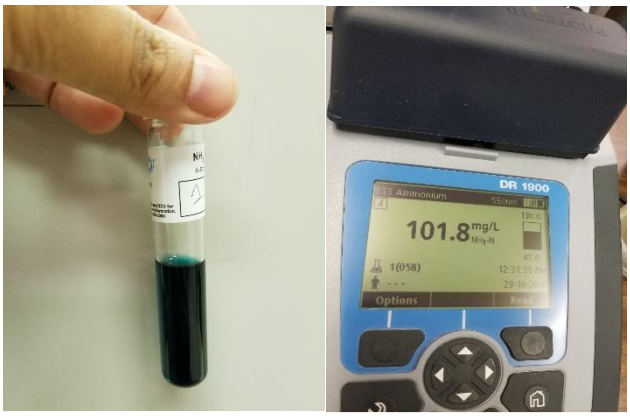

(a) (b)

Figure 3.17: CEC test of sample 15, (a) diluted leachate in the chemical, (b) ammonia determination.

3.4 Development of ANN Model

The architecture of an ANN model is determined based on the characteristics of the problem and knowledge of ANN. In this study, the feed-forward back propagation technique is used, and the nonlinear sigmoid function is chosen as the activation function. ANN models are usually developed following four different steps. In the first step, a database is divided into three different classes - training, testing, and validation. The training sets include around 50% of the total data and are selected randomly, including minimum and maximum values of the input data. The testing and validation sets are also selected randomly and contain about 25% of the data in each. In the second step, the opt hidden nodes and iteration of network is determined after training and testing the network. The three best-performing networks are chosen based on their statistics for comparison. In the third step, the three best networks are also validated using a validation data

set. For the final step, the selected three networks are re-trained using all the data in order to increase the prediction accuracy on the network structure that is determined in the previous step. The performance of the selected three networks is evaluated based on Mean Absolute Relative Error (MARE), Coefficient of Determination (R^2), and normalized Average Squared Error (ASE) as calculated using the following formulas:

$$\text{MARE} = \frac{\sum_{i=1}^{N} | X_i^P - X_i^A |}{N} \quad 3.8$$

$$R^2 = 1 - \frac{\sum_{i=1}^{N} (X_i^A - X_i^p)^2}{\sum_{i=1}^{N} (X_i^A - \overline{X_1})^2} \quad 3.9$$

$$\text{ASE} = \frac{\sum_{i=1}^{N} (X_i^A - X_i^p)^2}{N} \quad 3.10$$

where, X_i^A = Actual value, X_i^P = Predicted value, $\overline{X_1}$ = Mean of X_i^A, and N = Total number of data sets.

Basically ASE, MARE and R^2 are used for comparative assessment between different models to evaluate the performance. A 5% change in these parameters is assumed to represent a significant change in performance of the models. In this study, the performance of the models is classified as poor, moderate, good, high based on R^2 values. If the R^2 value fall between 0 to 0.19 the performance is classified as poor, 0.2 to 0.49 as moderate, 0.5 to 0.69 as good and 0.7 to 1 as high.

CHAPTER 4

PREDICTING GEOTECHNICAL PARAMETERS FROM ELECTRICAL RESISTIVITY USING DATA FROM THE LITERATURE

4.1 General

The ER method is a non-invasive surface geophysical method which is less time-consuming than traditional geotechnical methods and provides continuous spatial information about the soil. The limitation of the ER method is that the information is not in terms of engineering parameters. Correlation between geotechnical parameters and ER is needed to facilitate the use of ER information in geotechnical designs. The artificial neural network (ANN) is a powerful tool to develop correlations and predict parameters. In this chapter, data from the literature are used to develop several ANN models to predict saturation, CEC, water content, and dry density for remolded and undisturbed clay soil.

Performance of the ANN models is evaluated based on the mean absolute relative error (MARE), coefficient of determination (R^2) and the average squared error (ASE). Multilinear regression analysis is also performed to determine the correlation between parameters. Effectiveness of ANN models for predicting different parameters is compared to the results obtained from multilinear regression analysis. Performance of the ANN models developed for remolded and undisturbed soil samples are also compared4.2 Geotechnical Parameter

Geotechnical parameters used in this study are degree of saturation, CEC, water content and dry density. Degree of saturation is the ratio of the volume of water to the volume of voids.

Several researchers worked on the relationship between degree of saturation and ER. Rinaldi and Cuestas (2002), and Abu Hassanein et al. (1996) showed that degree of saturation is inversely proportional to ER. CEC is the total amount of negatively charged ions attached on the surfaces of soil by the positively charged ions (Ross and Ketterings, 1995). There are a couple of established relationships (Farrar and Coleman, 1967; Smit et al., 1985; and Yukselen and Kaya, 2006) between CEC and soil index properties like LL and PL. Several researchers (Giao, 2003; Bryson and Bath, 2009; Kibria, 2014; Bhatt and Jain, 2014; Ozcep et al, 2009; Osman et al, 2014) worked on correlation development between ER and water content. Some research is also found in the literature on the correlation between dry density and ER (Kibria, 2014).

4.3 Data from Literature

Two different data sets are acquired from literature (Kibria 2014). The first data set consisted of soil specimens collected from a slope along highway Loop 12 near Union Pacific Rail Road (UPRR), Dallas, Texas. The soil specimens were either remolded (44 measurements) or undisturbed (77 measurements). The remolded clay specimens included four soil types: (a) highly plastic clay, (b) low plastic clay, (c) Ca-bentonite, and (d) kaolinite. The undisturbed soil samples included a total six different types based on borehole location and depth. Experiments were performed at subsequent drying stages for undisturbed samples and at varied moisture content and dry unit weight for remolded samples. For this data set, the parameters were CEC, ER and degree of saturation. The second data set is based on soils collected along slopes of highway US 287 and US 67 in Midlothian, Ellis County, Texas. The measurements consisted of water content, ER and dry density on 73 remolded samples (Kibria 2011).

All the geotechnical parameters - water content, dry density, saturation, and CEC - were measured in the lab. Soil samples were also differentiated using sieve analysis, LL, PL, X-ray

fluorescent, and scanning electron microscope. The ERs were measured in the lab using super sting IP resistivity equipment. For remolded soil samples, a soil resistivity box was made with high strength plexiglass, and two circular stainless-steel electrodes were used for the undisturbed samples. Moisture content was varied in the ER test using distilled water (conductivity 12.94 μS).

The first data set consisted of 44 remolded samples and 77undisturbed samples. The second data set consisted of 73 remolded samples. Figure 4.1 shows the distribution of the actual data. For remolded samples, Figure 4.1(a) shows that saturation varies along with ER, but Figure 4.1(b) shows different ER values for the same CEC values. There are only four CEC values corresponding to different ER values. For undisturbed soil samples, Figure 4.1(c) shows only four different saturation values for the different ER values; Figure 4.1(d) shows that CEC varies with ER. Figure 4.1 (e) and (f) show that for the same dry density, different values of ER exist, and that for the same ER, different values of water content exist. The distribution of actual data can affect the distribution of the predicted data. If for different values of ER there are multiple values of saturation and CEC, this could affect the graphical prediction accuracy. The same thing may happen for same value of ER for varying water content and same value of dry density for varying ER.

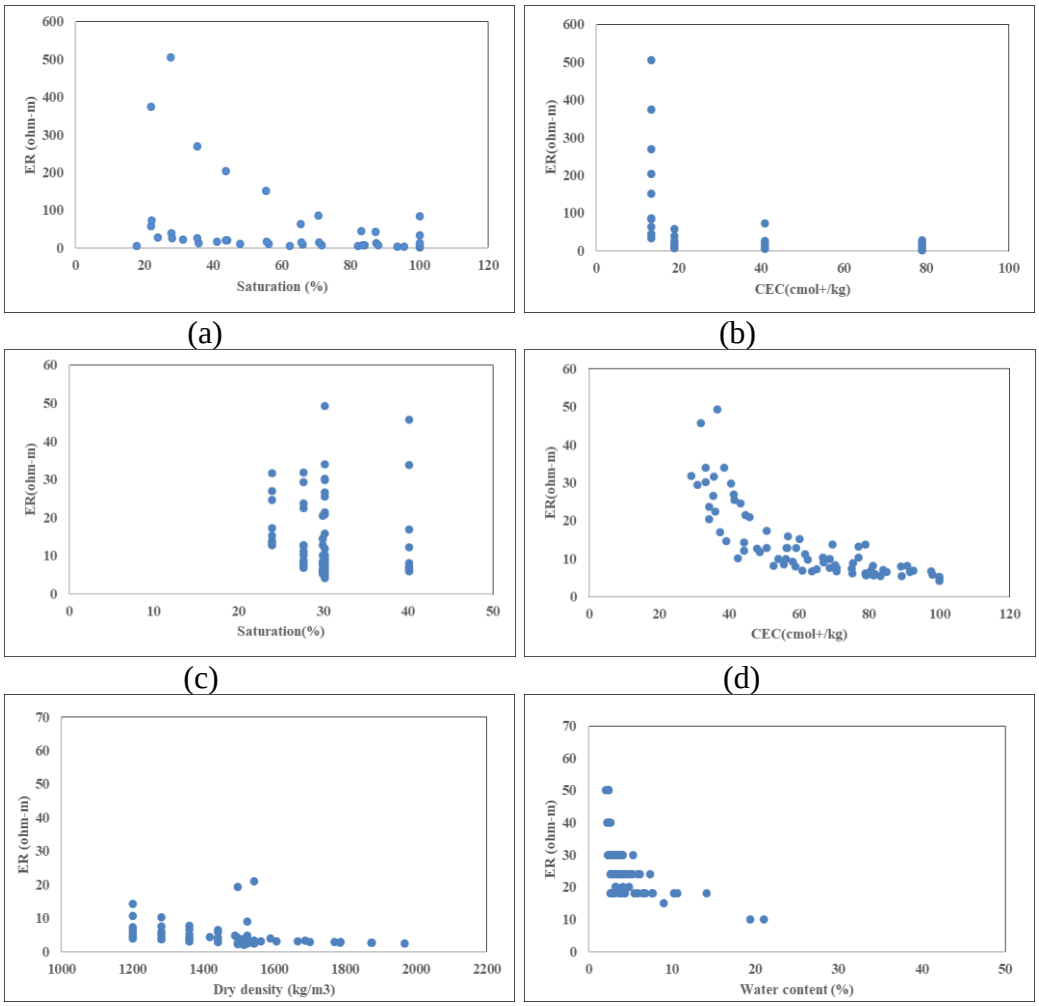

Figure 4.1: Actual data for (a) ER versus saturation, remolded samples, (b) ER versus CEC, remolded samples, (c) ER versus saturation, undisturbed samples, (d) ER versus CEC, remolded samples, (e) ER versus dry density, remolded samples, (f) ER versus water content, remolded samples.

4.4 Result and Analysis

4.4.1 Predicting ER for remolded versus undisturbed samples

The parameters and ranges for ANN model development are shown in Table 4.1. ANN models are developed to predict ER from CEC and saturation. From the first set of data of remolded samples, 44 data are subdivided with 24 for training, 10 for testing, and 10 for validation. Several ANN models are developed. The three best models and their statistics for training, testing,

validation and all-trained are shown in Table 4.2. Among them, the 2_ (1_1_500) _1 (input_ (initial hidden nodes_final hidden nodes_number of iteration) _output) is chosen as the best network based upon the lower ASE and MARE, and the higher R^2 in validation. The actual versus predicted graph is shown in Figure 4.2(a), which shows the data are well aligned with a 45-degree line. This represents good accuracy of the model for predicting ER.

Table 4.1: Parameters and ANN ranges.

Sample type	Parameters	Ranges	
		Max	Min
Remolded	CEC (cmol/kg)	87.15	5.86
	Saturation (%)	99	8.28
	ER (ohm-m)	530.82	0.01
Undisturbed	CEC (cmol/kg)	108.77	21.01
	Saturation (%)	42.11	21.93
	ER (ohm-m)	54.84	0
Remolded	Water Content (%)	55.33	4.96
	Dry Density (kg/m^3)	2473.85	883.26
	ER (ohm-m)	23.40	0.2

ANN models are also developed for predicting ER from CEC and saturation measured on undisturbed field samples. The statistics of the best all-trained trained are shown in Table 4.3 along with statistics of best model based on the remolded samples. The statistics show good accuracy in predicting ER using either undisturbed or remolded soil samples. However, the model based upon remolded samples has lower ASE and higher R^2 but higher MARE. ASE is the first criteria for evaluating the performance of ANN model. The lower the ASE, the higher the accuracy and the more reliability in prediction. This suggests that predicting ER using remolded samples gives better accuracy. This is further illustrated in Figure 4.2, where the predicted versus actual graph of the all-trained models shows more scatter for the undisturbed soil sample data than for the remolded soil sample. The well-aligned data with the 45-degree line represents the very high accuracy of the model for remolded samples in comparison to the model built with undisturbed

soil samples. Comparing Figure 4.2(a) and Figure 4.2(b) shows that the accuracy of the model of remolded samples is higher than the model of undisturbed soil samples. Therefore, the model built with remolded samples is more accurate than the model built with undisturbed soil samples.

Table 4.2: Statistical accuracy measures of ANN model predicting ER from CEC and saturation (remolded samples).

Model architecture	2_ (1_1_500) _1	2_ (2_2_500) _1	2_ (3_3_500) _1
Training			
ASE	0.0069	0.0078	0.0083
MARE	65.64	80.78	84.57
R^2	0.87	0.85	0.84
Testing			
ASE	0.0018	0.0019	0.0020
MARE	58.57	69.50	71.51
R^2	0.88	0.88	0.88
Validation			
ASE	0.0019	0.0021	0.0023
MARE	48.94	55.27	57.89
R^2	0.90	0.89	0.89
All-trained			
ASE	0.0037	0.0042	0.0040
MARE	58.64	71.03	68.49
R^2	0.89	0.88	0.88

Table 4.3: Comparison of ANN models predicting ER between remolded and undisturbed samples.

Sample type	Input Parameters	Model structure	ASE	MARE	R^2
Remolded	CEC Saturation	2_ (1_1_500) _1	0.0037	58.64	0.89
Undisturbed	CEC Saturation	2_ (4_4_200) _1	0.0072	21.27	0.78

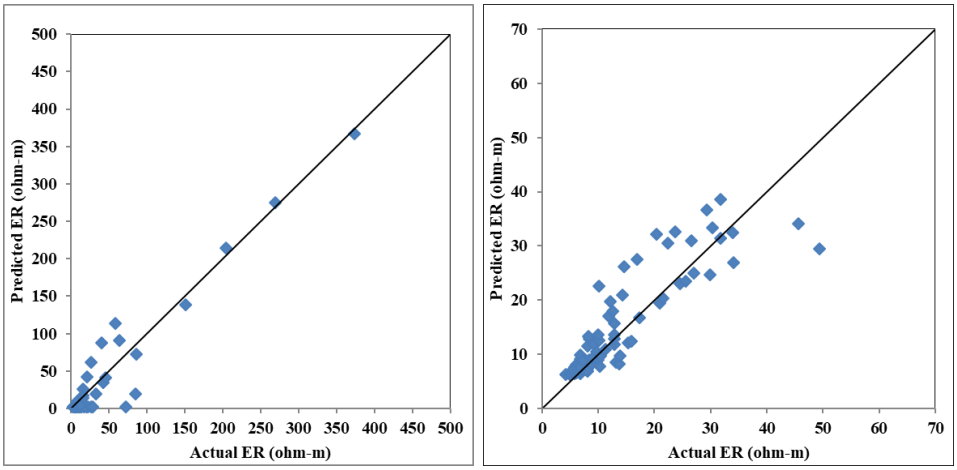

(a) (b)

Figure 4.2: Comparison of ANN models predicting ER (a) remolded samples (input: CEC and saturation), (b) undisturbed samples (input: CEC and saturation).

4.4.2 Predicting saturation for remolded versus undisturbed samples

Saturation is an important soil parameter, and knowing its spatial distribution is important for many applications. Prediction models are now developed for saturation solely from ER and, subsequently, for saturation from both ER and CEC. Models are developed using measurements on remolded and undisturbed samples. Statistics of the four models are listed in Table 4.4. The results show that the prediction model based on undisturbed samples has better performance than the model based on the remolded samples. This could be due to the number of data points. The undisturbed soil samples model has more data in comparison to remolded soil model. When CEC is added as an input, the performance of the models for both remolded and undisturbed samples are improved. Significant improvements are observed for the remolded soil model in comparison to the undisturbed soil model. However, the model based on the remolded samples shows better performance than undisturbed sample model. Figure 4.3 shows the predicted versus actual graphs of all-trained data for these four models. For remolded samples, the graphs show that the data are more scattered when only ER is taken as input (Figure 4.3 (a)) than when ER and CEC are used as inputs (Figure 4.3 (c)). Similarly, scatter is reduced for the undisturbed samples by including

CEC. For remolded samples the range of the data has a wide spread in comparison to the undisturbed model. For the undisturbed models straight lines are observed, which means that for the same value of actual saturation, different predicted saturation values exist. A similar pattern is observed in actual data set for ER versus saturation shown in Figure 4.1(c). It proves that the performance of the ANN model depends on the actual data set.

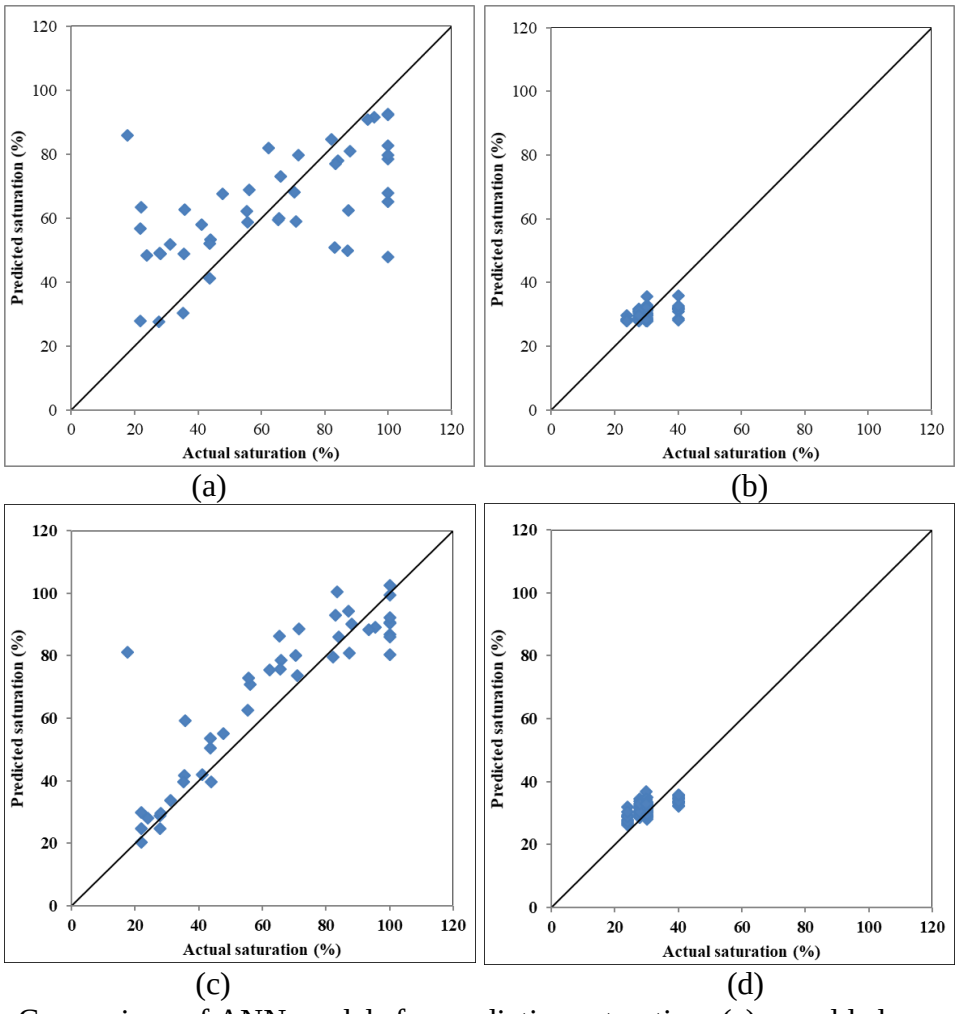

Figure 4.3: Comparison of ANN models for predicting saturation: (a) remolded samples (input: ER), (b) undisturbed samples (input: ER), (c) remolded samples (input: ER and CEC), (d) undisturbed samples (input: ER and CEC).

Table 4.4: Comparison of ANN models for predicting saturation between remolded and undisturbed samples.

Sample type	Input Parameters	Model structure	ASE	MARE	R^2
Remolded	ER	1_ (2_5_6200) _1	0.0474	40.99	0.36
Undisturbed	ER	1_ (1_11_20000) _1	0.0404	9.70	0.17
Remolded	CEC, ER	2_ (2_5_100) _1	0.0182	21.99	0.78
Undisturbed	CEC, ER	2_ (7_7_700) _1	0.0366	10.75	0.33

4.4.3 Predicting CEC for remolded versus undisturbed samples

CEC is a time-consuming measurement that must be performed on a laboratory sample. The ability to predict the CEC from ER or with the addition of saturation would be very beneficial. Four different ANN models are developed to predict CEC for undisturbed and remolded samples. Statistics of the all-trained best selected networks for these four models are shown in Table 4.5. The statistics show that ER has moderate correlation with CEC for remolded samples and good correlation with undisturbed soil samples. Also the undisturbed soil sample model for predicting CEC from ER performs with better accuracy than the remolded soil sample model. After adding saturation as input, the ANN models for both undisturbed and remolded soil samples are improved. Significant improvement is observed in the case of remolded samples. But the undisturbed soil sample model performs better when CEC is predicted from ER along with saturation. The undisturbed soil model has more data points than the remolded soil sample, which could affect the accuracy of the model. Figure 4.4 shows the predicted versus actual graphs of the four models for predicting CEC. The graph shows that data are more scattered in Figure 4.4 (a) and (b) in comparison to (c) and (d), which shows the improvement in prediction after adding saturation as input. A straight line pattern is observed for remolded soil samples which follows the same pattern of actual data shown in Figure 4.1(b). Comparison of Table 4.4 and 4.5 shows that ER can predict

CEC better than saturation, which could be due to the sensitivity of ER to the surface conductivity of clay soil, which is also related to CEC.

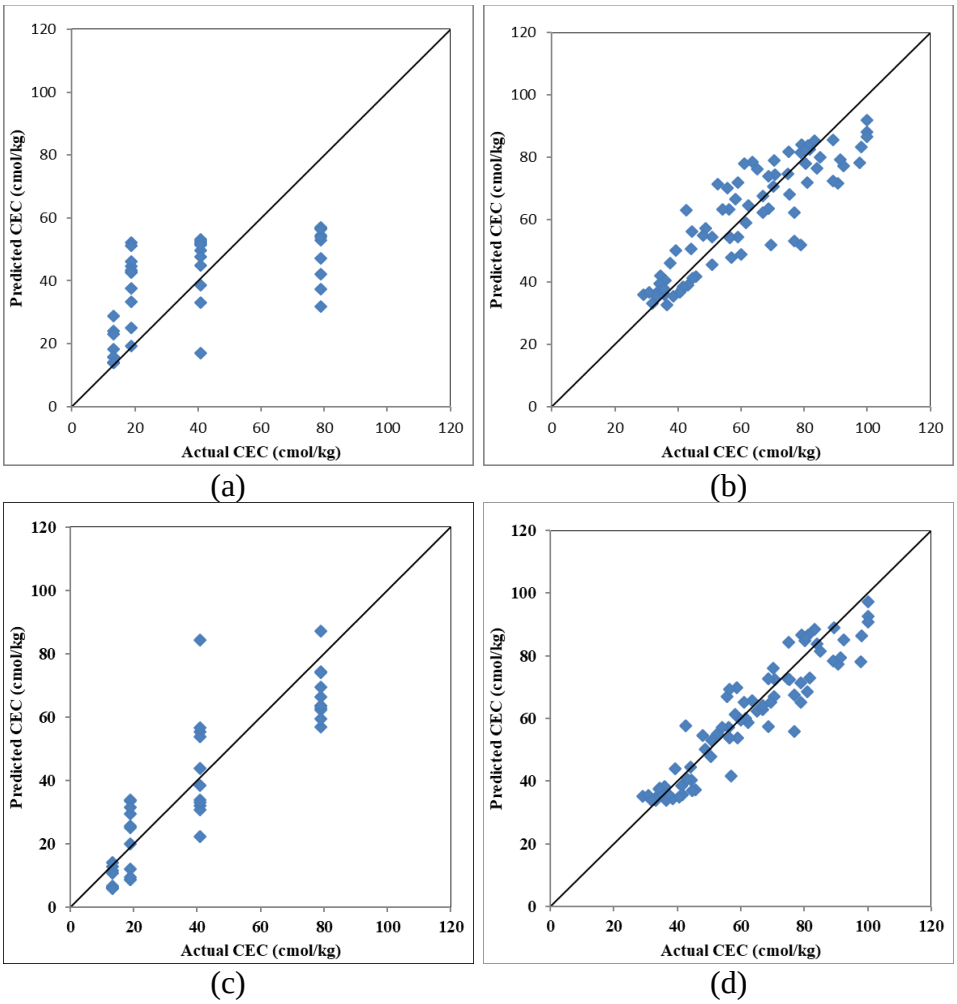

Figure 4.4: Comparison of ANN models predicting CEC: (a) remolded samples (input: ER), (b) undisturbed samples (input: ER), (c) remolded samples (input: ER and saturation), (d) undisturbed samples (input: ER and saturation).

Table 4.5: Comparison of ANN models predicting CEC between remolded and undisturbed samples.

Sample type	Input Parameters	Model structure	ASE	MARE	R^2
Remolded	ER	1_ (1_1_2100) _1	0.0606	50.42	0.39
Undisturbed	ER	1_ (7_8_100) _1	0.0125	12.95	0.76
Remolded	Saturation, ER	2_ (3_7_200) _1	0.0309	35.90	0.74
Undisturbed	Saturation, ER	2_ (2_3_100) _1	0.0069	9.26	0.87

4.4.4 Comparison of ANN models for predicting dry density and water content

The ER depends on porosity, saturation, clay content and the microscopic arrangement of the soil grains as it controls the pore structure. The dry density depends on the porosity, the arrangement of soil grains, and, to some extent, the mineralogy. Therefore, ANN models are developed to evaluate the correlation between dry density and ER. The models are based on 73 soil data from US 287 and US 67 in Midlothian, Ellis County, Texas. To start we ignore the influence of moisture content and determine relations between dry density and ER. Subsequently, the water content is added as an input to the model. The statistics of the models are shown in Table 4.6, which indicate that ER has moderate correlation with dry density and it improves when water content is added as input. The predicted versus actual graph of these two models is shown in Figure 4.5. Even though statistics show a clear improvement in predicting dry density after adding water content as input, it is hard to see the difference from this figure. The straight-line patterns are observed in the predicted versus actual graph, which is due to the pattern of the actual data set shown in Figure 4.1(e).

Table 4.6: Comparison of ANN models predicting dry density.

Sample type	Input Parameters	Model structure	ASE	MARE	R^2
Remolded	ER	1_ (3_12_20000) _1	0.0068	7.53	0.42
Remolded	Water content ER	2_ (9_12_20000) _1	0.0047	5.85	0.59

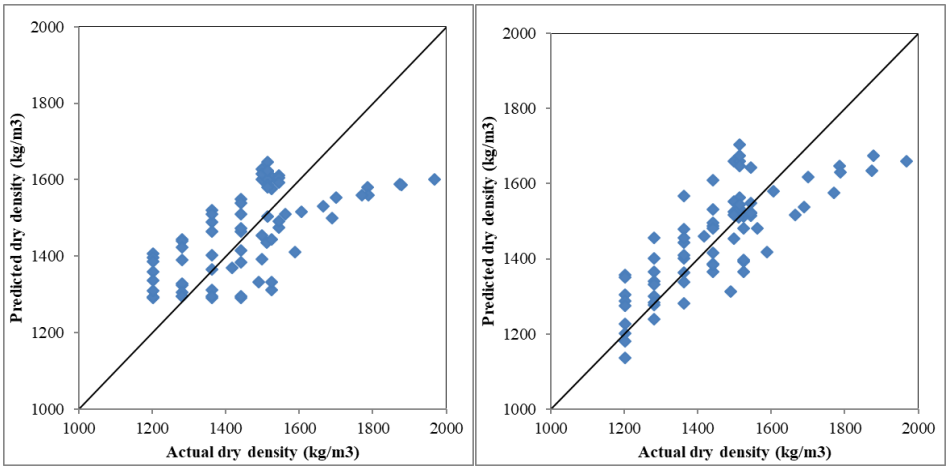

(a) (b)

Figure 4.5: Comparison of ANN models predicting dry density (a) input: ER, (b) input: ER and water content.

The presence of water has a strong influence on the conduction of electricity in soils. Historically, ER has been used to infer the presence of water in soils. Using the 73 soil data from US 287 and US 67 in Midlothian, Ellis County, Texas, ANN models are developed to predict water content from ER and subsequently ER along with dry density. The statistics of the models are shown in Table 4.7. Statistics show that ER has good correlation with water content and, that after adding dry density, the prediction performance of the model improves. However, it is hard to see this improvement in the predicted versus actual graph of these two models shown in Figure 4.6. Comparison of Table 4.6 and Table 4.7 indicates that ER can predict water content better than dry density. This is attributed to the fact that ER is more sensitive to water content than porosity.

Table 4.7: Comparison of ANN models predicting water content.

Model	Input Parameters	Model structure	ASE	MARE	R^2
Remolded	ER	1_ (1_12_2900) _1	0.0122	17.34	0.59
Remolded	Dry density ER	2_ (1_12_1300) _1	0.0098	15.08	0.66

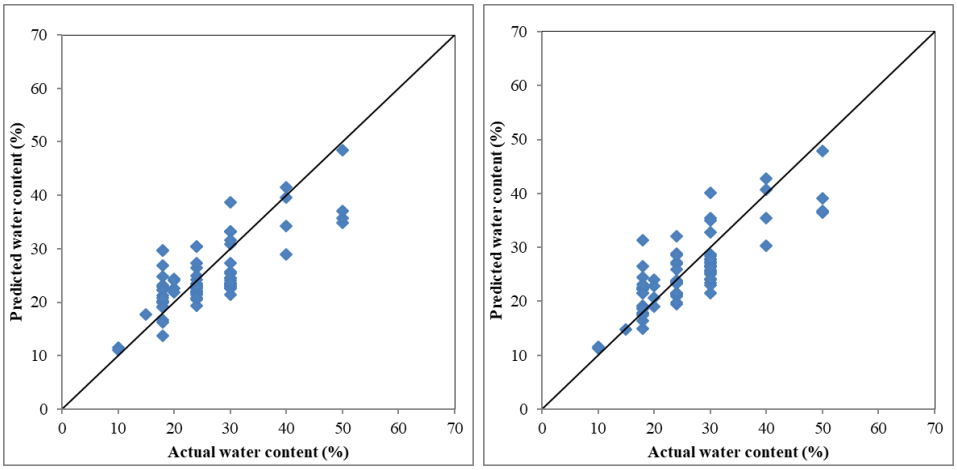

(a) (b)

Figure 4.6: Comparison of ANN models predicting water content (a) input: ER, (b) input: ER and dry density.

4.5 Comparison of Regression and ANN

Multilinear regression is applied to predict geotechnical parameters and ER to compare the performance of ANN with multilinear regression. The multilinear regression analysis is conducted using Excel. Table 4.8 shows the root mean squared error (RMSE), MARE (Equation 3.8), and unnormalized ASE (Equation 3.10) calculated using unnormalized actual and predicted data and R^2 (Equation 3.9).

The RMSE is defined as

$$\text{RMSE} = \sqrt{\frac{\sum_{i=1}^{N}(X_i^A - X_i^P)^2}{N}} \tag{4.1}$$

where, X_i^A = Actual value, X_i^P = Predicted value, $\overline{X_1}$ = Mean of X_i^A ,N = Total number of data.

Statistics show that for all the models, RMSE, MARE, and ASE are higher, and R^2 are lower for regression-based models in comparison to ANN-based models. That proves the better performance accuracy of ANN in comparison to regression. Significant improvement in performance from regression to ANN is observed in the case of remolded samples more so than undisturbed samples.

Table 4.8: Comparison of ANN and regression models.

Model	Soil type	Regression				ANN			
		RMSE	ASE	MARE	R^2	RMSE	ASE	MARE	R^2
Predicting ER from CEC and saturation	Remolded	82.95	6881.1	404.54	0.31	34.22	1175.4	58.64	0.9
	Undisturbed	9.34	87.2	82.73	0.61	4.56	20.8	21.02	0.78
Predicting CEC from ER and saturation	Remolded	23.27	541.5	74.87	0.19	14.3	204.7	35.9	0.75
	Undisturbed	12.25	150.2	17.75	0.61	7.31	53.5	9.18	0.87
Predicting CEC from ER	Remolded	23.65	559.5	76.89	0.16	23.65	559.5	76.89	0.39
	Undisturbed	12.56	157.8	17.71	0.59	9.82	96.45	12.95	0.76
Predicting Saturation from ER and CEC	Remolded	25.23	636.7	49.36	0.18	13.77	189.8	21.99	0.78
	Undisturbed	4.17	17.3	9.17	0.03	3.83	14.6	10.61	0.34
Predicting Saturation from ER	Remolded	25.65	657.9	51.17	0.15	22.19	492.7	40.99	0.36
	Undisturbed	4.27	18.2	8.82	0.004	4.02	16.2	9.71	0.17
Predicting dry density from ER and water content	Remolded	10.29	105.9	8.73	0.09	6.86	47.0	5.85	0.59
Predicting dry density from ER	Remolded	10.30	106.1	8.65	0.08	8.21	67.4	7.53	0.42
Predicting water content from ER and dry density	Remolded	7.18	51.5	21.9	0.31	4.99	24.9	15.08	0.66
Predicting water content from ER	Remolded	7.191	51.7	21.82	0.31	5.57	31.0	17.34	0.59

4.6 Conclusion

ER is predicted from the geotechnical parameters and, after that, geotechnical parameters are predicted from ER alone as well as from ER in conjunction with other geotechnical parameters for both remolded and undisturbed soil samples. Regression-based models are also developed to compare the performance of ANN-based models and regression-based models. ANN models are compared in terms of soil sample preparation - both remolded and undisturbed - using only ER as

input and then adding other geotechnical parameters as input along with ER. Analysis shows that ER can predict CEC better than saturation. This could be due to the dependence of ER on the surface conductivity of clay soil. For predicting ER and saturation, remolded soil models showed better performance; for predicting CEC, undisturbed soil models showed better performance. Again, the number of data points are greater for undisturbed soil models than remolded soil models. So, it is hard to tell from this analysis which type of sample preparation can give better results. Correlation of ER with water content is stronger than the correlation of ER with dry density. The reason could be the lower sensitivity of ER to mechanical properties. Adding additional geotechnical parameters with ER as input improved the prediction capacity of the models. And the improvements are more significant for remolded samples than undisturbed samples.

Overall ER shows good sensitivity to CEC, saturation, dry density and water content. ANN shows better performance than regression for all the cases but significant differences are observed for remolded samples.

CHAPTER 5

PREDICTING GEOTECHNICAL PARAMETERS FROM SEISMIC WAVE VELOCITY USING DATA FROM THE LITERATURE

5 .1 General

Non-destructive geophysical seismic methods are effective for investigating soil without affecting the inherent mechanical properties, but the information is not in terms of engineering parameters that are used for the design of infrastructure. Conventional geotechnical methods are invasive, point based and time-consuming. Developing correlations between geotechnical and geophysical methods could solve the associated problems. The current research is focused on developing models to forecast geotechnical parameters from seismic wave velocity using the artificial neural networks (ANNs) technique. Published seismic wave velocity, LL, PL, water content, and dry density from field and laboratory measurements are used to develop ANN models. Performance of the ANN models is assessed based on mean absolute relative error (MARE), average squared error (ASE), and coefficient of determination (R^2). Due to the small number of data, models are developed both with the validation step as well as without the validation step, which saves more data for training. The performance of the models is improved by using more data for training. For predicting water content and dry density, two different types of models are developed – one with velocity and one without velocity. These are compared to assess the performance of adding velocity as an input parameter. Models incorporating the velocity information yield better predictions in most cases. Multilinear regression analysis is also

performed and a comparison of the two methods indicates that ANN models outperform multilinear regression models.

5.2 Data Collections

This study uses data from a report on seismic wave velocity published by the Engineering Research Institute of Iowa State University, Ames, Iowa (Hogan and Handy, 1996). Highway embankments constructed of three types of soils were chosen for field and lab tests. They tried to correlate laboratory seismic wave velocity with the water content and dry density measured in lab, and field seismic wave velocity with in-place moisture density. They aimed to find a more economical and less time-consuming solution as conventional geotechnical tests are time-consuming. The types of soils investigated are shown in Table 5.1. Field tests were conducted on the embankment side-slope and sampled for lab measurement. A total of 35 data were generated from the field measurements and 34 data from laboratory measurements. An additional loess soil similar to the silty loam was included in the laboratory measurements.

Table 5.1:Type of soil used for the tests.

Soil Type	Liquid limit	Plasticity index
Clay loam	23	9
Silty clay (gray)	30	13
Silty clay (brown)	40	18
Silty loam	32	6
Loess	32	6

Micro-seismic refraction tests were conducted to measure seismic velocities in the field. The equipment consists of three components: an impact source, a receiving transducer, and a seismic timer. A model 217 Micro-Seismic Timer and a transducer were used for these micro-seismic refraction tests. A tack hammer was used as the impact source on a 5/8-inch diameter steel

ball bearing to transmit the energy into the ground. Seismic measurements were taken along a 2 ft line at 3-in intervals. A total of 10 first-arrival measurements were collected at each station. The seismic wave velocities were calculated from distance-time plots. At the midpoint of the seismic line, a standard rubber balloon volumetric density measurement (according to ASTM D2167-15) and a water content measurement were performed for the field samples.

In the laboratory, compacted samples of 4-inch diameter by 4.58 in high were prepared to determine seismic wave velocities. Standard and modified AASHO compaction tests procedures were followed to prepare the samples. Water content, dry density for lab samples (total 34) were determined in lab and LL, plasticity index for lab, and field samples for individual soil types (total 5) were also determined in the laboratory.

5.3 ANN Models

ANN models are developed to predict seismic wave velocity, water content, and dry density using the data sampled from the lab and field experiments. Separate ANN models are developed using lab data, field data, and lab and field data combined. The field data contains 35 datasets, and the lab data includes 34 datasets. As the number of data is limited, two different ANN approaches are used for predicting seismic wave velocity. The first approach is the typical approach described in chapter three, where the data is used for training, testing, and validation. Around 50% of data is used for training, 25% for testing, and 25% for validation. In the second approach, the validation stage is excluded so that 75% data is used for training and 25% for testing. The parameters used for developing models are shown in Table 5.2, along with their ranges.

Table 5.2: Parameters and ranges.

Type of data	Parameters	Ranges	
		Max	Min
General	Plasticity Index	21.87	2.03
	LL	45.43	17.39
Field	Dry density (kg/m^3)	2240.58	1465.69
	Water content (%)	18	3.87
	Velocity (m/s)	1128.99	67.12
Lab	Dry density (kg/m^3)	2240.58	1465.69
	Water content (%)	20.53	4.74
	Velocity (m/s)	1675.07	57.48
Field plus Lab	Dry density (kg/m^3)	2246.59	1484.71
	Water content (%)	20.96	3.13
	Velocity (m/s)	1705.07	7.23

5.3.1 ANN Models for Predicting Seismic Wave Velocity

Seismic wave velocity is predicted using lab and field data separately and together through the development of ANN models. Six different models are developed following the two approaches, with validation and without validation.

5.3.1.1.ANN Models Using Field Data

ANN models are developed to predict velocity using LL, plasticity index, water content, and dry density. Several models are developed, and the best three networks are selected based on the statistical measures and opt hidden nodes presented in Table 5.3. The statistics show that ASE, MARE and R^2 of all three networks are very close to each other in training, testing, and all-trained. But the network 4_ (4_4_3100) _1 (where network structure is denoted as input_ (initial hidden nodes_final hidden nodes_iteration) _output) shows the best results in the validation stage. Network 4_ (4_4_3100) _1 is chosen as best among those three. The predicted versus actual graph

for network 4_ (4_4_3100) _1 is shown in Figure 5.1(a). The statistics and predicted versus actual graph indicate that the accuracy of predicting velocity is marginal.

Table 5.3: Statistical accuracy measures of model for predicting seismic wave velocity using field data, with validation).

Model architecture	4_ (1_1_2100) _1	4_ (2_2_2100) _1	4_ (4_4_3100) _1
Training			
ASE	0.0151	0.0152	0.0152
MARE	19.61	19.87	19.75
R^2	0.30	0.30	0.30
Testing			
ASE	0.0122	0.0121	0.0121
MARE	21.72	21.70	21.56
R^2	0.26	0.28	0.27
Validation			
ASE	0.0153	0.0149	0.0147
MARE	18.54	18.63	18.49
R^2	0.25	0.28	0.29
All			
ASE	0.0132	0.0132	0.0133
MARE	18.87	19.01	19.04
R^2	0.34	0.34	0.34

Due to the small number of field data, the validation stage is omitted so that more data is available to train the network. The input and output parameters and their ranges are the same as the previous model. Network 4_ (2_4_2900) _1 is chosen as the best network. For further comparison, the statistics of the best models with all data are shown. The predicted versus actual graph for network 4_ (2_4_2900) _1 is shown in Figure 5.1(b). The statistics are presented in Table 5.4, and the predicted versus actual graph indicates that the accuracy of predicting velocity is increased after omitting validation, but the overall performance is still marginal.

5.3.1.2 ANN models using lab data

The performance of lab data to predict velocity is analyzed through the development of ANN models. Network 4_ (2_2_200) _1 is chosen as the best among the three networks, and the

predicted versus actual graph is shown in Figure 5.1(c). The statistics and graph indicate that the accuracy of the velocity predictions is good. The results compared in Table 5.4 also indicate that the errors are much lower, and the R^2 values are much higher for the network trained using lab data compared to the network trained using field data.

The ANN models are developed to predict velocity without validation. Network 4_ (1_5_100) _1 is chosen as the best network among the three. Excluding the validation helps to minimize the errors and increases the R^2 values. Accordingly, the accuracy of the model is improved without the validation stage. The predicted versus actual graph shown in Figure 5.1(d) and the statistics presented in Table 5.4 indicate that the accuracy of the velocity predictions is good. The results also show that the errors are much lower, and the R^2 values are much higher for the network trained using lab data in comparison to the network trained using field data.

5.3.1.3 ANN models using field and lab data

The ANN models are developed using field and lab data together to predict the seismic wave velocity. LL, plasticity index, water content, and dry density are used as input parameters. The best three models are selected for further analysis based on minimum ASE, minimum MARE, maximum R^2, and opt hidden nodes. Among those three models, network 4_ (1_2_2900) _1 gives the minimum ASE, minimum MARE, and maximum R^2 in validation. So, network 4_ (1_2_2900) _1 is chosen as the best network. The statistics are shown in Table 5.4. and the predicted versus actual graphs for the best network shown in Figure 5.1(e). indicates that the accuracy is marginal. The errors are higher even though the R^2 values improve after combining lab and field data in comparison to the models trained with lab and field data separately.

The ANN model for field and lab data combined are also developed without the validation stage. Network 4_ (5_10_20000) _1 is chosen as the best network and had significantly smaller

errors and increased R^2 values than the model with validation. The predicted versus actual graph is shown in Figure 5.1(f) and the statistics indicate that predicting velocity is good.

The comparison of the results in Table 5.4 indicates that the errors are higher, and the R^2 values are lower for the network trained using field data, and the errors are lower and the R^2 values are higher for the network trained using lab data. The statistical measures for the network trained using field data and lab data together are in between the network statistics of lab data and field data.

Table 5.4: Comparing ANN models (predicting seismic wave velocity).

Model		Model structure	ASE	MARE	R^2
Field	with validation	4_ (4_4_3100) _1	0.0133	19.04	0.34
	without validation	4_ (2_4_2900) _1	0.0128	19.34	0.37
Lab	with validation	4_ (2_2_200) _1	0.0079	14.86	0.71
	without validation	4_ (1_5_100) _1	0.0058	13.33	0.80
Field plus Lab	with validation	4_ (1_2_2900) _1	0.0174	30.75	0.50
	without validation	4_ (5_10_20000) _1	0.0075	18.53	0.78

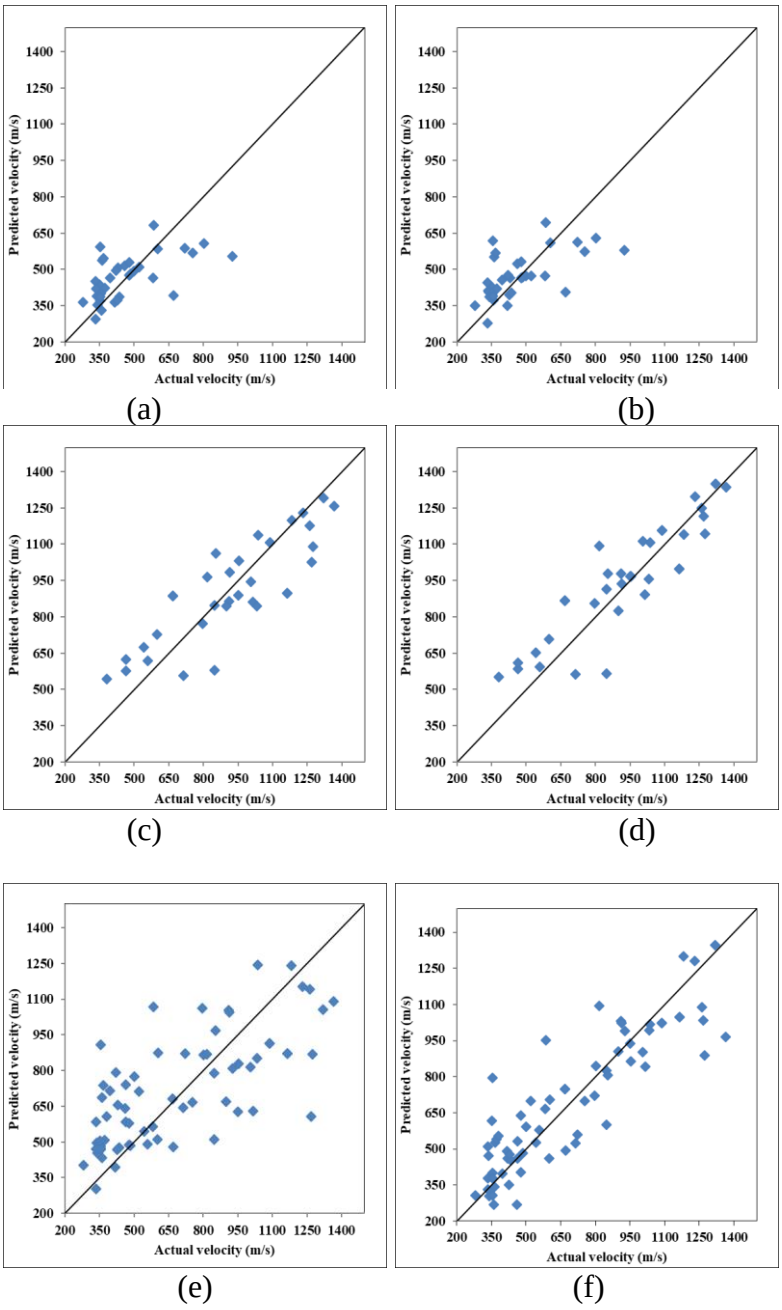

Figure 5.1: Graphical prediction accuracy of model for predicting seismic wave velocity, (a) field, with validation, (b) field, without validation, (c) lab, with validation, (d) lab, without validation, (e) field plus lab, with validation, (f) field plus lab, without validation

5.3.2 ANN models for predicting water content

ANN models are developed to predict water content using lab and field data separately and together. The models are developed without validation. Six different models are developed

without validation and models are developed with and without velocity as input to evaluate if velocity helps in predicting water content.

5.3.2.1 Using field data with velocity

ANN models are developed using field data to predict water content from LL, plasticity index, velocity and dry density. Network 4_ (1_5_100) _1 is chosen as the best performing network. The predicted versus actual graph for the best network is shown in Figure 5.2(a) and the statistics presented in Table 5.5 indicate that the accuracy of predicting velocity is good.

With the same number of classified data and ranges, ANN models are developed to predict water content but omitting seismic wave velocity from the input parameters. Network 3_ (2_3_1000) _1 is chosen as the best performing model among the three. The predicted versus actual graph is shown in Figure 5.2(b) and the statistics presented in Table 5.5 indicate good accuracy in predicting water content. The results presented in Table 5.5 indicate that the errors increase and the R^2 value decreases when the velocity is omitted as input. So, the results indicate that including seismic wave velocity improves the prediction of water content.

5.3.2.2 Using lab data

ANN models are developed using lab data to predict water content from LL, plasticity index, velocity and dry density. Network 4_ (3_3_100) _1 is chosen as best networks and the statistics are shown in Table 5.5. The predicted versus actual graphs are shown in Figure 5.2(c) and statistics indicate that the accuracy of predicting moisture content is high. The results compared in Table 5.5 also indicate that the errors are much lower and the R^2 values are much higher using lab data in comparison to using field data.

Excluding seismic wave velocity from input parameters but keeping the other parameters and ranges, the same ANN network 3_ (4_4_100) _1 is chosen as the best performing model. The predicted versus actual graph for the best network is shown in Figure 5.2(d) and the statistics indicate good accuracy in predicting water content. After omitting velocity from the input parameters, the errors increase and the R^2 value decreases. So, the results compared in Table 5.5 indicate that seismic wave velocity helps to predict water content. The results also indicate that the errors are much lower and the R^2 values are much higher for the network built using lab data in comparison to the network built using field data.

5.3.2.3 Using field plus lab data

Lab and field data are combined to develop ANN models to predict water content from LL, PL, dry density, velocity. Network 4_ (3_3_1000) _1 is the best network and the predicted versus actual graph, shown in Figure 5.2(e), and statistics indicate that the accuracy of predicting water content is good. The results indicate that the errors are higher and the R^2 values are lower for the network built using field data and lab data together in comparison to the network built using lab data and field data separately. So mixing field and lab data together lowers the performance of the model.

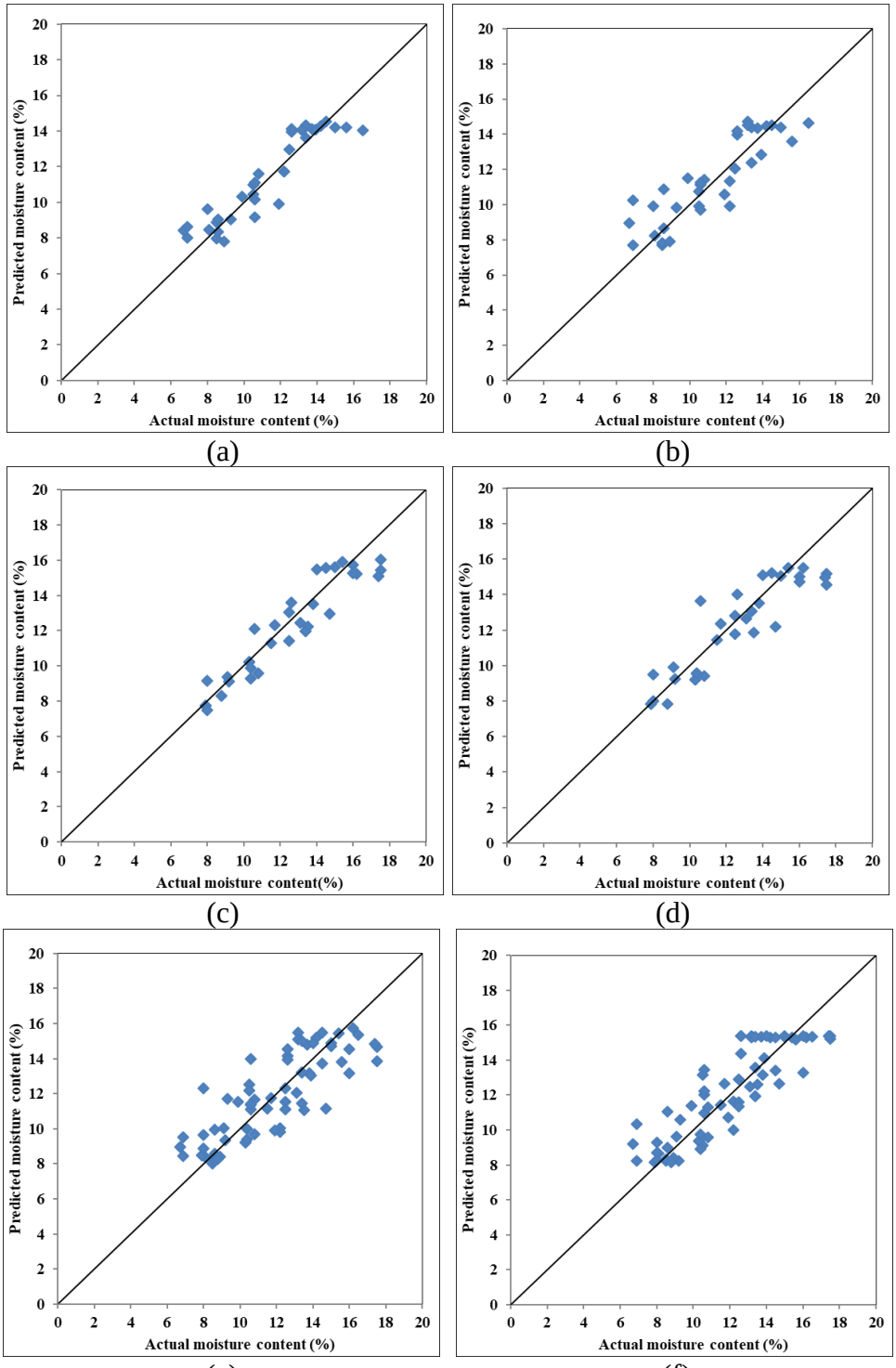

Figure 5.2: Graphical prediction accuracy of model for predicting moisture content, (a) field, with velocity, (b) field, without velocity, (c) lab, with velocity, (d) lab, without velocity, (e) field plus lab, with velocity, (f) field plus lab, without velocity.

The predicted versus actual graph for the best network omitting seismic wave velocity from the input parameters is shown in Figure 5.2(f). The statistics indicate good accuracy in predicting water content. After omitting velocity from the input parameters, the ASE has increased, even though the MARE has decreased and the R^2 value has increased. So, the results do not clearly indicate whether the seismic wave velocity helps to better predict water content. The results are almost the same for the model built using field data and field data and lab data together. But the errors are much lower and the R^2 values are higher for the network built using lab data in comparison to the network built using field and lab data together.

Table 5.5: Comparing ANN models (predicting water content).

Model		Model structure	ASE	MARE	R^2
Field	with velocity	4_ (1_5_100) _1	0.0051	7.78	0.85
	without velocity	3_ (2_3_1000) _1	0.0087	10.68	0.75
Lab	with velocity	4_ (3_3_100) _1	0.0043	6.63	0.89
	without velocity	3_ (4_4_100) _1	0.0051	7.69	0.82
Field plus Lab	with velocity	4_ (3_3_1000) _1	0.0083	11.61	0.67
	without velocity	3_ (3_11_19800) _1	0.0087	2.944	0.75

5.3.3 ANN models for predicting dry density

ANN models are developed to predict dry density using lab and field data separately and together. Due to the limited amount of data the validation step is omitted for these models to reserve more data for training for better accuracy. Six different models are developed with varying input parameters.

5.3.3.1 Using field data

Dry density is predicted using LL, plasticity index, velocity and water content. Network 4_ (3_5_100) _1 is the best performing network and the predicted versus actual graph, shown in

Figure 5.3(a), and the statistics presented in Table 5.6 indicate that the accuracy of predicting the dry density is high.

Using the same data set but omitting seismic wave velocity from the input parameters, network 3_ (4_4_2000) _1 is the best performing model. The predicted versus actual graph is shown in Figure 5.3(b), and the statistics indicate good accuracy in predicting dry density. Omitting velocity from the input parameters causes the errors to increase and the R^2 value to decrease significantly. The conclusion is that seismic wave velocity helps to predict dry density.

5.3.3.2 Using lab data

The best network and statistics using laboratory LL, plasticity index, velocity and water content as input parameters to predict dry density are shown in Table 5.6. The predicted versus actual graph is shown in Figure 5.3(c), and the statistics indicate that the accuracy of predicting dry density is high. Compared to the lab data in Table 5.6, the errors are lower and the R^2 values are higher for the network built using field data.

Keeping the other criteria the same and excluding velocity to predict dry density is best represented by network 3_ (4_4_500) _1. The statistics are shown in Table 5.6, and the predicted versus actual graph is shown in Figure 5.3(d). The statistics indicate good accuracy in predicting dry density. Omitting velocity from the input parameters, the errors decrease and the R^2 increases, as shown in Table 5.6. But the differences are not that significant. The results indicate that including seismic wave velocity does not enhance the prediction of dry density using lab data. The results of the without velocity models also indicate that the errors are lower and the R^2 values are higher for the network built using lab data in comparison to the network built using field data.

5.3.3.4 Using field plus lab data

Network 4_ (9_9_400) _1 is chosen as the best ANN model when using field and lab data to predict dry density and the velocity is included as input. The predicted versus actual graph is shown in Figure 5.3(e).and the statistics are presented in Table 5.6. The accuracy of predicting dry density is good, but the errors are higher and the R^2 values are lower in comparison to the network built using lab data and field data separately. So mixing field and lab data together lowers the performance of the model.

The best ANN model developed using field and lab data and omitting seismic wave velocity is represented by network 3_ (3_11_19800) _1. The predicted versus actual graph shown in Figure 5.3(f) and the statistics indicate good accuracy in predicting dry density. Omitting velocity from the input parameters results in ASE increases and R^2 value decreases, even though MARE decreases. So, the results do not indicate clearly that seismic wave velocity helps to predict dry density.

Table 5.6: Comparing ANN models (predicting dry density).

Model		Model structure	ASE	MARE	R^2
Field	with velocity	4_ (3_5_100) _1	0.0032	1.81	0.91
	without velocity	3_ (4_4_2000) _1	0.0068	2.90	0.80
Lab	with velocity	4_ (4_4_100) _1	0.0056	2.52	0.85
	without velocity	3_ (4_4_500) _1	0.0051	2.42	0.86
Field plus Lab	with velocity	4_ (9_9_400) _1	0.0077	3.00	0.78
	without velocity	3_ (3_11_19800) _1	0.0087	2.94	0.75

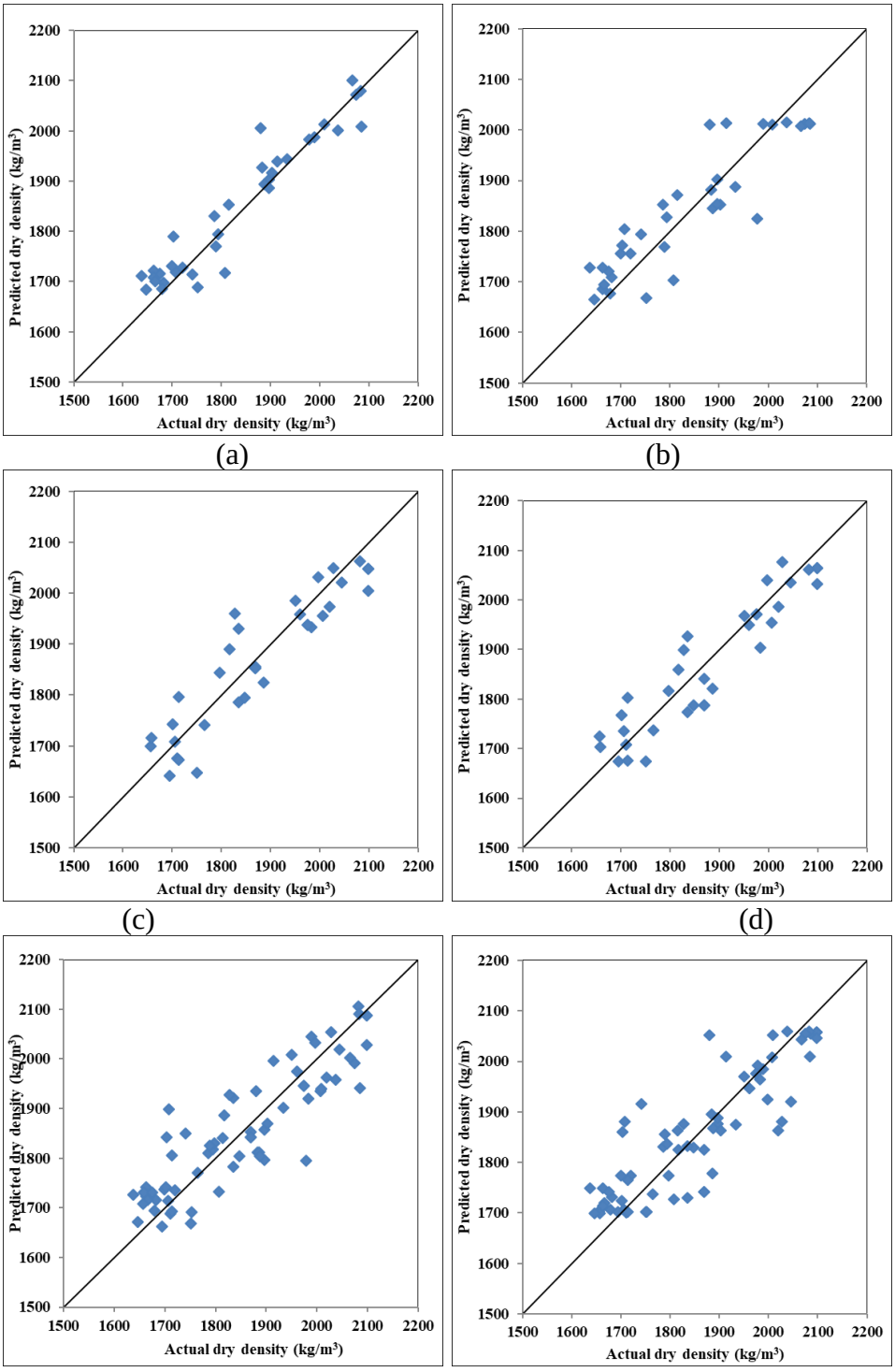

Figure 5.3: Graphical prediction accuracy of model for predicting dry density, (a) field, with velocity, (b) field, without velocity, (c) lab, with velocity, (d) lab, without velocity, (e) field plus lab, with velocity, (f) field plus lab, without velocity.

5.4 Comparison between ANN and regression models

Regression analysis is a statistical method of determining the strength and characteristics of the relationship between dependent and independent variables. Multiple linear regression analyses are performed using Excel with the same databases used for all the developed ANN models. The performance of the models is analyzed based on RMSE, MARE, ASE and R^2. Comparison between the regression models shows better coefficient of determination for the lab data than the field and lab data, and field data showed lower coefficient of determination than lab and field plus lab data. Regression analysis also resulted in better coefficient of determination for predicting water content and dry density in comparison to predicting seismic wave velocity. The lowest errors are observed in regression analysis for the case of lab data and predicting dry density for all types of data.

Table 5.7: Comparison of ANN and regression models.

Model		ANN				Regression			
		RMSE	ASE	MARE	R^2	RMSE	ASE	MARE	R^2
Predicting velocity	F	394	155616	19.3	0.37	403	162712	18.8	0.34
	L	403	162650	13.3	0.80	465	216368	15.4	0.72
	F+ L	483	233701	18.5	0.78	772	596434	30.8	0.43
Predicting water content	F	1.0	1.0	7.7	0.85	1.5	2.3	12	0.66
	L	1.0	1.0	6.6	0.89	0.9	0.9	6.5	0.88
	F+ L	1.6	2.6	11.6	0.67	1.6	2.7	12	0.66
Predicting dry density	F	2.7	7.5	1.8	0.91	4.9	24.2	3.3	0.69
	L	3.4	11.6	2.5	0.85	3.3	11.0	2.4	0.85
	F + L	4.1	17.5	3	0.78	4.4	19.5	3.1	0.75

Note: Field (F), Lab (L)

Table 5.7 presents the statistical measures for ANN and regression models. Here ASE is calculated using unnormalized actual and predicted values. For the ANN models, ASE were calculated using normalized actual and predicted values. To compare ANN models with regression models unnormalized ASE is used. Root mean squared error (RMSE) are also calculated using

Equation 4.1 to compare ANN and regression models. For all the cases, ANN models resulted in better R^2 values and less error in comparison to regression analysis. Significant improvements are observed for the case of field data for predicting water content, dry density and for field & lab data for predicting seismic wave velocity. So it appears that ANN shows better accuracy in prediction in comparison to regression analysis.

5.5 Conclusion

The aim of this study is to predict geotechnical parameters from seismic wave velocity and other geotechnical parameters using a published data set. ANN and regression models are developed to predict seismic wave velocity from geotechnical parameters and also to predict some geotechnical parameters using seismic wave velocity in conjunction with other geotechnical parameters. The geotechnical parameters used here are plasticity index, LL, dry density, and water content.

The standard procedure for ANN model development is training, testing, and validation. Due to the limited amount of data, the validation step is ignored in some cases to use more data for training. The statistics indicated that the performance of the models are improved by using more data for training as shown in Table 5.4 and Figure 5.1. Both laboratory and field data are analyzed separately and combined. The correlation between parameters for lab data is better in comparison to field and field plus lab data for both ANN and regression. The coefficient of determinations are higher, and RMSE, ASE, MARE are lower for ANN models than the regression models.

For most cases, the seismic wave velocity helps to predict water content and dry density. The results showed promising statistics for seismic wave velocity prediction models as a cost-

effective, less time-consuming, and non-destructive way to collect soil information for engineering design and analysis of infrastructures.

CHAPTER 6

PREDICTING GEOPHYSICAL PARAMETERS FROM GEOTECHNICAL PARAMETERS

6.1 Introduction

Geological and geotechnical engineers work in close cooperation to cover the essential investigation and analysis for civil engineering projects such as earth dam analysis, landslide evaluation, slope stability analysis, factor of safety evaluation for foundations, etc. Both are an integral part of a design team to complete a project. Soil parameters investigated by geotechnical methods are used for the design of foundations, retaining walls, dams, levees and so on. Geotechnical investigations are precise but are point measurements based on drilled boreholes and laboratory measurements on disturbed and undisturbed soil samples collected from the field. For a large construction area or already built infrastructure, the destructive nature and point based approach of geotechnical methods can be time-consuming and sometimes impossible to carryout. Geophysical investigations can, in many cases, create a map of the whole area without disturbing the structure and in less time than geotechnical approaches. Using geophysical information in engineering problems will help lower the project cost, and reduce completion time with higher confidence.

In this chapter, the laboratory geophysical and geotechnical measurements described in Chapter 3 are analyzed using ANN techniques. Geophysical and geotechnical experiments are conducted on the **same soil sample** compacted according to the standard proctor method. Different combinations of sand, silt and clay proportions are used to prepare clay and sandy-clay synthetic

samples

The dependence of the geophysical parameters (ER, P-wave velocity, and S-wave velocity) on geotechnical parameters is examined. The ANN outputs are geophysical properties and the inputs are various combinations of geotechnical properties. The analysis first examines the dependence on individual geotechnical inputs. Then the analysis is generalized to include multiple geotechnical inputs based on theoretical formulations in the literature, i.e., Archies's Law, Waxman Smith equation, Gassmann's formulation. These models are subsequently modified by replacing some of the geotechnical parameters with more easily obtainable geotechnical parameters to evaluate optimal measurement approaches.

6.2 Data from Laboratory Measurements

The geotechnical measurements can be subdivided into two groups. The first group is properties that depend solely on the soil type: soil mix proportions (SMP), Atterberg limits, specific surface area, SG, and CEC. There are 26 independent measurements of each parameter in this group. The second group of properties depends on the soil type and degree of compaction associated with the proctor test: moisture content and dry density, void ratio, saturation, and porosity. There are 155 measurements in this group. Cohesion is measured on a specific soil type and compacted at opt or near opt moisture, so there are 26 measurements. The measurements are compiled in Appendices A1 and A2. The data derived from the proctor test is further subdivided into below opt moisture content (77 data), at opt moisture content (26 data) and above opt moisture content (52 data). The geophysical measurements are a function of soil type and proctor compaction. Geophysical measurements at opt moisture content are used when correlated with the geotechnical measurements in group 1.

6.2.1 ER predictions from a Single Input

Statistics of ANN models to predict ER from individual geotechnical parameters are shown in Table 6.1. The overall statistics show that ER has good correlation with water content and saturation when all data are used for ANN model development. Other parameters show poor to moderate correlation with ER. The reason is that each soil measurement has other parameters that are changing. For at opt models, only 26 data are available. This limited amount of data could have an adverse effect on the prediction accuracy. Parameters related to clay type properties show relatively lower values than others.

Statistics of ANN models to predict ER using all data from water content show good correlation of ER with water content. ANN models are also developed to predict ER from water content by separately considering data at below opt, at opt, and above opt. The statistics show that accuracy of the model is better at below opt in comparison to above opt. The reason is that when the sample is close to full saturation (above opt), the conductivity remains fairly constant (Bai at al., 2013). Figure 6.1 (a) shows that with the increase of water content, ER decreases significantly below opt, but much less above opt. Increasing water content makes the sample more conductive and reduces ER. Statistics of ANN models to predict ER from saturation using all data shows that the accuracy of the model is good. Separate ANN models at below opt, at opt and above opt show that performance of the model decreases at above opt for the same reason as the water content. Figure 6.1 (b) shows that degree of saturation is inversely proportional to ER for the case of below opt, at opt and above opt. Statistics presented in Table 6.1 show that CEC is moderately correlated with ER. Figure 6.1 (c) shows that CEC is inversely correlated with ER. CEC is the capacity of the soil to hold exchangeable cations. CEC increases with the increase of clay fraction. CEC is

also affected by the type of clay minerals. Large clay fraction in the soil makes the soil more conductive and reduces ER.

Statistics show that PL can predict ER better than LL and that SL shows better accuracy and good correlation with ER in comparison to LL and PL. Figures 6.1 (d), (e), (f) show that with an increase of LL, PL, and SL, the ER decreases. The reason is that Atterberg limits are higher for soils that contain higher percentages of fines or clay, and that tends to reduce the ER (Hassanein et al., 1996). Statistics of the prediction model to predict ER from specific surface area shows that ER is moderately correlated with specific surface area. Figure 6.2 (a) shows that ER decreases with the increase of specific surface area. Specific surface area is correlated with clay size fraction (Petersen et al., 1996). Clay soils with large specific areas need more water to reach the LL (Mitchell and Soga, 2005). This means that with the increase of specific surface area, the electric conductivity increases and resistivity decreases.

Statistics of the ANN model to predict ER from cohesion shows that ER is poorly correlated with cohesion. There could be other influential parameters that are changing at the same time that may be used as inputs to get better predictions. Figure 6.2 (b) shows that with an increase of cohesion, the ER decreases. The reason is that cohesion is related to the amount of clay in the soil and is positively correlated with the increase of clay fraction (Akayuli et al., 2013). With the increase of clay fraction, electric conductivity increases so ER decreases. This makes cohesion inversely proportional to ER.

ANN models to predict ER from dry density show poor correlation. ANN models at below opt, at opt and above opt show that the sensitivity of the decreasing rate of ER is high at below opt, and that above opt sensitivity of ER to dry density is very low. Figure 6.2 (c) shows that with an increase of ER, dry density decreases for the case of below opt. But for at opt and above opt,

with the increase of dry density, ER increases. For below opt soil, with the increase of dry density, water content increases and samples become more conductive so ER decreases. Therefore dry density is inversely proportional relationship to ER. But at above opt, dry density decreases with the increase of water content and the sample becomes more conductive, so ER decreases. This indicates a directly proportional relationship between ER and dry density. ANN models built with all data show that void ratio is moderately correlated with ER. Separate ANN models at below opt, at opt and above opt predict less sensitivity of ER to void ratio at above opt in comparison to below opt. Figure 6.2 (d) shows that ER is positively correlated with void ratio at below opt and at opt, but above opt ER is negatively correlated with void ratio. At below opt, with the decrease of void ratio water content increases, so the sample becomes more conductive and ER decreases. That's why at below opt, void ratio and ER are positively correlated. At above opt, with the increase of void ratio , water content increases and ER decreases. This makes relationship between void ratio and ER at above opt inversely proportional. Statistics of ANN models to predict ER from SG show that there is almost no correlation between these two parameters. Figure 6.2 (e) implies the same thing. So it appears that ER is most sensitive to water content and saturation, less sensitive to parameters related to clay content and moisture such as CEC, Atterberg limits, surface area, even less sensitive to dry density, void ratio, and cohesion, and shows almost no sensitivity to SG.

Table 6.1: Statistical accuracy of ANN models for predicting ER from single geotechnical parameters.

Input		ANN network	ASE	MARE	R^2
Water content	All	1_ (5_5_1100) _1	0.0026	18.54	0.68
	Below opt	1_ (3_12_20000) _1	0.0061	7.20	0.64
	At opt	1_ (1_1_300) _1	0.0165	7.67	0.30
	Above opt	1_ (6_6_1200) _1	0.0086	5.85	0.23
Saturation	All	1_ (12_12_100) _1	0.0038	25.40	0.56
	Below opt	1_ (6_6_2100) _1	0.0077	11.05	0.44
	At opt	1_ (6_7_100) _1	0.0204	7.63	0.17
	Above opt	1_ (8_8_200) _1	0.0110	5.71	0.07
CEC	At opt	1_ (1_5_100) _1	0.0117	19.47	0.38
LL	At opt	1_ (2_2_3100) _1	0.0141	21.10	0.27
PL	At opt	1_ (6_6_100) _1	0.0122	21.15	0.38
SL	At opt	1_ (6_6_100) _1	0.0111	18.96	0.42
Surface area	At opt	1_ (3_3_3100) _1	0.0138	21.02	0.26
Cohesion	At opt	1_ (4_5_19100) _1	0.0150	20.56	0.19
Dry density	All	1_ (9_12_20000) _1	0.0069	35.23	0.17
	Below opt	1_ (6_12_20000) _1	0.0199	4.54	0.13
	At opt	1_ (1_3_100) _1	0.0225	3.94	0.18
	Above opt	1_ (6_6_100) _1	0.0089	3.05	0.04
Void ratio	All	1_ (2_9_20000) _1	0.0067	35.32	0.20
	Below opt	1_ (10_12_20000) _1	0.0177	10.34	0.14
	At opt	1_ (1_1_1200) _1	0.0204	9.58	0.14
	Above opt	1_ (2_9_2000) _1	0.0079	7.21	0.08
SG	At opt	1_ (1_1_100) _1	0.0189	27.42	0.005

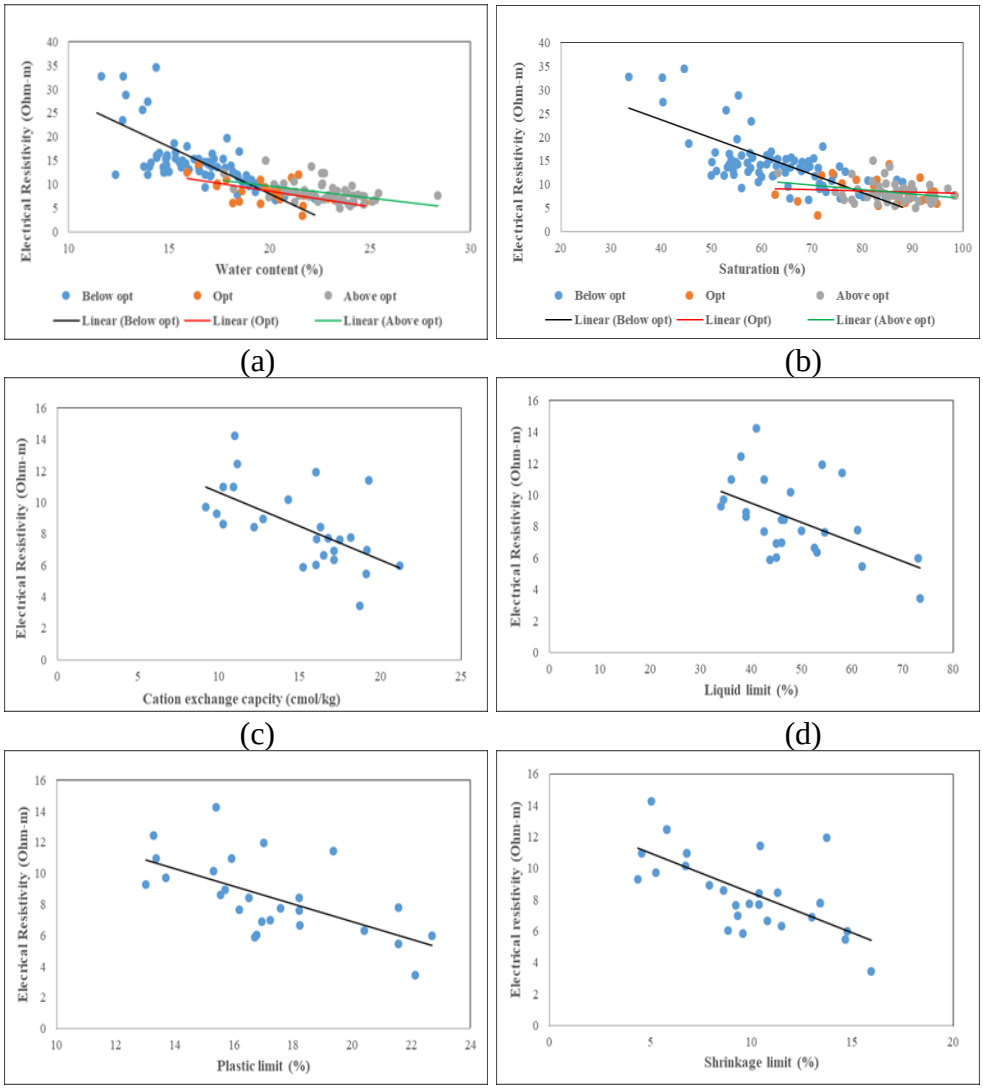

Figure 6.1: ER versus (a) water content, (b) saturation, (c) CEC, (d) LL, (e) PL, (f) SL

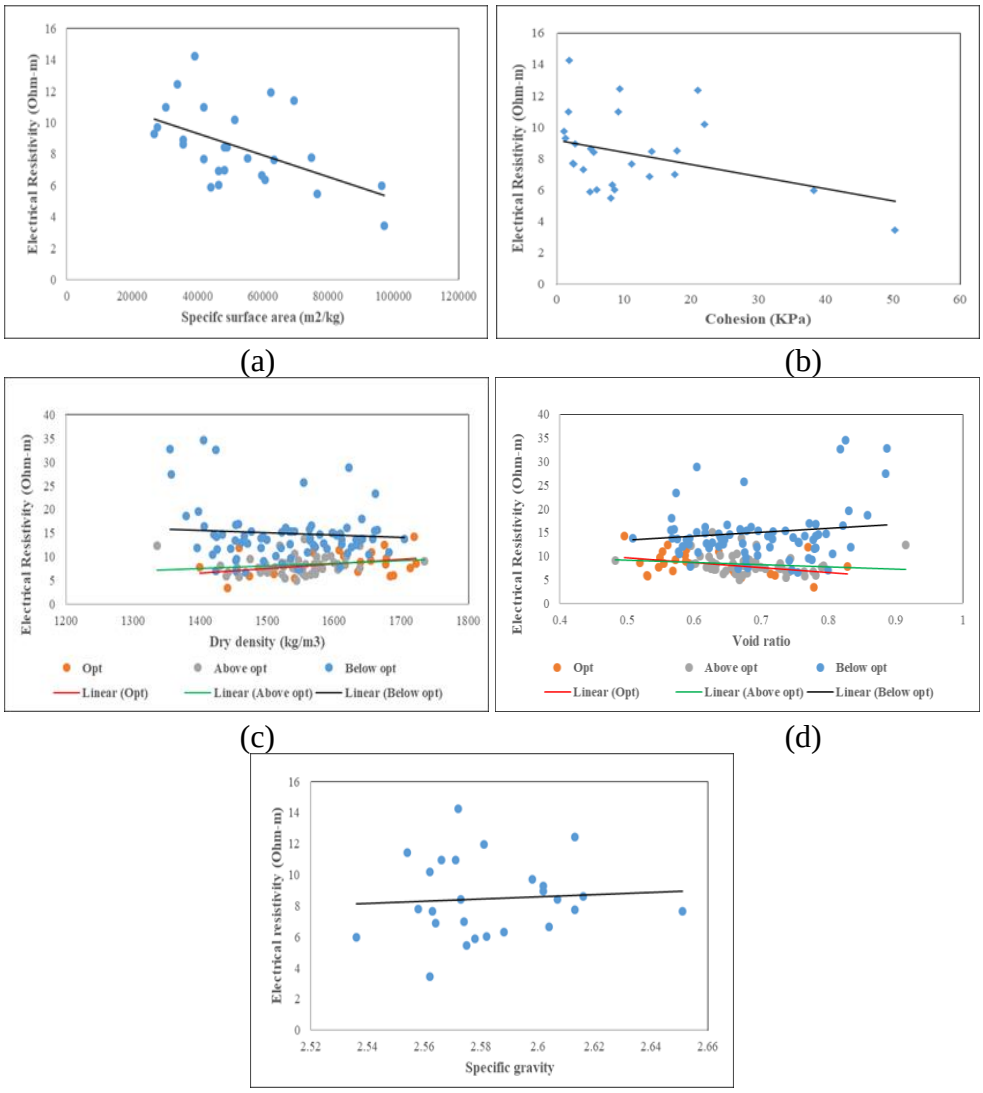

Figure 6.2: ER versus (a) surface area, (b) cohesion, (c) dry density, (d) void ratio, (e) SG.

6.2.2 Predicting ER from Multiple Inputs

Archie's (1942) first law is a relationship between the bulk resistivity of soil and the porosity for a fully-saturated clean sand or coarse-grained material. This model assumes that the primary pathway for electric current is through the pore fluid. For partially saturated sand, Archie's (1952) second law has an explicit dependence on saturation. This suggests that void ratio and saturation would be good input parameters. The assumption of clean sand is usually not valid for most soils because they contain clay minerals. The presence of clay minerals allows for electric

current to flow along the surface of the clay minerals. A measure of the clay might be accounted for by using the soil mixture proportions as input. Waxman-Smits (1968) developed a relationship for the effective electrical conductivity of soils that includes surface conduction. This surface conduction is sometimes modeled to be proportional to the CEC of the soil. Therefore, the sample CEC could be used as an input.

Various ANN models are developed for various combinations of void ratio, saturation, soil mixture proportions and CEC. The statistics of these ANN models, shown in Table 6.2., indicate that ANN model accuracy is higher when using multiple geotechnical parameters as input. At first, following Archie's second law, ER is predicted from void ratio and saturation. Statistics show that the accuracy of predicting ER from void ratio and saturation is high. To increase the prediction accuracy of the model, SMP is added as input and the results show that the accuracy of the model in predicting ER is improved. Following the Waxman Smits relationship, the CEC could be an important parameter. Two different models are developed without the soil type and then with soil type. After adding CEC with void ratio and saturation, the accuracy of the model increased and, after adding soil properties, the statistics show that the accuracy of the model in predicting ER is very high. This agrees with Waxman-Smits's law of predicting ER for soil with clay fraction.

As correlation between ER and void ratio is moderate (Table 6.1), another model is developed to predict ER from CEC and saturation and SMP, but excluding void ratio. Statistics show that the accuracy of the model is very close to the model for predicting ER with void ratio. So the void ratio has less influence on ER in comparison to CEC and saturation.

Other ANN models are developed by replacing the geotechnical parameters with more easily obtainable geotechnical parameters. It is assumed that void ratio can be replaced by dry density and saturation by water content and the CEC by the different Atterberg limits: LL, PL or SL. The

statistics of these models are shown in Table 6.3. Statistics show that accuracy of the model in predicting ER from dry density, water content, LL and SMP is high, but is lower than void ratio, saturation, CEC and SMP model. After that LL is replaced by PL to observe the difference in performance and the statistics show that accuracy of the model is improved. Replacing PL with SL improves the performance of the model even more and is very close to void ratio, saturation, CEC and SMP model. Replacing dry density by wet density shows that the performance of the model in predicting ER from wet density, water content, SL and SMP is almost the same as the model predicting ER from void ratio, saturation, CEC and SMP. Figure 6.3 shows the predicted versus actual graph of these two models. The graphs show that the two graphs are almost identical. So the best alternative combination is wet density, water content, SL and SMP. An ANN model is developed exluding dry density to predict ER, and the statistics show that the accuracy of the model has little change. Water content influences ER more in comparison to dry density. Several other ANN models are developed to predict ER from different combinations of geotechnical parameters. ER is predicted from saturation, SL, and SMP, and also from water content, CEC, and SMP. The statistics show that the accuracy of both models is high. ER is also predicted from water content, saturation, SL and SMP, and the accuracy of the model is very high - almost the same as the model predicting ER from wet density, water content, SL and SMP.

Table 6.2 : Statistical accuracy measures of ANN models for predicting ER from multiple geotechnical parameters (validation of Archie's and Waxman smith's formula)

Input	ANN network	ASE	MARE	R^2
Void ratio, saturation	2_ (2_12_20000) _1	0.0017	17.59	0.79
Void ratio, saturation, SMP	5_ (2_3_13100) _1	0.0012	16.42	0.85
Void ratio, saturation, CEC	3_ (2_7_20000) _1	0.0013	16.28	0.83
Void ratio, CEC, saturation, SMP	7_ (1_8_20000) _1	0.0007	13.78	0.90
Saturation, CEC, SMP	5_ (4_9_19100) _1	0.0009	15.91	0.88

Table 6.3: Statistical accuracy measures of ANN models for predicting ER from multiple geotechnical parameters (using different combinations of geotechnical parameters as input)

Input	ANN network	ASE	MARE	R^2
Dry density, water content, LL, SMP	6_ (2_2_600) _1	0.0021	17.74	0.77
Dry density, water content, PL, SMP	6_ (5_7_14100) _1	0.0009	15.19	0.88
Dry density, water content, SL, SMP	6_ (1_12_5000) _1	0.0008	14.80	0.89
Wet density, water content, SL, SMP	6_ (4_12_5900) _1	0.0008	13.98	0.90
Water content, SL, SMP	5_ (9_10_7100) _1	0.0016	16.89	0.80
Saturation, SL, SMP	5_ (1_3_20000) _1	0.0012	16.93	0.84
Water content, CEC, SMP	5_ (5_11_1100) _1	0.0016	18.49	0.81
Water content, saturation, SMP	5_ (8_12_19200) _1	0.0008	14.93	0.89

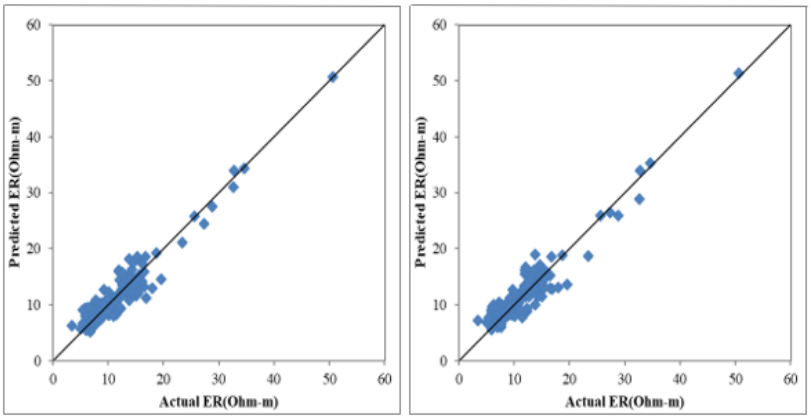

(a) (b)

Figure 6.3: Predicted versus actual graph of predicting ER from (a) void ratio, saturation, CEC, soil mix proportion, (b) wet density, water content, SL, soil mix proportion.

6.3 Predicting P-Wave

6.3.1 Single Input

The statistics of the ANN models are shown in Table 6.4. Overall statistics show that the correlations are poor except for dry density and void ratio, specifically at opt. The experimental setup is such that multiple parameters are varying at the same time. So it is expected that the

sensitivity will be less with individual parameters with P-wave velocity. At opt showed good sensitivity because at opt there is less variability in comparison to below and above opt. There are multiple points below opt and above opt for a single soil mix proportions with varying dry density and water content, which is adding more variability. Even though in that case, at opt data are limited and the presence of less variability is the reason for having better correlation than below and above opt.

P-wave velocity is predicted from water content, dry density, void ratio and saturation separately for the data at below opt, opt and above opt. Dry density has sensitivity at below opt and above opt, with a good sensitivity at opt in comparison to below and above opt. Void ratio is sensitive at opt and above opt. But the performance in predicting P-wave velocity from individual geotechnical parameters is not good. Statistics show that saturation has sensitivity at below and at opt and water content has sensitivity at below opt. The relationship pattern of P-wave velocity with water content, dry density, void ratio and saturation are also analyzed. P-wave velocity depends on bulk modulus, mass density and shear modulus. With the increase of dry density, P-wave velocity increases because for fluid-filled particulate material like soil, bulk modulus is a function of void ratio, bulk density of fluid, bulk density of skeleton, bulk density of solid grains, and mass density is a function of fluid saturation, void ratio, density of fluid, and density of grains. Here, P-wave velocity is dominated by bulk modulus more than mass density. Bulk modulus is inversely proportional to void ratio. So velocity increases with the decreases of void ratio and increases with the increases of dry density, as shown in Figures 6.4 (d) and (b). Bulk modulus is positively correlated with saturation. That's why with the increase of water content/ degree of saturation, bulk modulus increases, which causes an increase of P-wave velocity as shown in Figures 6.4 (a) and (b). Statistics show that LL, PL, SL, SG, specific surface area, and CEC are poorly correlated

with P-wave velocity. These geotechnical parameters are strongly dependent on the consistency of the clay soils and clay fractions. Whereas P-wave velocity depends on lots of other factors also, such as stiffness, mass density, confinement, stress, soil skeleton, etc., it is not possible to have good correlation from those individual parameters with P-wave velocity. For this research cohesion is determined from unconfined compression tests by compacting the separate sample following the same water content and soil proportions with an aim to replicate the same sample used for determining P-wave velocity. Statistics show cohesion is poorly correlated with P-wave velocity. This could be a confinement issue, for a change in soil skeleton in the replicated soil sample as well as other influencing parameters that need to be added to predict P-wave velocity. So further ANN models are developed to predict P-wave velocity from multiple geotechnical parameters.

Table 6.4: Statistical accuracy measures of ANN models for predicting P-wave velocity from single geotechnical parameters.

Input		ANN network	ASE	MARE	R^2
Dry density	Below opt	1_ (7_10_6100) _1	0.0108	11.50	0.14
	At opt	1_ (2_4_8100) _1	0.0105	11.43	0.38
	Above opt	1_ (2_4_20000) _1	0.0137	12.43	0.12
Void ratio	Below opt	1_ (1_1_100) _1	0.0125	12.42	0.01
	At opt	1_ (2_4_7100) _1	0.0103	11.10	0.39
	Above opt	1_ (2_5_500) _1	0.0257	18.26	0.12
Saturation	Below opt	1_ (3_3_19100) _1	0.0109	11.77	0.12
	At opt	1_ (1_1_600) _1	0.0147	14.02	0.19
	Above opt	1_ (1_1_400) __1	0.0161	13.96	0.04
Water content	Below opt	1_ (1_1_400) _1	0.0108	11.50	0.1
	At opt	1_ (1_1_100) _1	0.0172	14.59	0.0004
	Above opt	1_ (2_7_19900) _1	0.0155	13.08	0.03
LL	At opt	1_ (4_4_600) _1	0.0171	14.57	0.0002
PL	At opt	1_ (5_5_19600) _1	0.0168	14.16	0.005
SL	At opt	1_ (4_4_5100) _1	0.0168	14.46	0.004
SG	At opt	1_ (1_1_1100) _1	0.0170	14.41	0.0005
Surface area	At opt	1_ (4_4_19200) _1	0.0182	15.12	0.004
CEC	At opt	1_ (1_1_8800) _1	0.0125	14.35	0.001
Cohesion	At opt	1_ (1_1_100) _1	0.0292	185.07	0.003

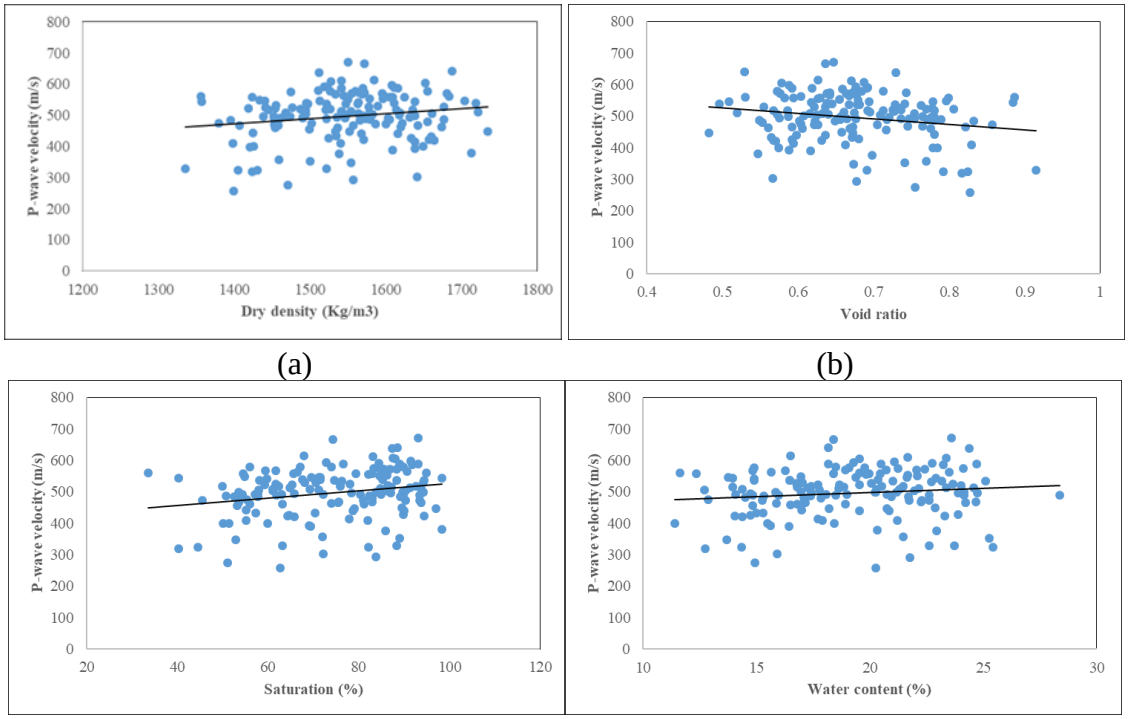

Figure 6.4: P-wave velocity versus (a) dry density, (b) void ratio, (c) saturation, (d) water content.

6.3.2 Multiple Input

P-wave velocity increases with the stiffness of the material and decreases with its mass density (inertia). For fluid-filled porous media, the effective bulk modulus is provided by Gassmann (see equation 2.25). Seismic wave propagation in granular materials like soil is more complicated due to the complex behavior of the solid skeleton that depends on the "strength" of the grain contacts. The grain contacts are influenced by the applied effective stress and internal forces associated with capillary forces and electrical forces at the grain surface. The P-wave velocity can also be dependent on the degree of compaction and cementation.

Based on the models for the individual parameters (Table 6.4), ANN models are developed for dry density, water content and SMP as inputs. Separate ANN models are developed for the data at below opt moisture, at opt moisture and above opt moisture. The statistics of the ANN models are shown in Table 6.5. The statistics show that after adding multiple geotechnical parameters as

inputs, the prediction accuracy increases significantly. At first, P-wave velocity is predicted from dry density, water content and SMP. At below opt, the accuracy of predicting ER is high. The accuracy of the model for predicting P-wave velocity at opt is high in comparison to below opt. Performance of the ANN model at above opt is moderate and accuracy is low in comparison to below and at opt ANN models. After that, ANN models are developed to predict P-wave velocity from void ratio, saturation and SMP. At below opt and opt, the accuracy of the model in predicting P-wave velocity if high, and at above opt the accuracy is moderate. The at opt model shows the best performance among the three models. And the performance of the models in predicting P-wave from water content, dry density, void ratio, and saturation are very close to each other. Water content, dry density, void ratio, saturation and SMP are combined to predict P-wave velocity. The performance of the model did not improve after combining water content, dry density, saturation and void ratio. Here, at below and at opt models showed better accuracy in predicting P-wave velocity in comparison to ANN model at above opt.

Table 6.5: Statistical accuracy measures of ANN models for predicting P-wave velocity from multiple geotechnical parameters.

Input		ANN network	ASE	MARE	R^2
Dry density, water content, SMP	Bellow opt	5_ (10_11_4100) _1	0.0032	6.40	0.74
	At opt	5_ (4_5_900) _1	0.0030	5.80	0.84
	Above opt	5_ (3_3_20000) _1	0.0081	9.42	0.49
Void ratio, saturation, SMP	Bellow opt	5_ (10_12_20000) _1	0.0030	6.15	0.76
	At opt	5_ (6_7_100) _1	0.0039	6.07	0.79
	Above opt	5_ (9_9_4300) _1	0.0089	9.77	0.45
Dry density, water content, void ratio, saturation, SMP	Bellow opt	7_ (7_8_2100) _1	0.0033	6.42	0.74
	At opt	7_ (2_3_700) _1	0.0041	6.44	0.77
	Above opt	7_ (3_3_2100) _1	0.0092	10.33	0.43

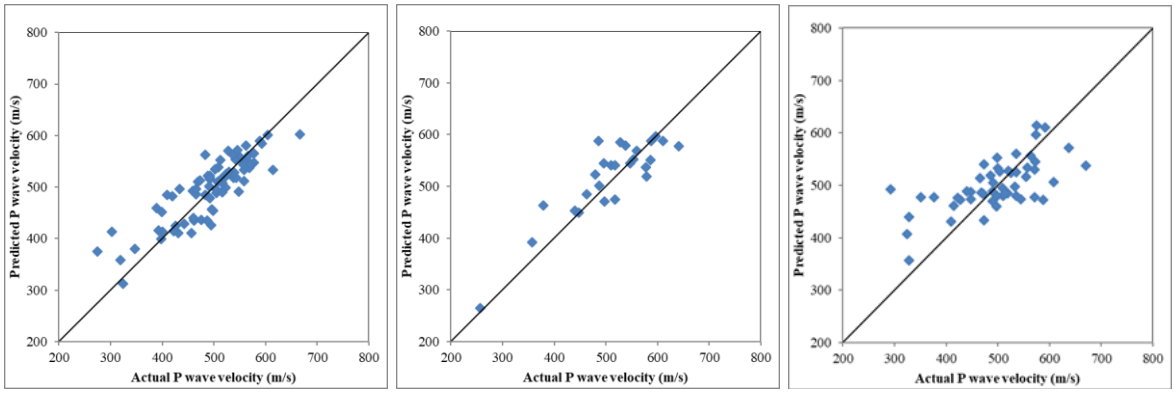

(a) (b) (c)

Figure 6.5: Predicted versus actual graph of predicting P-wave velocity from (a) dry density, water content, void ratio, saturation, soil mix proportion at below opt, (b) opt, (c) above opt.

The predicted versus actual graph for predicting P-wave velocity from water content, saturation, void ratio, dry density and SMP are shown in Figure 6.5. The graphs also show that data are well aligned with a 45-degree line at below, at opt and scattered at above opt. From the analysis, it is evident that P-wave velocity is correlated with water content, saturation, dry density, saturation and SMP, all of which play an important role in predicting P-wave velocity. Though the individual parameters do not show good performance combined, those parameters show high accuracy in predictions. As all the parameters are changed together and they all are correlated with P-wave velocity, using only one parameter to predict P-wave velocity cannot show good accuracy. To get better accuracy in performance, influencing parameters should be combined as input for predicting P-wave velocity.

6.4 Predicting S-Wave

6.4.1 Single Input

The statistics of the ANN models are shown in Table 6.6. Overall statistics show that the correlations are poor. The experimental setup is such that multiple parameters are varying at the same time. So it is expected that there will be less sensitivity with individual parameters with S-wave velocity. At opt showed good sensitivity because at opt there is less variability in comparison

to below opt and above opt. There are multiple points at below and at above opt for a single soil mix proportions with varying dry density and water content, which is adding more variability.

The statistics of the ANN models for individual geotechnical parameters are shown in Table 6.6. S-wave velocity is also predicted from water content, dry density, void ratio and saturation separately for the data at below opt, opt and above opt. Dry density and void ratio are sensitive to S-wave velocity at opt. Statistics show that water content has sensitivity at below opt and saturation has sensitivity at opt. The relationship pattern of S-wave velocity with water content, dry density, void ratio and saturation are also analyzed. S-wave velocity does not depend on bulk modulus like P-wave velocity but depends on shear modulus and mass density. S-wave is more dominated by shear modulus than mass density. Mass density is a function of saturation and void ratio. At the presence of water, the soil shear modulus of the granular skeleton remains unaffected. So, shear modulus depends on void ratio. With the decrease of void ratio, shear modulus increases which causes an increase of S-wave velocity. Dry density increases along with S-wave velocity due to the decrease in void ratio. Saturation and water content are shown to be inversely proportional to S-wave velocity because saturation is proportional to mass density and mass density is inversely proportional to S-wave velocity.

Statistics show that LL, PL, SG, specific surface area and CEC are poorly correlated with S-wave velocity. These geotechnical parameters are strongly dependent on the consistency of the clay soils, and clay fractions. Whereas S-wave velocity depends on lots of other factors also, such as stiffness, mass density, confinement, stress, soil skeleton, etc., it is not possible to have good correlation from those individual parameters with S-wave velocity. Statistics show the sensitivity of S-wave velocity to SL. For this research, cohesion is determined from unconfined compression tests by compacting the separate sample following the same water content and soil proportions

with an aim to replicate the same sample used for determining S-wave velocity. Statistics show cohesion is not correlated with S-wave velocity. This could be a confinement issue, for change in soil skeleton in the replicated soil sample as well as other influencing parameters that need to be added to predict S-wave velocity. So further ANN models are developed to predict S-wave velocity from multiple geotechnical parameters.

Table 6.6: Statistical accuracy measures of ANN models for predicting S-wave velocity from single geotechnical parameters.

Input		ANN network	ASE	MARE	R^2
Dry density	Below opt	1_ (2_2_15100) _1	0.0006	10.80	0.01
	At opt	1_ (1_2_400) _1	0.0123	9.57	0.16
	Above opt	1_ (1_1_300) _1	0.0273	16.74	0.00003
Void ratio	Below opt	1_ (1_2_19800) _1	0.0064	10.86	0.02
	At opt	1_ (1_6_1000) _1	0.0129	9.85	0.13
	Above opt	1_ (5_5_6100) _1	0.0272	16.58	0.005
Saturation	Below opt	1_ (3_3_19100) _1	0.0065	10.75	0.002
	At opt	1_ (3_3_400) _1	0.0132	10.04	0.10
	Above opt	1_ (1_1_1100) _1	0.0272	16.87	0.009
Water content	Below opt	1_ (2_5_6700) _1	0.0047	10.13	0.27
	At opt	1_ (1_1_100) _1	0.0148	10.59	0.003
	Above opt	1_ (9_9_2100) _1	0.0268	16.55	0.02
LL	At opt	1_ (1_6_20000) _1	0.0143	9.79	0.01
PL	At opt	1_ (1_1_300) _1	0.0146	10.42	0.01
SL	At opt	1_ (5_6_20000) _1	0.0119	8.82	0.17
SG	At opt	1_ (1_1_300) _1	0.0146	10.46	0.02
Surface area	At opt	1_ (2_2_100) _1	0.0152	10.75	0.01
CEC	At opt	1_ (1_1_500) _1	0.0147	10.45	0.002
Cohesion	At opt	1_ (6_6_20000) _1	0.0286	177.53	0.02

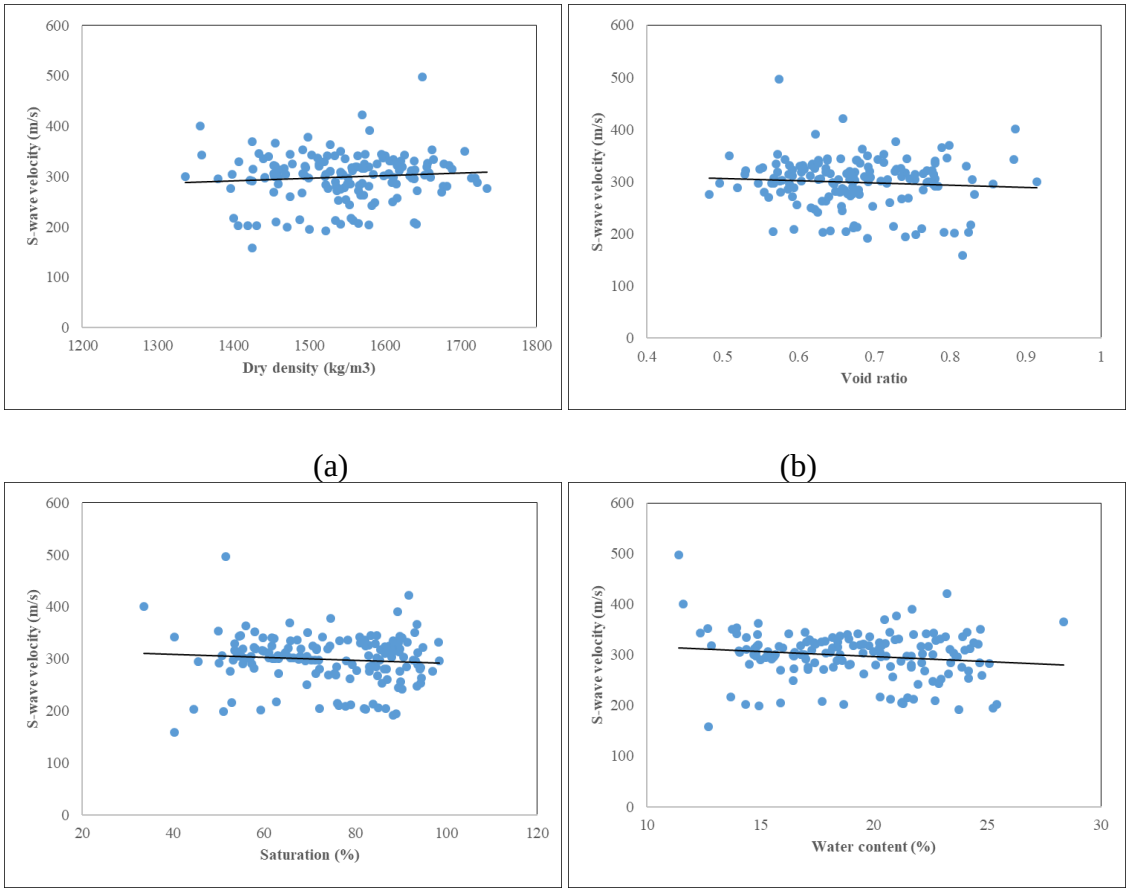

Figure 6.6: S-wave velocity versus (a) dry density, (b) void ratio, (c) saturation, (d) water content.

6.4.2 Multiple input

For fluid-filled porous media, the description is provided by Gassmann (see equation 2.25) and does not have a fluid effect on the shear modulus. However, the S-wave propagation in granular materials is influenced by the applied effective stress and internal forces associated with fluid capillary forces and electrical forces at the grain surface. The S-wave velocity can also be dependent on the degree of compaction and cementation. Based on the models for the individual parameters (Table 6.6), ANN models are developed for dry density, water content and SMP as inputs. Statistics of the ANN models in predicting S-wave velocity are shown in Table 6.7.

Statistics show that after adding multiple parameters as input, the prediction accuracy increases significantly.

At first S-wave velocity is predicted from water content, dry density and SMP. At below opt, the accuracy of the model in predicting S-wave velocity is good. Statistics at opt show that accuracy of the model is moderate. At above opt the accuracy of the ANN model is poor. After that, S-wave velocity is predicted from void ratio, saturation and SMP. Similar phenomena are observed as with the ANN models predicting S-wave velocity from dry density, water content, and SMP. At below opt, the accuracy is good; at opt, the accuracy is moderate; and at above opt, the accuracy is poor. Water content, dry density, void ratio, saturation and SMP are combined to predict S-wave velocity. Statistics show that the performance did not improve after combining water content, dry density, void ratio and saturation. SL is added along with the other geotechnical parameters of the previous model. The statistics show that at below opt the performance of the model did not improve but at opt and above opt the performance of the model improved significantly. The predicted versus actual graph of predicting S-wave velocity from water content, dry density, void ratio, saturation, SL and SMP are shown in Figure 6.7. Graphs show that the data are aligned with 45-degree line with little scattering. At above opt, data are more scattered in comparison to below and at opt. At above opt, most of the models show poor performance in predicting S-wave velocity. From the analysis it is evident that S-wave velocity is correlated with water content, saturation, dry density, saturation and SMP – all of which play an important role in predicting S-wave velocity. Though the individual parameters did not show good performance, combined those parameters showed high accuracy in predictions. As all the parameters are changed together and they all are correlated with S-wave velocity, using only one parameter to

predict S-wave velocity cannot show good accuracy. To get better accuracy in performance, influencing parameters should be combined as input for predicting S-wave velocity.

Table 6.7: Statistical accuracy measures of ANN models for predicting S-wave velocity from multiple geotechnical parameters.

Input		ANN network	ASE	MARE	R^2
Dry density, water content, soil mix proportion	Below opt	5_ (4_5_4100) _1	0.0022	7.22	0.66
	At opt	5_ (3_3_5000) _1	0.011	8.52	0.24
	At above opt	5_ (8_8_300) _1	0.026	16.66	0.03
Void ratio, saturation, soil mix proportion	Below opt	5_ (1_2_20000) _1	0.0030	8.75	0.53
	At opt	5_ (4_4_3800) _1	0.0109	8.58	0.25
	At above opt	5_ (9_9_100) _1	0.0226	16.71	0.02
Dry density, water content, void ratio, saturation, soil mix proportion	Below opt	7_ (2_2_20000) _1	0.0027	8.31	0.58
	At opt	7_ (2_2_3900) _1	0.0106	8.21	0.27
	At above opt	7_ (5_5_100) _1	0.0270	16.77	0.02
Dry density, water content, void ratio, saturation, SL, soil mix proportion	Below opt	8_ (3_3_5100) _1	0.0032	9.02	0.51
	At opt	8_ (1_3_100) _1	0.0072	8.09	0.53
	At above opt	8_ (4_6_1100) _1	0.0141	10.74	0.49

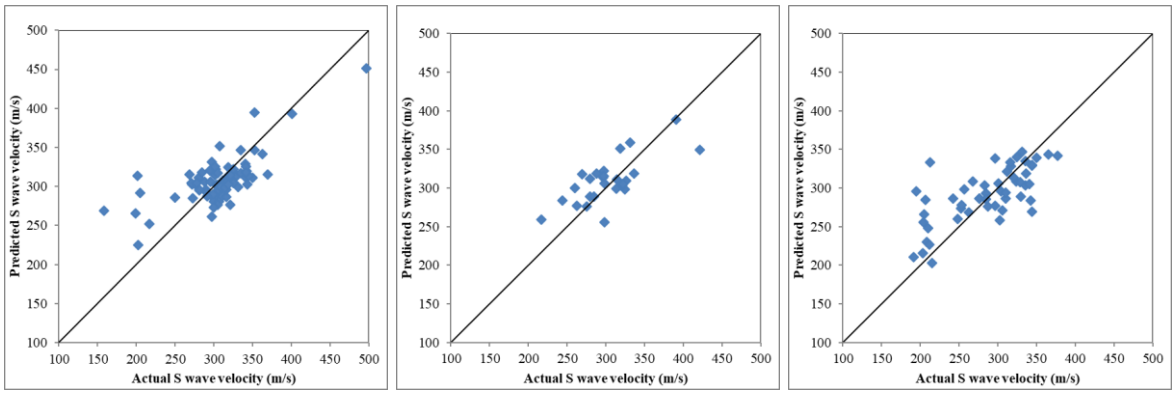

(a) (b) (c)

Figure 6.7: Predicted versus actual graph of predicting S-wave velocity from (a) dry density, water content, void ratio, saturation, SL, soil mix proportion at below opt, (b) at opt.

6.5 Conclusion

Three geophysical parameters - ER, P-wave and S-wave velocity - are predicted from geotechnical parameters for clay and sandy clay soils through ANN model development.

The analysis shows that water content and saturation have good correlation with ER; CEC, LL, PL, SL, surface area, void ratio have moderate correlation with ER; cohesion and dry density have poor correlation with ER; and SG has almost no correlation with ER.

Water content and saturation are inversely correlated with ER. This is because an increase of water content and saturation allows more current through the interconnecting pores and is consistent with Archie's Law. ER deceases as the LL, PL, SL, specific surface area, CEC, and cohesion increase. These geotechnical parameters are correlated with clay fraction. With the increase of clay fraction, LL, PL, SL, and specific surface area increase and make the sample more conductive thereby reducing ER. With the increase of ER, dry density decreases for the case of below opt. But at opt and above opt, with the increase of dry density ER increases. At below opt, with the increase of dry density, water content increases, samples becomes more conductive, and so ER deceases. But at above opt, dry density decreases with the increase of water content as the sample is becoming more conductive, so ER deceases. The relationship of void ratio with ER is just the opposite of dry density.

Multiple geotechnical parameters can predict ER with high accuracy. Prediction models of ER from void ratio, CEC, saturation, SMP showed very high accuracy, which agrees with the Waxman-Smits formula. Void ratio can be replaced by wet/ dry density, saturation by water content, and CEC by Atterberg limits to predict ER with similar accuracy. Void ratio and dry density are less sensitive to ER in comparison to saturation and water content.

Water content, dry density, saturation, and void ratio show poor correlation with P-wave velocity when used individually. In general, P-wave velocity increases with an increase of water content, dry density and saturation, and decreases with the increase in void ratio. Atterberg limits, SG, specific surface area, and CEC are not sensitive to P-wave velocity. Cohesion did not show

sensitivity with P-wave velocity. After combining geotechnical parameters, the ANN prediction models showed good accuracy in predicting P-wave velocity. P-wave velocity can be predicted from water content, dry density, and SMP with high accuracy at below opt moisture content and at opt but with moderate accuracy at above opt moisture content. Void ratio, saturation, and SMP can also predict P-wave velocity with high accuracy at below and opt and moderate accuracy at above opt. Combining water content, dry density, void ratio, saturation and soil mix proportion did not improve the performance of predicting P-wave velocity.

Water content, dry density, saturation, and void ratio showed little sensitivity to S-wave velocity when used individually. However, in general S-wave velocity increases with the increase of dry density and decreases with the increase of water content, saturation and void ratio. Atterberg limits, SG, specific surface area, and CEC are not sensitive to S-wave velocity, but SL has sensitivity to S-wave velocity. Cohesion did not show sensitivity with S-wave velocity. After combining geotechnical parameters, the ANN prediction models improved. S-wave velocity can be predicted from water content, dry density, and SMP with good accuracy below opt water content and with moderate accuracy at opt. Void ratio, saturation, and SMP can also predict S-wave velocity with good accuracy at below opt moisture content and moderate accuracy at opt. Combining water content, dry density, void ratio, saturation and soil mix proportion did not improve the performance of predicting S-wave velocity.

CHAPTER 7

PREDICTING GEOTECHNICAL PARAMETERS FROM GEOPHYSICAL PARAMETERS

7.1 General

Correlations between geophysical and geotechnical parameters are necessary for optimal use of geophysical information in engineering assessments. In this chapter, ANN models are developed to evaluate the added benefit of including geophysical information to predict geotechnical parameters. For example, to what accuracy can geophysical parameters along with an estimate of the SMP be used to predict geotechnical parameters for a large area in order to minimize the time and effort. Geophysical parameters, namely ER, S-wave, P-wave velocities, are used separately as inputs for predicting geotechnical parameters. Geotechnical parameters of interest are: Atterberg limits, SG, cohesion, CEC, surface area, water content, dry density, void ratio, and saturation. ANN models are developed to predict individual geotechnical parameters from one geophysical parameter and the SMP. The ANN models are then generalized to predict multiple geotechnical parameters. For P-wave and S-wave velocity, ANN models are developed separately for data at below opt moisture, at opt moisture content, and above opt moisture content.

7.2 Using ER as input

Chapter 6 described models to predict ER from individual geotechnical parameters. Water content and saturation have good correlation with ER. LL, PL, SL, CEC, void ratio, and surface area have moderate correlation, and cohesion and dry density showed poor correlation

Incorporating multiple parameters as input improved the performance of the prediction models. In this section, the ER along with SMP are used as inputs to predict geotechnical parameters.

ER measurements at opt or near opt water content (total 26 data) are used for ANN model development for cohesion and soil type related properties and do not change with compaction such as: Atterberg limits (LL, PL, SL), SG, CEC, and specific surface area. As the number of data is limited for these cases, the validation step is excluded in order to use more data for training. For other geotechnical parameters, such as water content, dry density, void ratio and saturation, the data at different compaction stages are used (155 data points), and the entire ANN model development approach (training, testing, validation, all trained) is followed.

7.2.1 Single geotechnical output

The statistical accuracy of the ANN models for predicting individual geotechnical parameters from ER along and SMP is shown in Table 7.1. The performance of the models varies as expected. In general, it appears that properties related to clay content are the best, followed by moisture related properties, and then porosity related properties. This agrees with the behavior of ER for clay containing soils.

Table 7.1: Statistical accuracy measures of predicting single geotechnical parameters from ER and SMP.

Input	Output	ANN network	ASE	MARE	R^2
SMP, ER	LL	4_ (2_2_100) _1	0.0027	4.80	0.89
SMP, ER	PL	4_ (1_6_100) _1	0.0013	2.80	0.95
SMP, ER	SL	4_ (3_3_100) _1	0.0043	11.78	0.84
SMP, ER	Cohesion	4_ (4_6_3100) _1	0.0018	48.12	0.93
SMP, ER	Surface area	4_ (2_4_2100) _1	0.0014	5.23	0.93
SMP, ER	CEC	4_ (5_5_300) _1	0.0046	7.65	0.86
SMP, ER	Saturation	4_ (1_5_20000) _1	0.0040	7.59	0.78
SMP, ER	Water content	4_ (10_10_7100) _1	0.0045	7.62	0.70
SMP, ER	Dry density	4_ (1_3_20000) _1	0.0051	2.17	0.68
SMP, ER	Void Ratio	4_ (7_8_20000) _1	0.0046	5.53	0.67
SMP, ER	SG	4_ (1_1_200) _1	0.0118	0.65	0.29

ANN models for predicting LL, PL, and SL show high accuracy. Atterberg limits are the water content limits that separate different phases of soil, such as semi-liquid, plastic and solid. These parameters are very well related to soil type and clay content. ER is also sensitive to water and clay content. So, predicting Atterberg limits from ER along with SMP gives high accuracy.

Table 7.1 shows the ASE, MARE and R^2 values for the ANN model to predict cohesion. SMP and the ER at opt or near opt moisture content (26 samples) are used. The statistics show high accuracy of the model in predicting cohesion. High accuracy in predicting cohesion might be attributed to the ER dependence on the surface conductivity of the cohesive soil.

Specific surface area also shows very high accuracy. Specific surface area of soil is related to water holding capacity, permeability, and swelling properties, and is closely associated with the ER sensitivity to the clay fraction.

The accuracy of the model for predicting CEC is also high. CEC is an important soil parameter which correlates with soil index properties, surface area, cement stabilized soil and swelling properties of bentonite. CEC depends on grain size distribution, the type and amount of

clay mineral, PH values, and the presence of organic matter. Since CEC is a time-consuming test, the use of ER may help to predict CEC in the lab and evaluate the CEC for large field areas.

The prediction model for saturation also shows high accuracy and this supports the relationship of the geotechnical parameters with the soil type and ER with water. Table 7.1 shows that the accuracy of the model for predicting water content is high. ER, which is affected by the water content, taken along with the soil mix proportions helps to predict water content. The models built for predicting void ratio and dry density show less coefficient of determination in comparison to the water content and saturation. This indicates lower sensitivity of ER to dry density and void ratio in comparison to saturation and water content.

The model using the ER at opt moisture content and SMP to predict SG is moderate. This means that there are other influential parameters that must be considered as inputs to increase the accuracy of the model. Only ER and SMP cannot predict SG well.

7.2.2 Multiple geotechnical outputs

Based on the previous results the geotechnical parameters are grouped based on dependence on clay, moisture content and void space. ER and SMP are used as inputs for Atterberg limits. Three output parameters are predicted using four input parameters. The statistics of the model shown in Table 7.2 indicate that ER and SMP are capable of predicting LL, PL, and SL with high accuracy. The accuracy of the combined output model is within the single output models. CEC is added to the output parameters now having four output parameters predicted from four inputs. The accuracy of this model is higher than the previous model. Again the accuracy lies with the model accuracy for the individual parameters.

Table 7.2: Statistical accuracy measures of predicting multiple geotechnical parameters from ER and SMP

Input	Output	ANN network	ASE	MARE	R^2
SMP, ER	LL, PL, SL	4_ (2_2_100) _3	0.0037	8.10	0.86
SMP, ER	LL, PL, SL, CEC	4_ (2_2_200) _4	0.0033	7.14	0.88
SMP, ER	Water content, Saturation	4_ (4_5_20000) _2	0.0049	4.96	0.68
SMP, ER	Dry density, Void ratio	4_ (4_5_19900) _2	0.0048	3.81	0.67
SMP, ER	Water content, Dry density, Void ratio, Saturation	4_ (1_3_20000) _4	0.0049	5.97	0.69

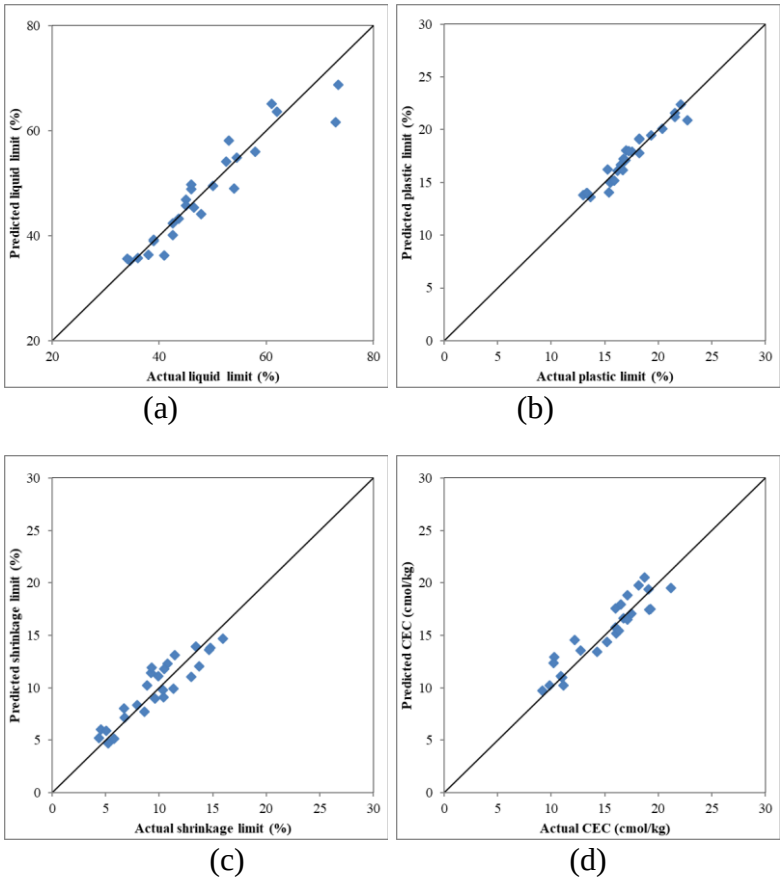

Figure 7.1: Predicted versus actual graph for predicting (a) LL, (b) PL, (c) SL, (d) CEC from soil mix proportion and ER.

The graphs of predicted versus actual for the LL, PL, SL, and CEC are shown in Figure 7.1. Figure 7.1 (a) shows a scattering of two data on the upper side, but overall the pattern is good. All the data are well aligned with the 45-degree line indicating the high accuracy of the model.

Water content and saturation depend on moisture whereas void ratio and dry density are based on porosity. The performance of the ANN model, shown in Table 7.2, is similar for both sets of parameters. The accuracy is close to the models for the individual parameters. Given the similarity in performance, a model is developed for water content, dry density, void ratio, and saturation. The statistics of the model indicate that there is no loss in accuracy by going to four output parameters. Figure 7.2 shows the predicted versus actual graph of water content, dry density, saturation and void ratio of these models. Well aligned data with the 45-degree lines indicates the good accuracy of the model.

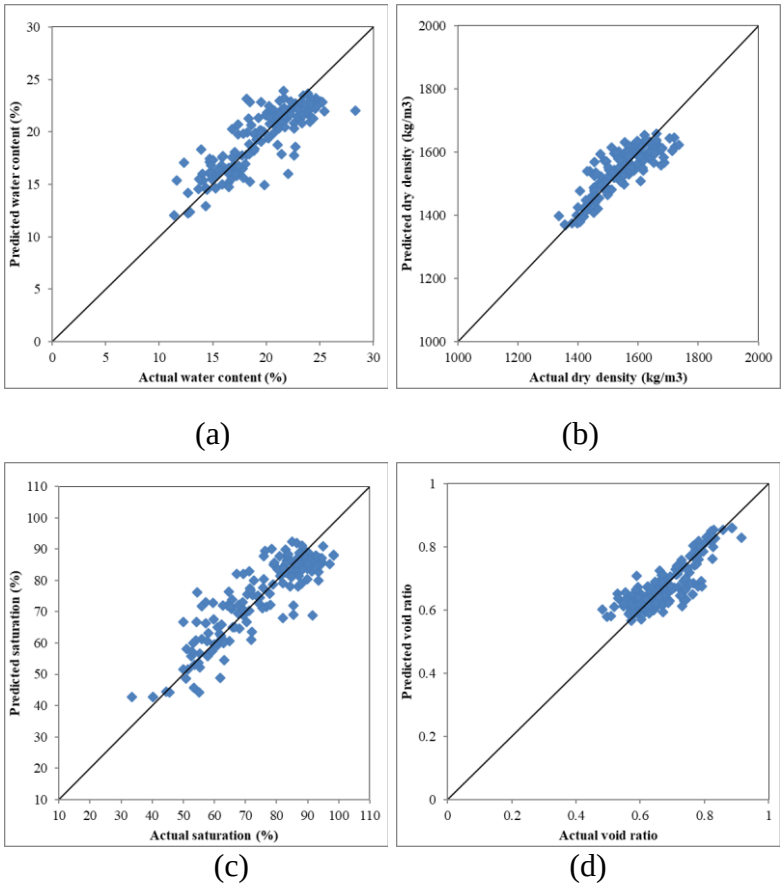

Figure 7.2: Predicted versus actual graph for predicting (a) water content, (b) dry density, (c) saturation, (d) void ratio from soil mix proportion, LL and ER.

7.3 Using P-wave as input

In Chapter 6 it is shown that Atterberg limits, SG, CEC, cohesion (unconfined shear strength) and surface area have almost no correlation with P-wave velocity. P wave velocity showed better dependence on water content, dry density, saturation and void ratio. In this section, models are developed for predicting these properties from P wave velocity and SMP. ANN models are developed separately for the data at below opt moisture content (77 data), at opt moisture (26 data) and above opt moisture content (52 data). Since the number of data at opt moisture is limited, the validation step is excluded in the ANN approach.

7.3.1 Single geotechnical output

The statistics of the models developed to predict water content, dry density, saturation and void ratio from P-wave velocity are shown in Table 7.3. The models based on P wave velocity as input are not as consistent as models using ER. The best models are for the dry density below and at opt moisture content and the void ratio. This may be because the density is indicative of the compaction which will be reflected in the soil stiffness that controls the P wave velocity.

Table 7.3: Statistical accuracy measures of predicting single geotechnical parameters from P-wave velocity and SMP.

Input	Output		ANN network	ASE	MARE	R^2
SMP, P	Water content	Below opt	4_ (10_12_19900) _1	0.0106	9.08	0.37
		At opt	4_ (1_1_100) _1	0.0105	6.15	0.53
		Above opt	4_ (1_1_15100) _1	0.0063	4.84	0.43
SMP, P	Dry density	Below opt	4_ (1_10_100) _1	0.0020	1.33	0.91
		At opt	4_ (5_5_6100) _1	0.0035	1.57	0.86
		Above opt	4_ (2_5_20000) _1	0.0040	2.17	0.56
SMP, P	Saturation	Below opt	4_ (1_1_20000) _1	0.0093	12.19	0.31
		At opt	4_ (1_1_100) _1	0.0179	7.98	0.33
		Above opt	4_ (3_6_20000) _1	0.0051	3.93	0.56
SMP, P	Void Ratio	Below opt	4_ (7_9_20000) _1	0.0048	7.78	0.61
		At opt	4_ (1_5_1000) _1	0.0030	4.37	0.87
		Above opt	4_ (4_5_19100) _1	0.0034	4.79	0.60

7.3.2. Multiple geotechnical outputs

Further ANN models are developed to predict multiple geotechnical parameters from P-wave velocity and SMP. Water content and dry density are predicted together using a single ANN model. The statistics of the model are shown in Table 7.4. The performance of the models is good at predicting water content and dry density, and is within the statistics for the individual predictions. The ANN models developed to predict saturation and void ratio perform similarly to the better individual model (void ratio). Including a combination of outputs appears to produce models that are more consistent across the compaction process. Figure 7.3 shows the predicted versus actual graph of predicting water content, dry density, void ratio and saturation It can be inferred from the graph that data are well aligned with a 45-degree line for dry density and void ratio in comparison to water content and saturation.

Table 7.4: Statistical accuracy measures of predicting multiple geotechnical parameters from p-wave velocity and SMP.

Input	Output		ANN network	ASE	MARE	R^2
SMP, P	Water content, Dry density	Below opt	4_ (3_3_1100) _2	0.0071	5.68	0.60
		At opt	4_ (5_5_900) _2	0.0067	3.75	0.70
		Above opt	4_ (7_7_19100) _2	0.0045	3.14	0.55
SMP, P	Saturation, void ratio	Below opt	4_ (1_3_8100) _2	0.0048	7.10	0.67
		At opt	4_ (1_2_1000) _2	0.0066	5.25	0.71
		Above opt	4_ (1_9_20000) _2	0.0030	3.70	0.70

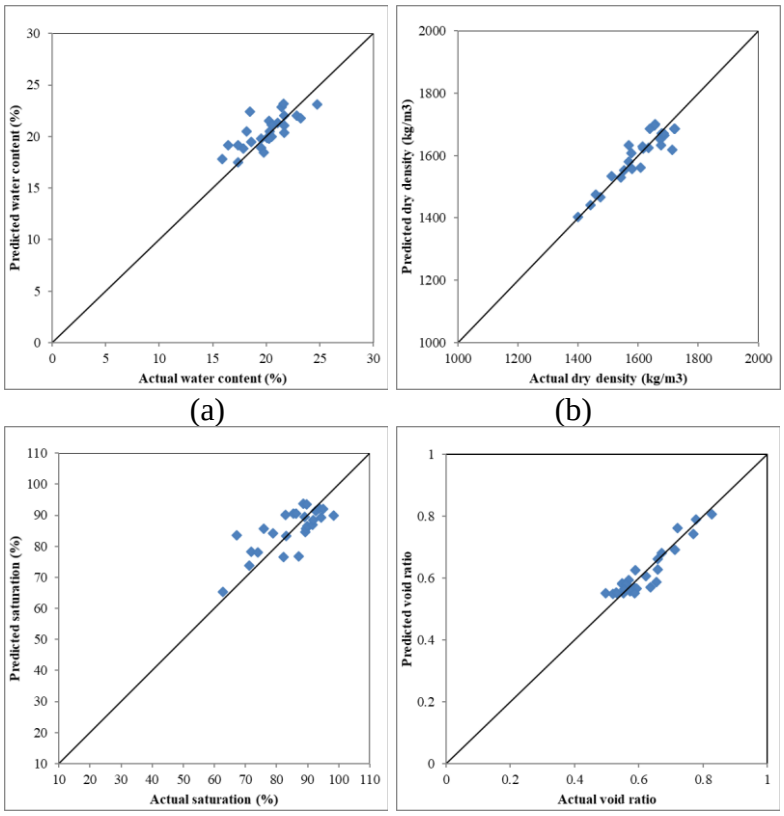

Figure 7.3: Predicted versus actual graph at opt for predicting (a) water content, (b) dry density, (c) saturation, (d) void ratio from soil mix proportion and P-wave velocity.

7.4 Using S-wave as input

The S-wave velocity is most commonly correlated with a cone penetration test. In Chapter 6, water content, dry density, saturation and void ratio provided the best results for predicting S wave velocity. In this section, the use of S wave velocity in combination with the soil mixture proportions is used to predict water content, dry density, saturation and void ratio at opt moisture content.

7.4.1 Single geotechnical output

The statistics of the models developed to predict water content, dry density, saturation and void ratio from S-wave velocity are shown in Table 7.5. Much like the P wave velocity, the S

wave velocity is better suited for predicting the dry density and void ratio than moisture content and saturation. Dry density at opt, which is an indicator of optimal compaction, is best correlated with P-wave velocity (0.86), followed by S wave velocity (0.78) and finally ER (0.68). S-wave velocity predicts dry density and void ratio better than ER, and ER predicts water content and saturation better than S-wave velocity.

Table 7.5: Statistical accuracy measures of predicting single geotechnical parameters from S-wave velocity and SMP.

Input	Output		ANN network	ASE	MARE	R^2
SMP, S	Water content	At opt	4_ (5_5_300) _1	0.0092	5.82	0.55
SMP, S	Dry density	At opt	4_ (1_1_200) _1	0.0060	2.23	0.78
SMP, S	Saturation	At opt	4_ (1_6_9100) _1	0.0073	5.90	0.49
SMP, S	Void Ratio	At opt	4_ (2_2_100) _1	0.0077	6.38	0.72

7.4.2. Multiple geotechnical outputs

The accuracy of models for predicting multiple geotechnical parameters from soil mixture proportions and S-wave velocity at opt is presented in Table 7.6. The model for predicting water content and dry density is good and within the performance of the individual models. The performance of the model for predicting saturation and void ratio is improved relative to predicting separately. Figure 7.4 shows the predicted versus actual graph of predicting water content, dry density, void ratio and saturation. It can be inferred from the graph that data is better aligned with a 45-degree line for dry density and void ratio in comparison to water content and saturation.

Table 7.6: Statistical accuracy measures of predicting multiple geotechnical parameters from S-wave velocity and SMP.

Input	Output		ANN network	ASE	MARE	R^2
SMP, S	Water content, Dry density	At opt	4_ (5_5_100) _2	0.0086	4.22	0.63
SMP, S	Saturation, Void Ratio	At opt	4_ (5_6_100) _2	0.0047	4.20	0.81

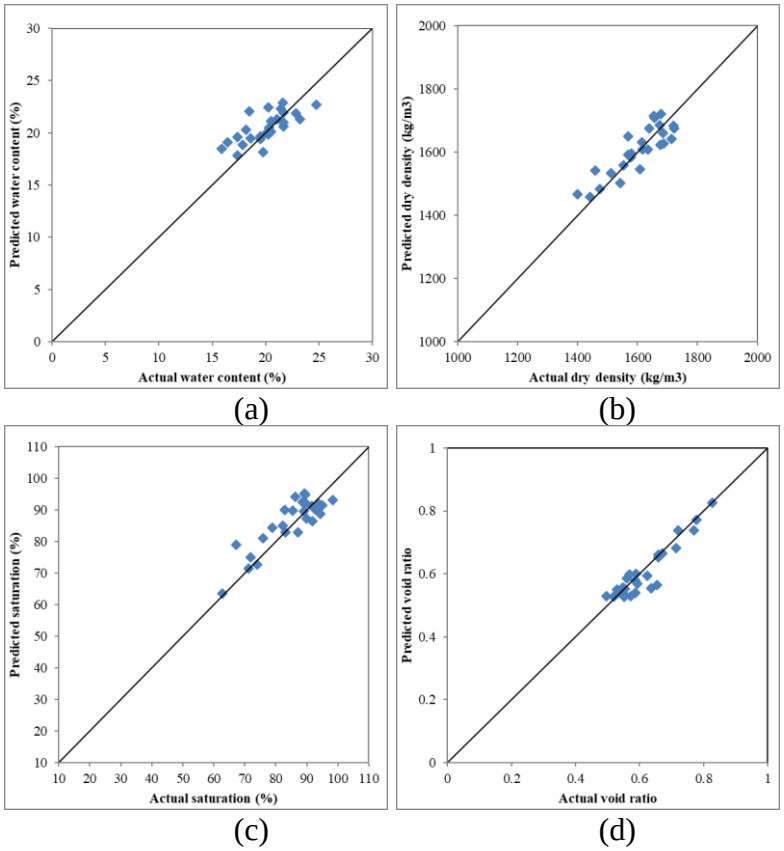

Figure 7.4:versus actual graph at opt for predicting (a) water content, (b) dry density, (c) saturation, (d) void ratio from soil mix proportion and S-wave velocity.

7.5 Conclusion

ANN models for predicting LL, PL, SL, water content, saturation, CEC, cohesion, and surface area from ER and SMP showed high accuracy due to the sensitivity of ER to clay and water. Dry density (R^2 = 0.68) and void ratio (R^2 = 0.67) showed good accuracy and SG (R^2 = 0.29) showed moderate accuracy. From the statistics of the ANN models, ER is more sensitive to water content and saturation in comparison to dry density and void ratio. Accuracy of the final ANN models for predicting multiple geotechnical parameters showed accuracy in between the ANN models for predicting single geotechnical parameters.

Analysis shows that P-wave is more sensitive to dry density and void ratio in comparison to water content and saturation. ANN models for predicting water content and dry density together

from P-wave velocity performance is in between the performance of the individual prediction model. The performance of the ANN models for predicting saturation and void ratio together is better than individual prediction model.

Similar to the P-wave velocity, the S-wave is more sensitive to dry density and void ratio in comparison to water content and saturation. Performance of predicting multiple geotechnical parameters (water content and dry density) show performance in between the performance of individual parameter prediction. Performance of predicting multiple geotechnical parameters (saturation and void ratio) show better performance than individual parameter prediction. ANN models for predicting dry density and void ratio from P-wave velocity is better than the models based on the S-wave velocity. ER predicts water content and saturation better than P-wave velocity, and P-wave velocity predicts void ratio and dry density better than ER. Similarly, ER predicts water content and saturation better than S-wave velocity, and S-wave velocity predicts void ratio and dry density better than ER. Therefore, there could be advantages to using all three geophysical properties as a combined input. This is discussed in the next chapter.

CHAPTER 8

PREDICTING GEOTECHNICAL PARAMETERS FROM COMBINED/MULTIPLE GEOPHYSICAL PARAMETERS

8.1 General

Erosion, excessive pore water pressure and ground water seepage are very common causes of earth dam failure. Compaction plays a very important role in earth dam construction and the maximum dry density at opt water content is an important parameter during construction. Dams are compacted within specified ranges of the maximum dry density. During operation, the loss of fine materials increases the void ratio and permeability which can lead to enhanced seepage and soil piping. Eventually this can lead to failure of the dam by internal erosion.

Geophysical methods can be used to provide a qualitative assessment of the earth dam by providing internal images of the structure. This information can supplement geotechnical information by providing continuous spatial data of the internal structure. Correlations between geophysical and geotechnical parameters allow for a more thorough assessment of the condition of the earth dam.

Interpretation of geophysical data can lead to multiple scenarios. In other words, the solution is not unique. For example, consider the impact of loss of fine material on the ER. Assuming the zone is fully saturated, this loss of fines increases the porosity and causes a decrease in ER (Archie's Law); however, the loss fines is a loss of clay and should therefore increase the

ER. One approach to reduce this non-uniqueness is to use information from multiple geophysical methods. In this chapter, water content, dry density, saturation and void ratio are predicted by combining geophysical parameters.

It was shown in Chapter 6 and 7 that water content, dry density, saturation and void ratio have correlations with ER, S-wave and P-wave velocity. It was further shown that using the SMP can increase the performance of the models. For earthen dams, the SMP is fairly well constrained for the various parts of the dam. However, this approach would assume that these properties are constant within each section of the dam which could be a source of error.

8.2 Predicting Water Content

In Chapter 7, ANN models were developed to predict water content using only one geophysical parameter at a time, with and without the use of soil mixture proportions. A summary of the best models is shown in Table 8.1. The best model using one geophysical parameter is with ER. The addition of SMP increases the performance of the model.

Table 8.1 :Summary of predicting water content from individual geophysical parameter and SMP

Input		ANN network	ASE	MARE	R^2
	Below opt	1_ (3_12_20000) _1	0.0061	7.20	0.64
ER	At opt	1_ (1_1_300) _1	0.0165	7.67	0.30
	Above opt	1_ (6_6_1200) _1	0.0086	5.85	0.23
	Below opt	4_ (2_11_20000) _1	0.0035	5.21	0.79
ER + SMP	At opt	4_ (6_6_100) _1	0.0104	6.46	0.55
	Above opt	4_ (4_4_1300) _1	0.0069	5.09	0.38
	Below opt	1_ (1_1_400) _1	0.0108	11.50	0.10
P	At opt	1_ (1_1_100) _1	0.0172	14.59	0.0004
	Above opt	1_ (2_7_19900) _1	0.0155	13.08	0.03
	Below opt	4_ (10_12_19900) _1	0.0106	9.08	0.37
P + SMP	At opt	4_ (1_1_100) _1	0.0105	6.15	0.53
	Above opt	4_ (1_1_15100) _1	0.0063	4.84	0.43
	Below opt	1_ (2_5_6700) _1	0.0047	10.13	0.27
S	At opt	1_ (1_1_100) _1	0.0148	10.59	0.003
	Above opt	1_ (9_9_2100) _1	0.0268	16.55	0.02
	Below opt	4_ (5_5_1100) _1	0.0129	10.28	0.25
S + SMP	At opt	4_ (5_5_300) _1	0.0092	5.82	0.55
	Above opt	4_ (7_9_900) _1	0.0043	4.05	0.61

8.2.1 Combined geophysical parameters`

The statistics of ANN models for different combinations of geophysical parameters in different compaction regimes, below opt moisture content, at opt moisture content and above opt moisture content, are shown in Table 8.2. The better models are those that include ER as an input and are compacted below opt moisture content. The addition of seismic information provides little improvement on the models below opt. However, the use of S and P wave velocity in addition to ER does improve the performance of the model at opt and above opt moisture content. Overall the best model is obtained using all three geophysical parameters and, compared to Table 8.1, is better than using ER individually - especially at and above opt moisture content.

Table 8.2: Statistical accuracy of ANN models for predicting water content from combined geophysical parameters.

Input		ANN network	ASE	MARE	R^2
ER, S	Below opt	2_ (4_9_19900) _1	0.0057	6.97	0.66
	At opt	2_ (1_1_200) _1	0.0191	8.26	0.30
	Above opt	2_ (4_7_4200) _1	0.0077	5.79	0.30
ER, P	Below opt	2_ (3_9_20000) _1	0.0058	7.06	0.65
	At opt	2_ (4_4_19700) _1	0.0129	7.14	0.34
	Above opt	2_ (7_7_1100) _1	0.0085	5.86	0.23
S, P	Below opt	2_ (6_11_19100) _1	0.0117	9.52	0.31
	At opt	2_ (3_4_16800) _1	0.0139	7.31	0.29
	Above opt	2_ (3_9_5300) _1	0.0092	5.83	0.16
ER, S, P	Below opt	3_ (6_12_20000) _1	0.0057	6.80	0.66
	At opt	3_ (3_6_100) _1	0.0086	6.17	0.57
	Above opt	3_ (6_6_11000) _1	0.0067	5.09	0.39

Predicted versus actual graphs for predicting water content for the highest performance networks at below opt, at opt and above opt are shown in Figure 8.1. Graphs show that some data are scattered and not perfectly aligned with a 45-degree line. Including some other geotechnical parameters may improve the performance.

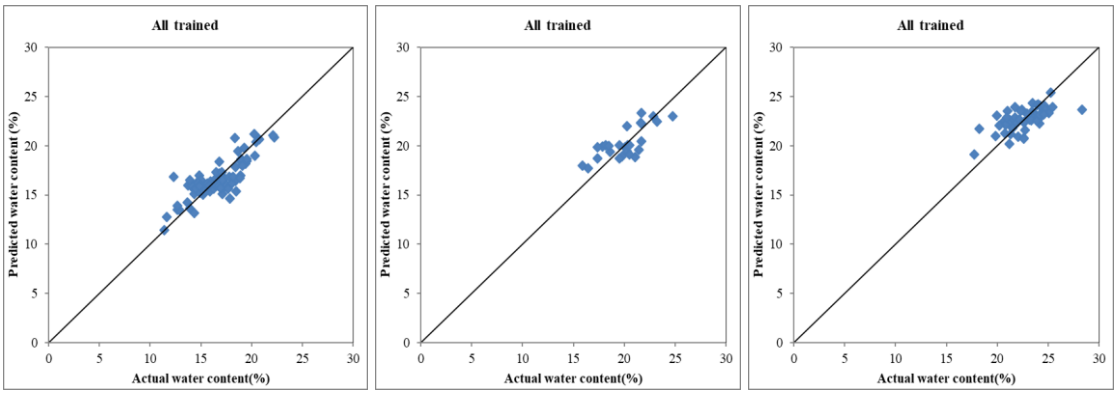

(a) (b) (c)

Figure 8.1: Predicted versus actual graph for predicting water content from ER, S and P-wave velocity at (a) below opt, (b) at opt, (c) at above opt.

The addition of the SMP increases the accuracy of all the models. The statistics of ANN models to predict water content using the three geophysical parameter and SMP as input are shown in Table 8.3. The statistics show that models including SMP have better performance. The use of three geophysical inputs is most important for data above opt moisture content. The predicted versus actual graph for these models are shown in Figure 8.2. The graphs show less scattering of the data and are well aligned with the 45-degree line. Comparison of the graphs shown in Figure 8.1 (c) and Figure 8.2 (c) shows the improvement in model prediction when SMP is added as input. Data are closer to the 45-degree and less scattered after adding geotechnical parameters as input.

Table 8.3: Statistical accuracy of ANN models for predicting water content from combined geophysical and SMP.

	Input	ANN network	ASE	MARE	R^2
Below opt	ER, S, P, SMP	6_ (2_7_20000) _1	0.0036	5.46	0.79
At opt	ER, S, P, SMP	6_ (5_5_100) _1	0.0086	5.89	0.57
Above opt	ER, S, P, SMP	6_ (8_9_2100) _1	0.0031	2.99	0.72

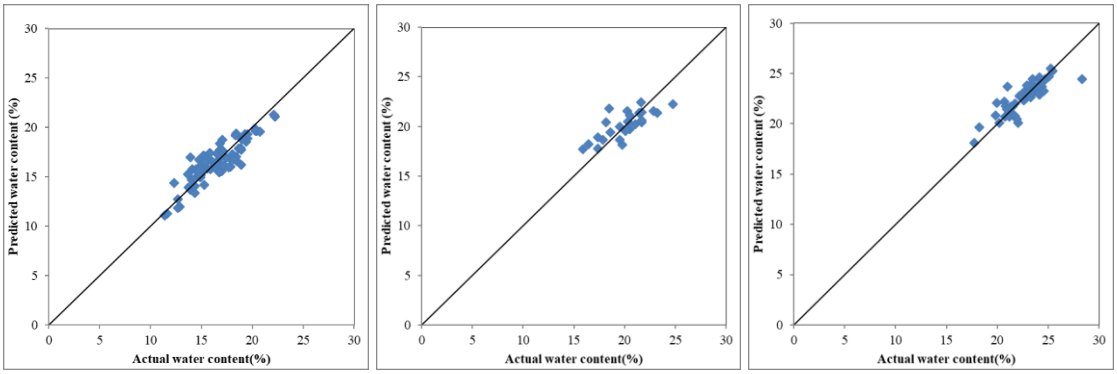

(a) (b) (c)

Figure 8.2: Predicted versus actual graph for predicting water content from (a) ER, S, P-wave velocity, SMP at below opt, (b) ER, S, P-wave velocity, SMP at opt, (c) ER, S, P-wave velocity, SMP at above opt.

Table 8.1 shows that ER along with SMP at below opt shows better performance and S along with SMP show better performance at opt and above opt. Comparison of these models with the combination of three geophysical parameters along with SMP shows that significant improvement is only observed at above opt.

8.3 Predicting Dry Density

ANN models were developed in Chapter 7 to predict dry density using only one geophysical parameter at a time, with and without the use of SMP. A summary of the best models is shown in Table 8.4. Models using a single geophysical input are poor. Addition of SMP provides a large improvement when combined with any of the geophysical inputs. The best models are for data below opt moisture content.

Table 8.4: Summary of predicting dry density from individual geophysical parameter and SMP

Input		ANN network	ASE	MARE	R^2
ER	Below opt	1_ (6_12_20000) _1	0.0199	4.54	0.13
	At opt	1_ (1_3_100) _1	0.0225	3.94	0.18
	Above opt	1_ (6_6_100) _1	0.0089	3.05	0.04
ER + SMP	Below opt	4_ (2_11_20000) _1	0.0014	1.01	0.93
	At opt	4_ (1_3_100) _1	0.0080	2.52	0.70
	Above opt	4_ (2_2_100) _1	0.0071	2.83	0.28
P	Below opt	1_ (7_10_6100) _1	0.0108	11.50	0.14
	At opt	1_ (2_4_8100) _1	0.0105	11.43	0.38
	Above opt	1_ (2_4_20000) _1	0.0137	12.43	0.12
P + SMP	Below opt	4_ (1_10_100) _1	0.0020	1.33	0.91
	At opt	4_ (5_5_6100) _1	0.0035	1.57	0.86
	Above opt	4_ (2_5_20000) _1	0.0040	2.17	0.56
S	Below opt	1_ (2_2_15100) _1	0.0006	10.80	0.01
	At opt	1_ (1_2_400) _1	0.0123	9.57	0.16
	Above opt	1_ (1_1_300) _1	0.0273	16.74	0.00003
S + SMP	Below opt	4_ (8_8_100) _1	0.003494	1.615	0.84
	At opt	4_ (1_1_200) _1	0.0060	2.23	0.78
	Above opt	4_ (3_3_100) _1	0.0066	2.71	0.28

8.3.1 Combined geophysical parameters

The statistics of ANN models to predict dry density for different combinations of geophysical parameters for different compaction regimes (below opt moisture content, at opt moisture content and above opt moisture content) are shown in Table 8.5. There is no consistent trend in model improvements for the different compaction regimes. Based on ASE, MARE and R^2

the best combinations are ER and P-wave at below opt, ER and S-wave at opt, and ER, S and P-wave at above opt.

Table 8.5: Statistical accuracy of ANN models for predicting dry density from combined geophysical parameters.

Input		ANN network	ASE	MARE	R^2
ER, S	Below opt	2_ (3_12_19100) _1	0.0217	4.77	0.04
	At opt	2_ (1_7_100) _1	0.0119	2.65	0.57
	Above opt	2_ (8_8_400) _1	0.0090	3.07	0.03
ER, P	Below opt	2_ (6_12_20000) _1	0.0179	4.23	0.21
	At opt	2_ (1_1_2100) _1	0.0178	3.61	0.34
	Above opt	2_ (2_3_100) _1	0.0086	2.97	0.07
S, P	Below opt	2_ (9_12_19900) _1	0.0182	4.24	0.19
	At opt	2_ (1_1_19900) _1	0.0201	3.84	0.25
	Above opt	2_ (9_9_100) _1	0.0087	3.04	0.05
ER, S, P	Below opt	3_ (10_10_20000) _1	0.0198	4.58	0.14
	At opt	3_ (6_6_200) _1	0.0196	3.87	0.31
	Above opt	3_ (1_5_200) _1	0.0054	2.55	0.53

Predicted versus actual graphs for predicting dry density for the highest performance networks below opt, at opt and above opt are shown in Figure 8.3. Graphs show that some data are scattered and not perfectly aligned with a 45-degree line. Including some geotechnical parameters might improve the performance.

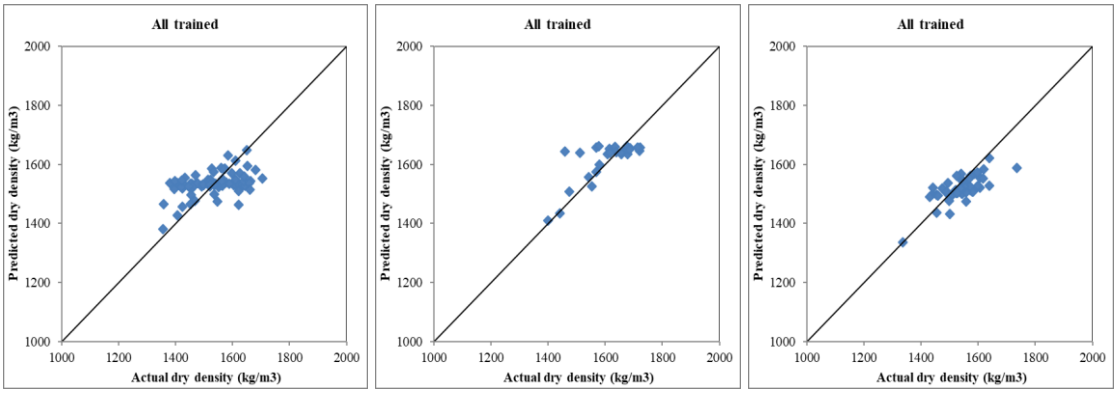

(a) (b) (c)

Figure 8.3: Predicted versus actual graph for predicting dry density from (a) ER and P-wave velocity at below opt, (b) ER, S-wave velocity at opt, (c) ER, S and P-wave velocity at above opt.

The statistics of ANN models to predict dry density using the best combination of geophysical parameter determined above and SMP as input are shown in Table 8.6. The statistics show that after including SMP as input, the performance of all the models improves. At below opt and at opt, SMP makes the prediction accuracy significantly better, while at above opt, the improvement is not that significant. The predicted versus actual graphs for these models are shown in Figure 8.4. The graphs show less scattering of the data and are well aligned with a 45-degree line. The improvements of the performance are observed after adding SMP as input from the comparison of the graphs shown in Figure 8.3 (a) to Figure 8.4 (a) and also Figure 8.3 (b) to Figure 8.4 (b). Data are closer to a 45-degree line and less scattered after adding geotechnical parameters as inputs.

Table 8.6: Statistical accuracy of ANN models for predicting dry density from combined geophysical and other geotechnical parameters.

Input		ANN network	ASE	MARE	R^2
Below opt	ER, P, SMP	5_ (1_5_100) _1	0.0013	1.03	0.94
At opt	ER, S, SMP	5_ (1_3_19100) _1	0.0038	1.65	0.86
Above opt	ER, P, S, SMP	6_ (5_5_15200) _1	0.0041	2.14	0.56

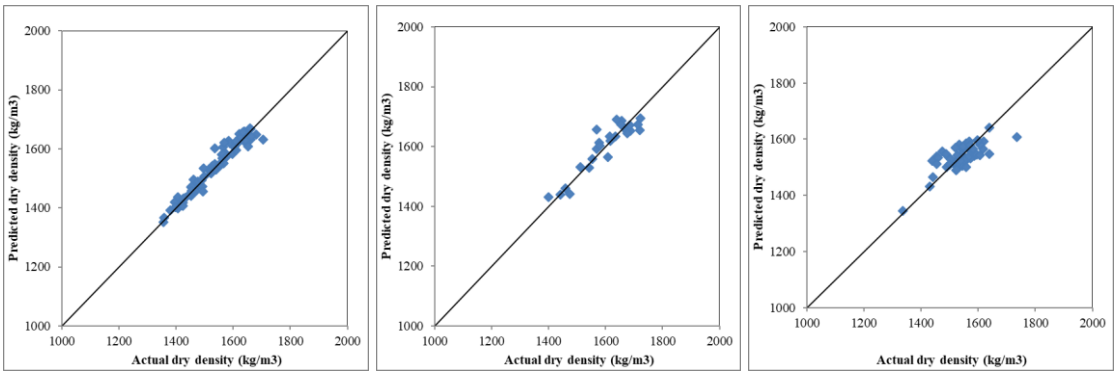

(a) (b) (c)

Figure 8.4: Predicted versus actual graph for predicting dry density from (a) ER, P-wave velocity, SMP at below opt, (b) ER, S-wave velocity, SMP at opt, (c) ER, S, P-wave velocity and SMP at above opt.

8.4 Predicting Saturation

A summary of the best ANN models developed for predicting saturation using only one geophysical parameter at a time, with and without the use of soil mixture, is shown in Table 8.7. The best models include ER for compaction below opt, P-wave velocity for compaction at opt moisture content and at above opt performances are very poor. The addition of SMP increases the performance of the models.

Table 8.7: Summary of predicting saturation from individual geophysical parameter and SMP

Input		ANN network	ASE	MARE	R^2
ER	Below opt	1_ (6_6_2100) _1	0.0077	11.05	0.44
	At opt	1_ (6_7_100) _1	0.0204	7.63	0.17
	Above opt	1_ (8_8_200) _1	0.0110	5.71	0.07
ER + SMP	Below opt	4_ (1_3_6900) _1	0.0041	7.17	0.69
	At opt	4_ (1_1_100) _1	0.0200	8.39	0.19
	Above opt	4_ (4_4_4100) _1	0.0063	4.43	0.47
P	Below opt	1_ (3_3_19100) _1	0.0109	11.77	0.12
	At opt	1_ (1_1_600) _1	0.0147	14.02	0.19
	Above opt	1_ (1_1_400) __1	0.0161	13.96	0.04
P + SMP	Below opt	4_ (1_1_20000) _1	0.0093	12.19	0.31
	At opt	4_ (1_1_100) _1	0.0179	7.98	0.33
	Above opt	4_ (3_6_20000) _1	0.0051	3.93	0.56
S	Below opt	1_ (3_3_19100) _1	0.0065	10.75	0.002
	At opt	1_ (3_3_400) _1	0.0132	10.04	0.10
	Above opt	1_ (1_1_1100) _1	0.0272	16.87	0.009
S + SMP	Below opt	4_ (1_1_100) _1	0.0132	14.21	0.13
	At opt	4_ (1_6_9100) _1	0.0073	5.90	0.49
	Above opt	4_ (1_1_100) _1	0.0109	5.61	0.09

8.4.1 Combined geophysical parameters

The statistics of ANN models to predict saturation for different combinations of geophysical parameters for different compaction regimes, below opt moisture content, at opt moisture content and above opt moisture content, are shown in Table 8.8.

The better models for samples compacted below opt moisture content are those that include ER. The addition of seismic information provides little improvement on the models below opt.

However, the use of S and P wave velocity in addition to ER does improve the performance of the models at opt and above opt moisture content. Overall the best models are obtained using all three geophysical parameters and are better than using just one geophysical input.

Table 8.8: Statistical accuracy of ANN models for predicting saturation from combined geophysical parameters.

Input		ANN network	ASE	MARE	R^2
ER, S	Below opt	2_ (1_1_1800) _1	0.0078	11.14	0.45
	At opt	2_ (1_6_100) _1	0.0117	5.49	0.54
	Above opt	2_ (7_7_100) _1	0.0108	5.45	0.09
ER, P	Below opt	2_ (1_6_9000) _1	0.0065	10.12	0.53
	At opt	2_ (3_6_100) _1	0.0110	5.72	0.56
	Above opt	2_ (6_6_300) _1	0.0106	5.55	0.11
S, P	Below opt	2_ (3_5_2000) _1	0.0080	11.53	0.45
	At opt	2_ (2_2_800) _1	0.0191	7.78	0.23
	Above opt	2_ (2_2_600) _1	0.0115	5.81	0.03
ER, S, P	Below opt	3_ (5_13_100) _1	0.0055	9.22	0.66
	At opt	3_ (5_7_100) _1	0.0105	5.14	0.59
	Above opt	3_ (1_1_500) _1	0.0106	5.50	0.11

Predicted versus actual graphs for predicting saturation for the highest performance networks at below opt, at opt and above opt are shown in Figure 8.5. Graphs show that some data are scattered and not perfectly aligned with a 45-degree line. Including some geotechnical parameters may improve the performance.

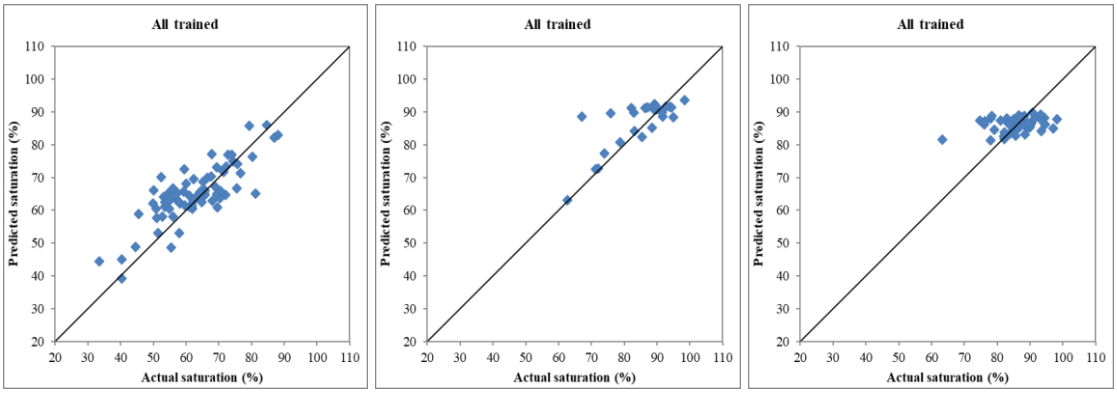

(a) (b) (c)

Figure 8.5: Predicted versus actual graph for predicting saturation from (a) ER, S and P-wave velocity at below opt, (b) at opt, (c) at above opt.

The statistics of ANN models to predict saturation using the three geophysical parameters and SMP as inputs are shown in Table 8.9. The statistics show that after including SMP as input, the performance of the model improves. The errors of the models decreased and R^2 increased. At below opt, SMP makes the prediction accuracy better; at opt and above opt, the performance significantly improved after adding SMP as input. The predicted versus actual graphs for these models are shown in Figure 8.6. The graphs show less scattering of the data and are well aligned with a 45-degree line. The improvements in the performance are observed after adding SMP as input from the comparison of the graphs shown in Figure 8.5 (b) to Figure 8.6 (b) and also Figure 8.5 (c) to Figure 8.6 (c). Data are closer to a 45-degree and less scattered after adding geotechnical parameters as input.

Table 8.9: Statistical accuracy of ANN models for predicting saturation from combined geophysical and other geotechnical parameters.

Input		ANN network	ASE	MARE	R^2
Below opt	ER, S, P, SMP	6_ (1_2_700) _1	0.0045	8.20	0.73
At opt	ER, S, P, SMP	6_ (3_4_200) _1	0.0046	3.72	0.80
Above opt	ER, S, P, SMP	6_ (8_8_7600) _1	0.0056	4.34	0.56

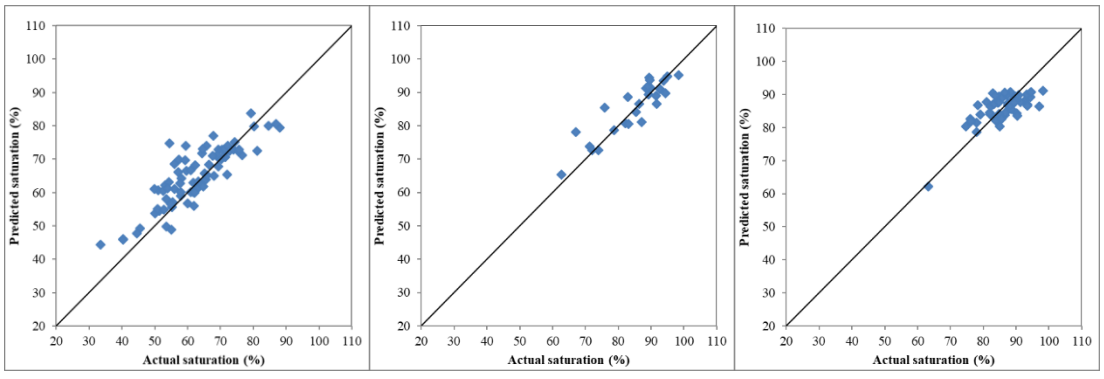

(a) (b) (c)

Figure 8.6: Predicted versus actual graph for predicting saturation from (a) ER, S and P-wave velocity, SMP at below opt, (b) ER, S and P-wave velocity, SMP at opt, (c) ER, S and P-wave velocity, SMP at above opt.

Statistics of Table 8.7 show that ER along with SMP at below opt, S along with SMP at opt, and P along with SMP at above opt show better performance. Comparison of these models with the combination of three geophysical parameters along with SMP shows that at below opt performance improves and at above opt performance improves significantly.

8.5 Predicting Void Ratio

A summary of the best ANN models developed to predict void ratio using only one geophysical parameter at a time, is shown in Table 8.10. Models without SMP as input are rather poor. Either geophysical parameter in conjunction with SMP produces models of moderate performance.

Table 8.10: Summary of predicting void ratio from individual geophysical parameter and SMP

Input		ANN network	ASE	MARE	R^2
ER	Below opt	1_ (10_12_20000) _1	0.0177	10.34	0.14
	At opt	1_ (1_1_1200) _1	0.0204	9.58	0.14
	Above opt	1_ (2_9_2000) _1	0.0079	7.21	0.08
ER + SMP	Below opt	4_ (5_11_1000) _1	0.0012	2.60	0.93
	At opt	4_ (1_1_100) _1	0.0089	6.66	0.66
	Above opt	4_ (3_4_700) _1	0.0054	6.44	0.43
P	Below opt	1_ (1_1_100) _1	0.0125	12.42	0.01
	At opt	1_ (2_4_7100) _1	0.0103	11.10	0.39
	Above opt	1_ (2_5_500) _1	0.0257	18.26	0.12
P + SMP	Below opt	4_ (7_9_20000) _1	0.0048	7.78	0.61
	At opt	4_ (1_5_1000) _1	0.0030	4.37	0.87
	Above opt	4_ (4_5_19100) _1	0.0034	4.79	0.60
S	Below opt	1_ (1_2_19800) _1	0.0064	10.86	0.02
	At opt	1_ (1_6_1000) _1	0.0129	9.85	0.13
	Above opt	1_ (5_5_6100) _1	0.0272	16.58	0.005
S + SMP	Below opt	4_ (9_9_100) _1	0.0034	3.97	0.82
	At opt	4_ (2_2_100) _1	0.0077	6.38	0.72
	Above opt	4_ (2_2_100) _1	0.0070	6.83	0.25

8.5.1Combined geophysical parameters

The statistics of ANN models for void ratio for different combinations of geophysical parameters and different compaction regimes are shown in Table 8.11. These models are better than those using just one geophysical input.

Overall, the best models are obtained using ER and P-wave for at below opt, and ER, S and P-wave for both at opt and above opt. The combination of ER and P-wave provides improvement to the model below opt whereas the combination of all three geophysical parameters improves the performance at opt and significantly improves the performance above opt moisture content.

Table 8.11: Statistical accuracy of ANN models for predicting void ratio from combined geophysical parameters.

Input		ANN network	ASE	MARE	R^2
ER, S	Below opt	2_ (11_12_20000) _1	0.0188	10.76	0.06
	At opt	2_ (1_1_3100) _1	0.0146	8.47	0.38
	Above opt	2_ (6_12_2900) _1	0.0069	6.64	0.20
ER, P	Below opt	2_ (1_5_20000) _1	0.0165	10.04	0.17
	At opt	2_ (1_2_700) _1	0.0148	8.98	0.4
	Above opt	2_ (4_7_6900) _1	0.0055	6.64	0.35
S, P	Below opt	2_ (1_2_16300) _1	0.0194	10.95	0.03
	At opt	2_ (1_1_100) _1	0.0237	11.50	0.12
	Above opt	2_ (3_3_5100) _1	0.0068	6.9	0.20
ER, S, P	Below opt	3_ (3_3_20000) _1	0.0188	10.84	0.05
	At opt	3_ (6_6_300) _1	0.0142	9.23	0.40
	Above opt	3_ (9_9_20000) _1	0.0042	5.86	0.50

Predicted versus actual graphs for predicting void ratio for the highest performance networks at below, at opt and above opt are shown in Figure 8.7. Graphs show that some data are scattered and not perfectly aligned with a 45-degree line.

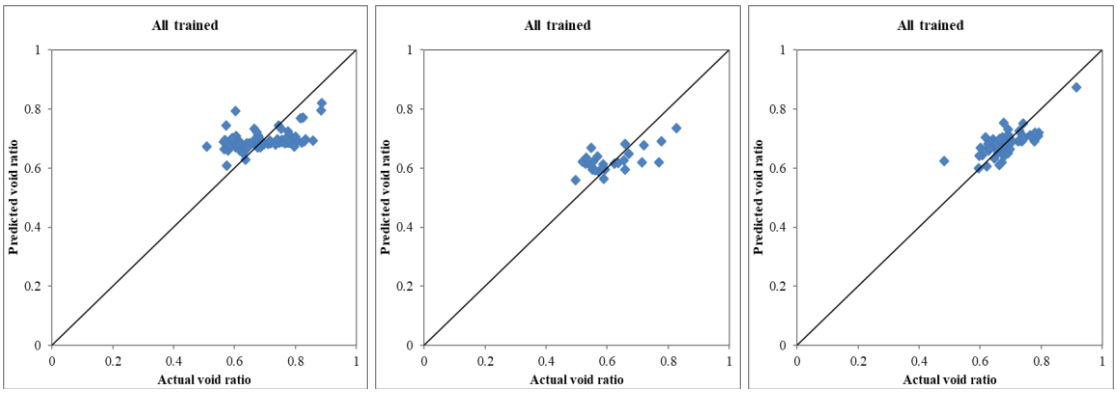

(a) (b) (c)

Figure 8.7: Predicted versus actual graph for predicting void ratio from (a) ER and P-wave velocity at below opt, (b) ER, S and P-wave velocity at opt, (c) ER, S and P-wave velocity at above opt.

The statistics of ANN models for the best combination of geophysical parameters determined above along with the SMP as input are shown in Table 8.12. The statistics show that after including SMP as input, the performance of the models improves significantly at below opt, at opt and above opt. The predicted versus actual graph for these models are shown in Figure 8.8. The improvement of the performance is observed after adding SMP as input from the comparison of the graphs shown in Figure 8.7 (a) to Figure 8.8 (a), Figure 8.7 (b) to Figure 8.8 (b) and also Figure 8.7 (c) to Figure 8.8 (c). Data are closer to a 45-degree and less scattered after adding geotechnical parameters as input.

Table 8.12: Statistical accuracy of ANN models for predicting void ratio from combined geophysical parameters.

	Input	ANN network	ASE	MARE	R^2
Below opt	ER, P, SMP	5_ (7_10_7200) _1	0.001	2.32	0.94
At opt	ER, P, S, SMP	6_ (1_1_200) _1	0.0041	5.11	0.87
Above opt	ER, P, S, SMP	6_ (4_5_2100) _1	0.0023	4.07	0.74

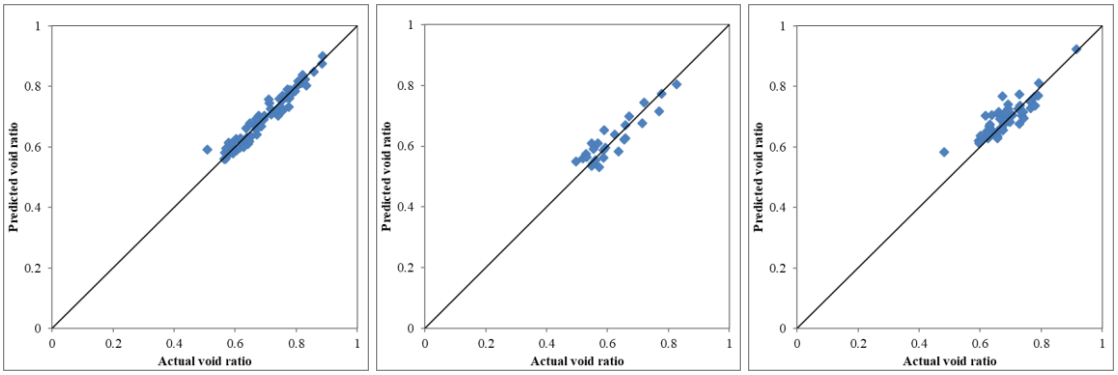

(a) (b) (c)

Figure 8.8: Predicted versus actual graph for predicting void ratio from (a) ER, P-wave velocity, SMP at below opt, (b) ER, S, P-wave velocity, SMP at opt, (c) ER, S, P-wave velocity, SMP at above opt.

Table 8.10 show that ER along with SMP at below opt shows better performance, and P along with SMP show better performance both at opt and above opt. Comparison of these models with the best combination of geophysical parameters along with SMP shows that significant improvement is only observed at above opt.

8.6 Predicting Water Content, Dry density, Void ratio, Saturation from Combined Geophysical Parameters

ANN models can predict several outputs up to the number of inputs. In Chapter 7 it was shown that models with more outputs can perform better than models with a single output. Table 8.13 shows the statistics for models predicting all four geotechnical properties - moisture content, void ratio, dry density and saturation - using the SMP and individual geophysical measurements. All models are close in performance. The best model is for data below opt and using ER and SMP as input. The models at opt are of intermediate performance using S wave velocity as input. The models above opt have lower performance with the ER as input producing the best model.

Table 8.13: Summary of predicting water content, dry density, void ratio, saturation from individual geophysical parameter and SMP.

Input		ANN network	ASE	MARE	R^2
ER + SMP	Below opt	4_ (10_10_20000) _4	0.0027	4.09	0.83
	At opt	4_ (6_6_100) _4	0.0106	5.68	0.57
	Above opt	4_ (8_9_1700) _4	0.0041	3.63	0.60
P + SMP	Below opt	4_ (6_7_1000) _4	0.0058	6.31	0.64
	At opt	4_ (2_4_100) _4	0.0061	4.20	0.73
	Above opt	4_ (5_7_300) _4	0.0045	3.81	0.57
S + SMP	Below opt	4_ (5_10_1000) _4	0.0046	5.51	0.74
	At opt	4_ (3_4_2500) _4	0.0053	3.81	0.76
	Above opt	4_ (8_10_100) _4	0.0051	4.27	0.49

Comparison of these models with the combination of three geophysical parameters shown in Table 8.14 indicate slight improvement in performance. Below opt shows an increase in R^2 of 0.02, no change in R^2 at opt and an increase in R^2 of 0.09 above opt.

Table 8.14: Statistical accuracy of ANN models for predicting water content, dry density, void ratio, saturation from combined geophysical parameters

Input		ANN network	ASE	MARE	R^2
ER+ P + S + SMP	Below opt	6_ (11_11_7000) _4	0.0022	3.65	0.86
	At opt	6_ (6_6_600) _4	0.0055	3.93	0.76
	Above opt	6_ (11_11_7000) _4	0.0031	3.16	0.69

8.6 Conclusion

Predicting water content using combinations of three geophysical parameters shows better performance versus single parameters. At below opt, SMP makes the prediction accuracy better, at opt the improvement is not that significant, and at above opt the performance is significantly improved after adding SMP as input.

To predict dry density, the combination of ER and P-wave provides improvement on the models below opt, a combination of ER and S-wave at opt, and a combination of three geophysical parameters at above opt significantly improves the performance. Including SMP with the best

combinations makes prediction accuracy significantly better at below opt and at opt, whereas at above opt, the improvement is not that significant.

To predict saturation, combinations of three geophysical parameters show better performance, which is similar to water content predictions. At below opt, adding SMP makes the prediction accuracy better; at opt and at above opt, the performance significantly improves after adding SMP as input.

To predict void ratio, the combination of ER and P-wave provides improvement on the models below opt. The combination of three geophysical parameters improves the performance at opt, but significantly improves at above opt. By including SMP as input, the performance of the models are improved significantly.

For predicting water content, dry density, void ratio, and saturation together from three geophysical parameters along with SMP shows only a slight improvement in performance.

CHAPTER 9

CONCLUSION

.

9.1 Conclusion

In the past, most of the correlations between ER and geotechnical parameters were developed using traditional regression analysis. An attempt was made to develop ANN models to predict geotechnical parameters from ER and seismic wave velocity separately using existing data sets in literature. Analysis of the published data set shows sensitivity of ER to CEC, saturation, water content and dry density. Results of the ANN models developed using published seismic data indicate that the performance of the models is improved after using more data for training. The correlation between parameters for lab data was better in comparison to field and field plus lab data. For most cases, the seismic wave velocity helps to predict water content and dry density, and ANN shows better performance than regression for all the cases.

ANN models do predict correlations between geophysical and geotechnical parameters with better accuracy than regression. However, the datasets are limited and a database of laboratory measurements was collected where measurements were obtained on the same sample. The soil types were constrained to typical materials used for the construction of earth dams - clay and sandy clay soil types. The geotechnical measurements consisted of two groups. The first group were properties that depend solely on the soil type: soil mix proportions (SMP), Atterberg limits,specific surface area, SG, and CEC. There were 26 independent measurements for each parameter in this group. The second group of properties depend on the soil type and the degree

of compaction associated with the proctor test: moisture content and dry density, void ratio, saturation, and porosity. There were 155 measurements in this group. Cohesion was measured on a specific soil type and compacted at opt or near opt moisture, so there are 26 measurements. The geophysical measurements consisted of ER, S-wave and P-wave velocity, and there were 155 measurements.

ANN models were developed to predict geophysical parameters from geotechnical parameters to assess the sensitivity of geotechnical parameters to ER, S-wave and P-wave velocity. Models for ER versus water content and saturation had good performance; for ER versus CEC, LL, PL, SL, surface area, and void ratio had moderate performance; for ER versus cohesion and dry density had poor performance; and ER versus SG had almost no correlation. Combinations of multiple geotechnical parameters were examined and revealed that ER could be predicted with better accuracy.

Water content, dry density, saturation, and void ratio had little influence on P-wave and S-wave velocity when used individually. However, after combining geotechnical parameters, the ANN prediction models showed good accuracy in predicting P-wave velocity and S-wave velocity. Atterberg limits, SG, specific surface area, and CEC did not affect the P-wave and S-wave velocity. SL showed a little sensitivity to S-wave velocity. Somewhat unexpectedly, cohesion did not show any influence on P-wave and S-wave velocity.

More applicable to problems of geotechnical assessment, ANN models were evaluated to predict geotechnical parameters from geophysical parameters with and without soil mix proportions as input. Incorporating soil mixture proportions significantly increased the

performance of the models. Using the soil mixture proportion appears feasible for earthen dams where each section is built with known mixtures. For other situations, unknown variations in the soil mixture proportions would lead to a source of error.

ANN models for predicting LL, PL, SL, water content, saturation, CEC, cohesion, and surface area from ER and SMP showed high accuracy due to the sensitivity of ER to clay content and water. Dry density (R^2 = 0.68) and void ratio (R^2 = 0.67) showed good accuracy, and SG showed moderate accuracy.

P-wave and S-wave velocity showed moderate sensitivity to dry density and void ratio at opt, but poor sensitivity to water content and saturation when individually predicted. But there is no sensitivity to Atterberg limit, surface area, SG, and CEC. P-wave and S-wave do not show sensitivity to cohesion due to the confining issue.

Multiple geotechnical were predicted from one geophysical input and SMP with good accuracy. ANN models for predicting dry density and void ratio from P-wave velocity were better than the models based on ER and the S-wave velocity. ER measurements predict water content and saturation better than seismic measurements. Results varied depending on the state of compaction, i.e. below opt moisture content, at opt or above opt moisture content. However such results suggest there could be advantages to using multiple geophysical properties as a combined input.

Subsequent analysis showed that the combination of three geophysical parameters provided models with better performance at predicting water content and saturation. Dry density was best predicted using a combination of ER and P-wave for soils compacted below opt, a

combination of ER and S-wave at opt, and a combination of three geophysical parameters at above opt. To predict void ratio, the combination of ER and P-wave provided improvement on the models below opt. Including SMP as input improves the performance of the models for all of the cases.

The final analysis was predicting all four geotechnical properties (water content, dry density, void ratio, saturation) using the three geophysical inputs along with SMP. These all-encompassing models had high performance below opt (R^2=0.82) and at opt (R^2=0.76), and moderate performance at above opt moisture content (R^2=0.69).

9.2 Recommendation for Future Research

For this research, variation in sand, silt and clay fractions within the clay and sandy clay soil types are used for correlation development. Correlation should be developed for other soil types. Two different types of clay, namely 80% kaolinite and 20% bentonite of the clay fraction, are used for this research. Different mixing proportions of kaolinite and bentonite can be used for further research. Synthetic soil samples are prepared through standard proctor compaction tests for the current research. Correlation should be developed for actual field soils in either remolded or undisturbed states.

The suite of geotechnical parameters could be expanded to include soil erodibility, permeability, cohesion, and angle of friction. Additional parameters, such as those from a penetration test that might be correlated with seismic wave velocity, should studied.

In this study, the proctor compaction test is used to prepare soil samples. This process leads to changes in several soil properties from sample to sample, and does not allow for investigating changes in only one soil parameter. Work could be conducted in triaxial cells to examine the importance of effective stress and over burden pressure, which are important factors

for seismic wave velocity. Future work could focus on experiments isolating individual parameters or replicating other soil processes. For example, samples could be produced by reducing the fine content due to flushing with water.

REFERENCES

Abidin, M.H.Z., Saad, R., Ahmad, F., Wijeyesekera, D.C., and Yahya, A.S. 2013. "Soil moisture content and density prediction using laboratory resistivity experiment." *IACSIT international journal of engineering and technology*, 5,731-735.

Abu-Hassanein, Z. S., Benson, C. H., and Blotz, L. R. 1996. "Electrical resistivity of compacted clays." *Journal of geotechnical engineering*, 122, 397-406.

Adewoyin, O., Joshua, E.O., and Akinwumi, I.I. 2017. "Evaluation of geotechnical parameters using geophysical data." *Journal of engineering and technology*, 49, 95-113.

Akayuli, C., Ofosu, B., Nyako, S.O., and Opuni, K.O. 2013. "The influence of observed clay content on shear strength and compressibility of residual sandy soils." International journal of engineering research and applications (IJERA), 3, 2538-2542.

Archie, G. E. 1952. "Classification of carbonate reservoir rocks and petrophysical considerations." *AAPG bulletin*, 36, 218–298.

Archie, G.E. 1942. "The electrical resistivity log as an aid in determining some reservoir characteristics." *Petroleum transactions of AIME*, 146, 54–62.

Association of state dam safety-ASDSO. 2019. "A 101 on dams."https://www.damsafety.org/dams101.

Bhatt, S., and Jain, P.K. 2014. "Correlation between electrical resistivity and water content of sand-a statistical approach." *American international journal of research in science, technology, engineering and mathematics*, 6, 115-121.

Bryson, L.S., and Bathe, A. 2009. "Determination of selected geotechnical properties of soil using electrical conductivity testing." *Geotechnical testing journal*, 32, 1-10.

Casagrande, A. 1932. "Research of Atterberg limits of soils." *Public roads*, 13, 121–136.

Das, B.M., and Sobhan, K. 1985. "Principles of geotechnical engineering." Global engineering, Eighth edition.

Dikmen, U. 2009. "Statistical correlations of shear wave velocity and penetration resistance for soils." *Journal of geophysics and engineering*, 6, 61-72

Farrar, D., and Coleman, J. 1967. "The correlation of surface area with other properties of nineteen British clay soils." *Journal of soil science*, 18, 118-124.

Federal emergency management agency. 2010. http://www.fema.gov/.

Federal emergency management agency. 2013. "Summary of existing guidelines for hydrologic safety of dams." United States dam inventory data, http://www.fema.gov/media-library/assets/documents/28555.

Gautam, D. 2017. "Empirical correlation between uncorrected standard penetration resistance (N) and shear wave velocity (V_S) for Kathmandu valley, Nepal." *Geomatics natural hazards and risk*, 8, 496-508.

Giao, P.H., Chung, S.G., Kim, D.Y., and Tanaka, H. 2003. "Electric imaging and laboratory resistivity testing for geotechnical investigation of pusan clay deposits." *Journal of applied geophysics*, 52,157-175.

Goh, A.T.C. 1995a. "Back-propagation neural networks for modeling complex systems." *Artificial intelligence in engineering*, 9, 143-151.

Goh, A.T.C. 1995c. "Modeling soil correlations using neural networks." *J. Computing in civil engrg. ASCE*, 9, 275-278.

Hassanein, Z.S.A., Benson, C.H., and Blotz, L.R. 1996. "Electrical resistivity of compacted clays." *Journal of geotechnical engineering*, 122, 397.

Hickey, C.J. 2012. "Rapid assessment of potential hazards in levees and earthen dams." SERRI project final report, National center of physical acoustics, University of Mississippi, USA.

Ho, M., Lall, U., Allaire, M., Devineni, N., Kwon, H. H., Pal, I., Raff, D., and Wegner, D. 2017. "The future role of dams in the United States of America." *Advancing earth and space science*, 982-998.

Hogan, J.M, and Handy, R.L. 1996. "Seismic wave velocity as a means of in-place density measurement." Final report-part 2 of 2, Engineering research institute, IOWA State University.

Irfan, F., and Syed, B. 2011. "Correlation of electrical resistivity with some soil properties for possible assessment of geotechnical problems: A conceptual…" *UMI-engineering science conference*, Kuala Lumpur, Malaysia.

Jaksa, M. B. 1995. "The influence of spatial variability on the geotechnical design properties of a stiff, over consolidated clay." Ph.D. thesis, The University of Adelaide, Adelaide.

Kalinski, R.J., and Kelly, W.E. 1993. "Estimating water content of soils from electrical resistivity." *Geotechnical testing journal*, 16, 323-329.

Kearey, P., Brooks, M., and Hill, I. 1984. "An introduction to geophysical exploration." Third edition, Wiley-Blackwell.

Kibria, G. 2014. “Determination of geotechnical properties of clayey soil from resistivity imaging (RI).” M.Sc. thesis, University of Texas at Arlington.

Kibria, G. 2014. “Evaluation of physico-mechanical properties of clayey soils using electrical resistivity imaging technique.” Ph.D. thesis, University of Texas at Arlington.

Loke., M.H. 2015. “Tutorial: 2-D and 3-D electrical imaging surveys.” *Geotomo software*, Malaysia.

Mayne, P.W., and Rix, G.J. 1995. “Correlations between shear wave velocity and cone tip resistance in natural clays.” *Soils and foundations,* 35, 107–110.

Mitchell, J. and Saga, K. 2005. “Fundamentals of soil behavior.” John Willey and sons, Inc., Hoboken, NJ.

Mohd, H.Z.A., Rosli, S., Fauziah, A., Devapriya, C.W., and Mohamed, F.T.b. 2012. “Seismic refraction investigation in near surface landslides at the Kindasang area in Sabah, Malaysia.” *Sciverse science direct, Procedia engineering*, 50, 516-531.

Najjar, Y.M., and Huang, C. 2007. “Simulating the stress-strain behavior of Georgia kaolin vis recurrent neural approach.” *Computers and geotechnics*, 34, 346-361.

National inventory of dams. 2009. US army corps of engineers (USACE), Corps map, http://geo.usace.army.mil/pgis/f?p=397:5:0::NO.

Osman, S.B.S., Fikri, M.N., and Siddique, F.I. 2014. “Correlation of electrical resistivity with some soil parameters for the development of possible prediction of slope stability and bearing capacity of soil using electrical parameters.” *Science and technology*, 22, 139-152.

Ozcep, F., Tezel, O., and Asci, M. 2009. “Correlation between electrical resistivity and soil-water content: Istanbul and Golcuk.” *International journal of physical sciences*, 4, 362-365.

Petersen, L., Moldrup, P., Jacobsen, O., and Rolston, D. 1996. “Relations between specific surface area and soil physical and chemical properties.” Soil science, 161, 9-12.

Rinaldi, V. A., and Cuestas, G. A., 2002. "Ohmic conductivity of a compacted silty clay." *J. Geotechnical and geoenvironmental engineering*, 128, 824-835.

Ross, D.S., and Ketterings, Q., 2012. “Recommended methods for determining soil cation exchange capacity.” https://s3.amazonaws.com/udextension/lawngarden/files/2012/10/CHAP9.pdf.

Santamarina, J.C., Klein, k. a., and Fam, M. A. 2001. “Soils and waves, particulate materials behavior, characterization and process monitoring.” John Wiley and sons, LTD.

Shahin, M. A., Jaksa, M. B., and Maier, H. R. 2000. “Predicting the settlement of shallow foundations on cohesionless soils using back-propagation neural networks.” Research report No. R 167, University of Adelaide, Adelaide.

Sharma, P. V. 1997. “Environmental and engineering geophysics.” Press syndicate of the University of Cambridge.

Shidlovskaya, A., Briaud, J.L., Chedid, M., and Keshavaza, M. 2016. “Erodibility of soil above the groundwater level: some test results.” *E3S web of conferences.*

Shirgiri, N. 2012. “Correlation between geotechnical and geophysical properties of soil.” M.Sc. thesis, University of Birmingham.

Siddiqui, F.I., and Osman, S.B.A.B.S. 2012. “Integrating geo-electrical and geotechnical data for soil characterization.” *International journal of applied physics and mathematics*, 2,104-106.

Smith, C.W., Hadas, A., Dan, J., and Koyumdjisky, H. 1985. “Shrinkage and Atterberg limits relation to other properties of principle soil types in Israel.” *Geoderma*, 35, 47-65.

Stephens, T. 2010 “Manual on small earth dams: A Guide to Siting, Design and construction.” FAO irrigation and drainage paper, http://www.fao.org/docrep/012/i1531e/i1531e00.pdf.

Sudha, K., Israil, M., Mittal, S., and Rai, J. 2009. “Soil characterization using electrical resistivity tomography and geotechnical investigations.” *Journal of applied geophysics*, 67, 74-79.

Tiwari, P., and Shah, M.V. 2015. “Correlation between index properties and electrical resistivity of hydrocarbon contaminated periodic marine clays.” *IOP conference series: Earth and environmental science,* International symposium on geohazards and geomechanics, Warwick, UK.

Waxman, M.H., and Smits, L.J.M. 1968. "Electrical conductivities in oil-bearing shaly sands." *SPE journal*, 8,107–122.

Yasarer, H., and Najjar, M. Y. 2014. “Characterizing the permeability of Kansas concrete mixes used in PCC pavements.” *ASCE journal*, 14, 1-8.

Yukselen, Y., and Kaya, A. 2006. “Prediction of cation exchange capacity from soil index properties.” *Clay minerals*, 41, 827-837.

APPENDICES

Table A1: Experimental results of geotechnical and geophysical laboratory tests (Part-1)

Soil Type	Silt (%)	Sand (%)	Clay (%)	Kaolinite (%)	Bentonite (%)	Atterberg Limit			Specific gravity	Specific Surface Area (m2/kg)	Cation exchange capacity (cmol/kg)
						LL (%)	PL (%)	SL (%)			
1	0	45	55	44	11	46	18.21	11.31	2.57	48214.29	16.30
2	5	45	50	40	10	46.5	16.51	10.39	2.61	49107.14	12.20
3	10	45	45	36	9	43.7	16.70	9.60	2.58	44107.14	15.20
4	15	45	40	32	8	39	15.54	8.63	2.62	35714.29	10.27
5	0	50	50	40	10	47.8	15.30	6.74	2.56	51428.57	14.30
6	5	50	45	36	9	42.5	15.92	6.81	2.57	41964.29	10.25
7	10	50	40	32	8	41	15.40	5.06	2.57	39285.71	11.00
8	15	50	35	28	7	36	13.36	4.59	2.57	30357.14	10.89
9	0	60	40	32	8	38	13.28	5.81	2.61	33928.57	11.14
10	5	60	35	28	7	34	13.02	4.40	2.60	26785.71	9.86
11	0	65	35	28	7	34.5	13.69	5.27	2.60	27678.57	9.20
12	0	20	80	64	16	73.5	22.12	15.94	2.56	97321.43	18.73
13	10	20	70	56	14	73	22.70	14.77	2.54	96428.57	21.21
14	20	20	60	48	12	54	17.00	13.73	2.58	62500.00	16.02
15	0	25	75	60	15	61	21.56	13.42	2.56	75000.00	18.18
16	10	25	65	52	13	53	20.40	11.48	2.59	60714.29	17.14
17	20	25	55	44	11	46	17.22	9.33	2.57	48214.29	19.18
18	0	30	70	56	14	62	21.56	14.65	2.58	76785.71	19.11
19	10	30	60	48	12	52.5	18.23	10.80	2.60	59821.43	16.48
20	20	30	50	40	10	45	16.95	12.99	2.56	46428.57	17.11
21	0	35	65	52	13	58	19.36	10.45	2.55	69642.86	19.29
22	10	35	55	44	11	50	17.57	9.91	2.61	55357.14	16.77
23	20	35	45	36	9	42.5	16.18	10.38	2.65	41964.29	16.05
24	0	40	60	48	12	54.5	18.21	9.24	2.56	63392.86	17.48
25	10	40	50	40	10	45	16.77	8.86	2.58	46428.57	16.00
26	20	40	40	32	8	39	15.69	7.93	2.60	35714.29	12.74

Table A2: Experimental results of geotechnical and geophysical laboratory tests (Part-2)

Soil Type	Dry density Kg/m^3	wet density Kg/m3	Water Content %	Void Ratio	Degree of Saturation (%)	True resistivity (Ohm-m)	P wave velocity (m/sec)	S wave velocity (m/sec)	Cohesion (kPa)
1	1527.233	1754.771	14.90	0.68	55.98	16.09	577.8	362.8	14.13
	1533.504	1782.798	16.26	0.68	61.71	15.33	566.6	341.1	
	1572.143	1880.286	18.40	0.64	74.37	12.04	666.7	325	
	1616.097	1947.308	**20.49***	0.59	89.06	8.43	587.9	322.3	
	1586.39	1944.871	22.60	0.62	93.49	9.90	471.8	247.9	
	1521.586	1882.723	23.73	0.69	88.38	8.77	328.2	191.3	
2	1562.918	1795.691	14.89	0.67	58.12	15.75	536.7	319.2	5.5
	1610.958	1903.731	18.17	0.62	76.63	12.67	589.4	334.3	
	1651.963	1974.58	19.53	0.58	88.07	10.53	604.7	302.7	
	1676.657	2013.149	**20.07***	0.55	94.29	8.42	528.2	279.9	
	1573.84	1929.907	22.62	0.66	89.85	10.08	489.5	343.6	
	1541.408	1922.108	24.70	0.69	93.14	7.44	587.9	350.3	
3	1569.363	1802.016	14.82	0.64	59.46	12.57	568	316.2	4.99
	1584.579	1846.119	16.51	0.63	67.87	12.81	614.2	304.3	
	1589.39	1860.057	17.03	0.62	70.58	11.78	529.4	325	
	1683.978	2013.075	**19.54***	0.53	94.90	5.87	559.8	321.4	
	1578.795	1915.064	21.30	0.63	86.76	8.37	508.7	203.7	
	1527.565	1880.298	23.36	0.69	87.57	8.62	607.8	310.3	
4	1618.932	1851.527	14.37	0.62	61.03	16.10	508	311.2	5.1
	1642.487	1923.265	17.09	0.59	75.45	13.74	466.1	271.5	
	1721.668	2042.029	**18.61***	0.52	93.71	8.61	509.8	288.2	
	1605.109	1925.642	19.97	0.63	82.95	7.28	557.1	305.9	
	1572.089	1924.399	22.41	0.66	88.29	6.40	572.1	316.2	
	1512.406	1881.236	24.39	0.73	87.43	7.75	637.6	324.5	
5	1563.781	1796.386	14.87	0.64	59.70	14.10	541.7	340.6	22
	1597.654	1847.774	15.66	0.60	66.45	15.04	562.5	301.2	
	1614.579	1895.421	**17.39***	0.59	75.94	10.16	517.7	285	
	1540.713	1875.74	21.21	0.66	81.99	10.57	409.8	204.7	
	1502.389	1826.497	22.29	0.71	80.98	7.33	473.7	342.1	
	1438.719	1783.651	23.89	0.78	78.40	5.95	496.8	335.7	
6	1534.709	1814.543	15.00	0.67	57.29	12.66	433.3	290	9.22
	1564.447	1856.413	17.78	0.64	71.26	13.49	505.4	271	
	1568.052	1874.449	**19.54***	0.64	78.78	10.97	439.8	262.3	
	1534.085	1852.112	20.73	0.67	79.08	8.90	447.4	212.1	
	1487.302	1827.179	21.48	0.73	75.99	7.66	518.8	214.7	
	1455.393	1785.772	22.70	0.76	76.33	6.78	533	210.1	

Table A2: Experimental results of geotechnical and geophysical laboratory tests (Part-2 continues)

Soil Type	Dry density Kg/m^3	wet density Kg/m3	Water Content %	Void Ratio	Degree of Saturation (%)	True resistivity (Ohm-m)	P wave velocity (m/sec)	S wave velocity (m/sec)	Cohesion (kPa)
7	1625.319	1825.949	12.34	0.58	54.51	12.05	558.5	343.1	1.85
	1704.834	1939.326	13.75	0.51	69.55	13.78	545.5	350.3	
	1719.037	2002.011	**16.46***	0.50	85.33	14.24	537.9	297.3	
	1734.902	2050.827	18.21	0.48	97.07	9.08	447.4	275.9	
	1605.512	1941.617	20.93	0.60	89.44	8.43	485.5	330	
	1582.531	1929.907	21.95	0.63	90.30	7.42	503.2	242.2	
8	1632.233	1872.426	14.72	0.58	65.78	13.63	494.7	301.2	1.71
	1641.128	1901.916	15.89	0.57	72.11	18.00	302.3	204.7	
	1655.608	1950.903	**17.84***	0.55	82.94	10.96	479.5	326.4	
	1565.068	1897.626	21.25	0.64	85.00	6.24	573.5	206.3	
	1519.343	1864.615	22.73	0.69	84.41	12.32	590.9	328.7	
	1474.595	1830.043	24.10	0.74	83.35	9.60	574.9	344.1	
9	1661.578	1872.389	12.69	0.57	57.90	23.41	505.4	352.4	9.37
	1663.877	1888.267	14.37	0.57	65.83	15.71	420.1	334.3	
	1674.451	1940.399	**15.88***	0.56	74.04	12.45	463.4	269.3	
	1638.687	1929.029	17.72	0.59	77.87	12.29	414.2	208.6	
	1595.019	1925.13	20.70	0.64	84.73	10.22	570.7	344.1	
	1557.302	1896.115	21.76	0.68	83.86	8.39	292.1	212.5	
10	1622.123	1830.616	12.85	0.60	55.36	28.84	475.6	318.4	1.34
	1633.941	1874.583	14.73	0.59	64.68	12.52	425.5	311.6	
	1638.681	1894.336	15.60	0.59	69.05	13.52	393.3	295.8	
	1654.891	1982.026	**19.77***	0.57	89.87	9.29	577.8	318.8	
	1618.131	1945.419	20.23	0.61	86.56	10.03	500	323.7	
	1599.9	1914.516	21.73	0.63	90.27	8.70	472.7	340.6	
11	1649.469	1837.416	11.39	0.58	51.48	50.64	400	496.8	1.06
	1657.579	1890.363	14.04	0.57	64.31	13.76	422.4	307.5	
	1660.178	1914.15	15.30	0.56	70.36	15.46	431.7	297.7	
	1677.419	1968.828	**17.37***	0.55	82.24	9.73	487.5	324.1	
	1596.835	1913.285	19.82	0.63	82.12	15.02	554.5	336.2	
	1555.372	1898.601	22.07	0.67	85.53	13.77	570.7	317.1	
12	1379.164	1589.311	15.24	0.86	45.52	18.67	473.7	295.1	50.33
	1406.613	1647.839	17.15	0.82	53.49	16.49	466.1	329.6	
	1418.536	1683.13	18.65	0.81	59.28	10.53	522.3	201.7	
	1423.902	1715.203	20.46	0.80	65.58	7.09	558.5	369.7	
	1440.697	1752.273	**21.63***	0.78	71.19	3.43	546.7	298.1	
	1441.499	1782.591	23.66	0.78	77.99	6.76	524.7	296.2	

Table A2: Experimental results of geotechnical and geophysical laboratory tests (Part-2 continues)

Soil Type	Dry density Kg/m^3	wet density Kg/m3	Water Content %	Void Ratio	Degree of Saturation (%)	True resistivity (Ohm-m)	P wave velocity (m/sec)	S wave velocity (m/sec)	Cohesion (kPa)
13	1421.255	1641.417	15.49	0.78	50.09	14.66	398.6	291.8	38.19
	1424.304	1666.374	17.00	0.78	55.22	14.29	442.3	291	
	1425.61	1688.077	18.41	0.78	59.94	11.56	399.3	314.5	
	1453.114	1776.206	22.23	0.75	75.66	7.06	468.9	268.3	
	1474.087	1838.707	**24.74***	0.72	87.08	5.98	495.8	259.7	
14	1470.411	1617.362	14.93	0.76	51.02	12.78	275	199	8.27
	1452.302	1662.121	17.41	0.78	57.82	13.52	495.8	321.4	
	1453.798	1690.588	16.80	0.78	55.93	9.29	460.6	300	
	1456.881	1698.045	18.50	0.77	61.87	16.91	488.5	300.4	
	1458.615	1726.353	**21.45**	0.77	71.96	11.95	357.8	298.1	
	1553.813	1771.526	23.38*	0.66	91.27	6.34	512	284.3	
15	1355.703	1513.173	11.62	0.89	33.50	32.72	559.8	400.7	21.02
	1357.152	1546.428	13.95	0.88	40.32	27.41	542.9	342.1	
	1395.776	1615.912	17.08	0.83	52.47	11.93	483.5	275.9	
	1397.857	1647.937	17.89	0.83	55.14	19.64	409.1	303.5	
	1399.672	1683.398	**20.27**	0.83	62.66	7.79	256.9	216.7	
	1335.797	1637.664	22.60*	0.91	63.18	12.35	328.2	300.4	
16	1424.029	1605.116	12.72	0.82	40.26	32.67	319.7	158.3	17.92
	1453.269	1675.904	15.32	0.78	50.78	16.72	487.5	306.3	
	1466.485	1698.63	15.83	0.76	53.57	14.33	498.9	316.2	
	1510.752	1790.256	**18.50**	0.71	67.15	6.34	579.2	336.7	
	1497.531	1811.996	21.00*	0.73	74.63	8.49	535.5	377.4	
	1490.46	1850.442	24.15	0.74	84.88	6.67	490.6	267.7	
17	1499.366	1721.406	14.81	0.72	53.18	13.61	456.1	297.3	17.58
	1520.568	1775.816	16.79	0.69	62.37	11.96	516.6	300	
	1535.316	1826.631	18.97	0.68	72.19	9.66	492.6	280.9	
	1545.99	1866.637	20.74	0.66	80.29	7.34	491.6	277.6	
	1552.467	1907.485	**22.87***	0.66	89.46	6.99	448.3	243.8	
	1458.516	1818.259	24.67	0.76	83.01	5.78	468	284.3	
18	1433.525	1676.683	16.96	0.80	54.85	14.69	548	345.1	8.1
	1445.823	1718.286	18.84	0.78	62.13	11.79	516.6	339.6	
	1454.55	1738.503	19.52	0.77	65.26	9.49	522.3	321	
	1468.18	1765.945	20.28	0.75	69.27	6.65	508.7	304.7	
	1541.486	1875.302	**21.66***	0.67	83.17	5.46	611	275.3	
	1544.366	1907.229	23.50	0.67	90.66	5.00	563.9	303.9	

Table A2: Experimental results of geotechnical and geophysical laboratory tests (Part-2 continues)

oil Type	Dry density Kg/m^3	wet density Kg/m3	Water Content %	Void Ratio	Degree of Saturation (%)	True resistivity (Ohm-m)	P wave velocity (m/sec)	S wave velocity (m/sec)	Cohesion (kPa)
19	1490.699	1759.95	18.06	0.75	62.98	13.89	492.6	305.5	8.65
	1495.258	1799.53	20.35	0.74	71.46	9.12	539.2	317.5	
	1550.195	1892.691	22.09	0.68	84.63	7.52	550.6	284.3	
	1569.497	1933.952	**23.22**	0.66	91.74	6.64	586.5	421.6	
	1556.985	1933.952	24.21*	0.67	93.75	5.99	466.1	312	
	1455.021	1867.564	28.35	0.79	93.50	7.63	489.5	365.6	
20	1405.275	1606.7	14.33	0.82	44.57	34.57	324.1	202.4	3.99
	1536.345	1789.549	16.48	0.67	63.17	15.33	459.7	272.4	
	1608.779	1904.426	18.38	0.59	79.36	7.83	557.1	288.2	
	1635.45	1971.046	**20.52**	0.57	92.67	6.91	517.7	297	
	1571.32	1937.133	23.28*	0.63	94.49	7.28	422.4	262.6	
	1547.735	1921.571	24.15	0.66	94.32	7.66	498.9	253.5	
21	1491.093	1698.947	13.94	0.71	49.94	11.96	516.6	352.9	13.78
	1494.25	1747.435	16.94	0.71	61.02	14.28	502.1	301.2	
	1523.138	1816.907	19.29	0.68	72.78	8.45	592.4	341.6	
	1607.97	1946.857	**21.08**	0.59	91.49	11.42	596.9	331.4	
	1550.687	1916.661	23.60*	0.65	93.16	6.86	670.5	296.2	
	1521.517	1903.183	25.08	0.68	94.41	6.35	535.5	283	
22	1521.416	1746.887	14.82	0.72	53.97	15.24	488.5	304.3	2.58
	1541.078	1806.841	17.25	0.70	64.78	15.35	512	309.1	
	1560.499	1858.314	19.08	0.67	73.94	10.88	577.8	318.8	
	1578.365	1920.134	**21.65**	0.66	86.31	7.74	553.2	279.9	
	1538.412	1891.472	22.95*	0.70	85.85	7.63	376.2	252.7	
	1500.328	1879.165	25.25	0.74	88.97	6.70	351.4	194.7	
23	1603.638	1829.495	14.08	0.65	57.17	14.60	491.6	304.7	2.37
	1611.062	1876.191	16.46	0.65	67.59	13.54	537.9	298.9	
	1681.316	1999.22	18.91	0.58	86.91	10.96	570.737	280.2	
	1713.336	2061.417	**20.32***	0.55	98.41	7.68	379.3	296.6	
	1638.361	2013.734	22.91	0.62	98.27	7.66	544.2	331.4	
	1526.93	1893.605	24.01	0.74	86.48	5.47	520	309.9	
24	1460.972	1694.28	15.97	0.75	54.26	13.05	490.6	313.7	11.11
	1477.053	1738.429	17.70	0.74	61.69	15.39	523.5	325	
	1512.748	1805.903	19.38	0.69	71.54	10.17	545.5	319.7	
	1579.422	1921.925	**21.69***	0.62	89.25	7.63	485.5	390.7	
	1524.771	1888.84	23.88	0.68	89.88	8.03	427	275.9	
	1430.138	1793.534	25.41	0.79	82.22	8.06	324.1	202.8	

Table A2: Experimental results of geotechnical and geophysical laboratory tests (Part-2 continues)

Soil Type	Dry density Kg/m^3	wet density Kg/m3	Water Content %	Void Ratio	Degree of Saturation (%)	True resistivity (Ohm-m)	P wave velocity (m/sec)	S wave velocity (m/sec)	Cohesion (kPa)
25	1565.664	1792.779	14.51	0.65	57.70	16.55	483.5	281.6	5.97
	1578.31	1842.96	16.77	0.64	68.08	14.75	528.2	318.8	
	1688.113	1994.675	**18.16***	0.53	88.55	6.03	641.1	314.1	
	1615.954	1952.658	20.84	0.60	89.99	8.28	439.8	256.3	
	1542.072	1883.539	22.14	0.67	84.78	7.94	509.8	302.3	
	1494.491	1861.739	24.57	0.73	87.19	7.41	514.3	320.5	
26	1554.721	1767.432	13.68	0.67	52.85	25.65	346.7	216.5	2.8
	1609.569	1874.132	16.44	0.62	69.36	14.86	389.4	249.5	
	1620.373	1926.677	18.90	0.61	81.19	10.86	461.5	331	
	1638.997	1970.888	**20.25***	0.59	89.68	8.93	497.9	313.7	
	1569.637	1901.916	21.17	0.66	83.75	8.42	498.9	287.1	
	1546.986	1905.108	23.15	0.68	88.32	9.20	535.5	335.2	

Note: * Cohesions are determined at opt or near opt moisture content
Optimum moisture contents are in bold letter

VITA

Fatema Tuz Johora graduated from Military Institute of Science and Technology, Bangladesh, with a Bachelor of Science in Civil Engineering in January 2014. After that, she Joined Military Institute of Science and technology as a lecturer. She worked there from January 2014 to August 2017. During that time, she was doing her part-time M.Sc. in Civil Engineering at Military Institute of Science and technology from October 2014 to August 2017. She was also working as a junior consultant engineer in Center for Advisory and Testing Service (CATS), Military Institute of Science and Technology (MIST), from January 2014 to August 2017. She entered The University of Mississippi, Oxford, Mississippi, in August 2017, and enrolled in a Civil Engineering Doctorate program. During her graduate study, she worked at the National Center for Physical Acoustics as a graduate research assistant from August 2017 to August 2021,

Her experience includes conducting research in the development of prediction models using ANN. She conducted extensive lab works to determine geotechnical properties such as Atterberg limits, water content, dry density, saturation, SG, CEC, void ratio, cohesion and so on. She also has expertise in electrical resistivity and seismic wave velocity lab measurements. In Bangladesh, she taught a couple of civil engineering courses at the undergrad level. She also has expertise in consultancy on a good number of structural and geotechnical projects. She has research experience on seismic vulnerability assessment of concrete buildings using OpenSees software. She has also research experience in correlation development with concrete compressive strength and ultrasonic pulse velocity.